



## City Research Online

### City, University of London Institutional Repository

---

**Citation:** Pal, Atasi (2013). Thulium-doped fibre laser in the 2  $\mu\text{m}$  wavelength region for gas sensing. (Unpublished Doctoral thesis, City University London)

This is the unspecified version of the paper.

This version of the publication may differ from the final published version.

---

**Permanent repository link:** <https://openaccess.city.ac.uk/id/eprint/2989/>

**Link to published version:**

**Copyright:** City Research Online aims to make research outputs of City, University of London available to a wider audience. Copyright and Moral Rights remain with the author(s) and/or copyright holders. URLs from City Research Online may be freely distributed and linked to.

**Reuse:** Copies of full items can be used for personal research or study, educational, or not-for-profit purposes without prior permission or charge. Provided that the authors, title and full bibliographic details are credited, a hyperlink and/or URL is given for the original metadata page and the content is not changed in any way.

# **Thulium-doped Fibre Laser in the 2 $\mu\text{m}$ Wavelength Region for Gas Sensing**

Thesis by

**Atasi Pal**

for the Degree of  
**Doctor of Philosophy**



**CITY UNIVERSITY  
LONDON**

London, United Kingdom

Submitted to City University London

2013

(Defended July 19, 2013)

# Declaration

This thesis is presented in fulfilment of the requirement for the degree of Doctor of Philosophy. The research reported in this doctoral thesis has been carried out at the City University London, UK and CSIR-Central Glass & Ceramic Research Institute, Kolkata, India mainly over the period 2009-2012. The author has contributed extensively to all aspects of the research work presented in this thesis. The work has not been submitted to any other University of Higher Education Institution or for any other academic award in this University. Where use has been made of previously published work or the work of other people, it has been fully acknowledged and fully referenced.

Author's Signature: -----  
Atasi Pal

## Supervisors:

-----  
**Professor Tong Sun**

Professor of Sensor Engineering  
City University London, UK

-----  
**Dr. Ranjan Sen**

Chief Scientist & Head Glass Division  
CSIR-Central Glass & Ceramic Research  
Institute, Kolkata, India

-----  
**Professor K T V Grattan**

Dean, City Graduate School  
City University London

# Acknowledgement

First and foremost I would like to express my profound gratitude to my academic advisors, Professor Tong Sun, Dr. Ranjan Sen and Professor K T V Grattan, for their able guidance, unconditional support, unceasing encouragement and above all, the freedom they gave me to choose research topics and plan work throughout my dissertation. I am grateful to Professor Sun for motivating me for doctoral research and for creating a friendly space in which ideas could be explored. She has also provided me with invaluable help in carefully planning and managing research projects, never allowing me to bother of the financial requirements to continue my Ph.D work. Dr. Sen carefully chalked out my plan of work at CSIR-CGCRI that can be extended further during my stay at City University London. Despite his busy schedule, he has always made time for discussion and support to overcome critical situations during this period. I would like to mention special thanks to Prof. Grattan for his invaluable suggestions for organizing the entire thesis. I have always appreciated his calm, precise and carefully evaluating manner. I have truly learned a lot during my thesis, which go beyond science itself, and will remain thankful to my supervisors for this.

This thesis is the result of my research work as a scientist at Fibre Optics and Photonic Division at CSIR-CGCRI, Kolkata. Of course, it would have been impossible without extensive help and co-operation of the group. Firm support and guidance of the then director Dr. Himadri Sekhar Maiti inspired me to initiate such collaborative research work and made it possible to spend long time at City University London for research work. Mr. Kamal Dasgupta, Head, Fiber Optics and Photonic Division, was always available for any help needed during this period. Dr. Anirban Dhar deserves special mention for his contribution in fabricating different kind of fibres required for my experiments. Dr. Shyamal Das and other members in the group were instrumental for providing all the support that I required numerous times.

It was my pleasant experience to be associated with the Sensor Research Group at School of Engineering and Mathematical Science, City University London where the friendly and informal work environment allows students from different continents to feel at ease right from day one. I am grateful to Dr. T. Venugopalan, Dr. Frederic Surre, Shuying Chen, Shuang Yao and Jie Cao for their patience and support to accommodate me in a new laboratory environment; for creating experimental setup as well as for helping me to sort out administrative process. I should acknowledge that without extensive support from Shuying, I may not be able to complete my scheduled work during my limited period of stay at City. During the last year of my work I truly enjoyed working together with Shuang Yao and Dr. Kort Bremer. In particular, I thank Kort for organizing a fruitful trip to cold and wet Limerick for performance testing of our laser. I would like to express my gratitude to Prof. Elfed Lewis, Director of the Optical Fibre Sensors Research Centre at University of Limerick to give us an opportunity of testing our laser in the gas sensor system at University of Limerick.

Last but not least, I wish to thank Anka Schwuchow, IPHT, Jena, Germany, Dr. K A Annapurna, Glass Division, CSIR-CGCRI and Dr. Reinhard Caspary, Technical University at Braunschweig who helped me to understand the spectroscopy of rare-earth.

# Abstract

The transition  ${}^3F_4 \rightarrow {}^3H_6$  of trivalent Thulium is widely studied for generating lasers at wavelength near 2  $\mu\text{m}$ . For decades, tuneable continuous wave narrow line-width sources in this wavelength region have been proved to be very useful as spectroscopic tools for trace gas detection. Semiconductor lasers are often not readily available at a reasonable cost with the specific wavelengths required to provide a close ‘match’ to the key absorption features of the gases of interest. Well-designed fibre laser-based systems, however, can overcome this limitation by offering potentially much wider wavelength ranges, coupled with their distinctive and valuable features such as stability, narrow line-width and high tuneability at room temperature. In this work, a compact ‘all-fibre’ laser system has been specifically designed, developed and evaluated, as this type of laser systems is highly desirable for ‘in-the-field’ applications. This takes full advantages of the active fibres based on silica glass host compared to other non-oxide glass hosts in terms of their chemical durability, stability and crucial structural compatibility with readily available telecommunication optical fibres. Ideal host composition for Thulium and efficient pumping scheme poses major challenges restricting the production of commercially deployable efficient ‘all-fibre’ lasers in the 2  $\mu\text{m}$  wavelength region. The aim of the thesis work is to address these challenges. The work presented in this thesis demonstrates a modulated Thulium-doped ‘all-fibre’ tuneable laser in the 2  $\mu\text{m}$  wavelength region suitable for detection of a number of gases of interest. The scope of work includes the fabrication and optimization of the active fibre with the core composition suitable for the creation of an effective Thulium-doped fibre laser. Co-doping of Ytterbium is explored to investigate the energy-transfer mechanism from Ytterbium to Thulium and thereby opening up the opportunity of using economic pump laser diodes emitting at around 0.98  $\mu\text{m}$ . In this respect, both Thulium- and Thulium/Ytterbium-doped single-mode single-clad silica optical fibres are designed and fabricated for a systematic analysis before being used as laser gain media. The optical

preforms having different host compositions, Thulium-ion concentrations and proportions of Ytterbium to Thulium are fabricated by using the Modified Chemical Vapour Deposition technique coupled with solution doping to enable the incorporation of rare-earth ions into the preforms. A thorough investigation of the basic absorption and emission properties of Thulium-doped silica fibres has been performed. The step-wise energy-transfer parameters in Thulium/Ytterbium-doped silica fibre have been determined quantitatively from spectroscopic measurements along with migration-assisted energy-transfer model. A set of tuneable Thulium-doped ‘all-fibre’ lasers, offering a narrow line-width in the 2  $\mu\text{m}$  wavelength region, is created by using fabricated Thulium-and Thulium/Ytterbium-doped fibres as gain media and fibre Bragg grating pairs under in-band pumping at 1.6  $\mu\text{m}$  and/or pumping by an economical laser diode at 0.98  $\mu\text{m}$ , utilizing Ytterbium to Thulium energy-transfer. The host composition and the dopant concentration in the single-mode single-clad fibre configuration are optimized to achieve maximum lasing efficiency. The tuning of laser wavelength has been achieved by using relaxation/compression mechanism of the fibre Bragg grating pair used to confine the laser cavity. A new set of laser resonators has also been formed by using a combination of a high reflective fibre Bragg grating with a low reflective broadband mirror, fabricated at the end of the fibre through silver film deposition, to enable only one fibre Bragg grating to be tuned. The stability of the laser output power, line-width and shape have been monitored throughout the tuning range. This is followed by the design of a compact, high-Q, narrow line-width and low threshold microsphere laser resonator, operating in the 2  $\mu\text{m}$  wavelength region, by coupling a Thulium-doped silica microsphere to a tapered fibre. In the microsphere, laser emission occurred at wavelengths over the range from 1.9 to 2.0  $\mu\text{m}$  under excitation at a wavelength of around 1.6  $\mu\text{m}$ . The designed modulated tuneable Thulium-doped ‘all-fibre’ laser, operating at a wavelength range centred at a wavelength of 1.995  $\mu\text{m}$ , has been tested for CO<sub>2</sub> gas detection. Both the modulation of the fibre laser, through pump source modulation and the ‘locking’ detection mechanism have been utilized to eliminate laser intensity noise and therefore to obtain a compact gas sensor with high sensitivity. The absorption spectrum, the line-strength and the concentration level of CO<sub>2</sub>, have been

monitored using the absorption spectroscopic technique. The measured minimum detectable concentration of CO<sub>2</sub> obtained using the system confirms the claim that it is capable of detecting trace gases at the ppm level. The stable laser performance achieved in the sensor system illustrates its potential for the development of practical, compact yet sensitive fibre laser based gas sensor systems.

# Contents

## Acknowledgement

## Abstract

## Glossary of Acronyms

<b>1 Introduction</b>	2
1.1 Aims and Objectives	7
1.2 Structure and Design of the Thesis	8
References	10
<b>2 Rare-earth-doped Fibres, Fibre Lasers and Their Applications</b>	12
2.1 Background	12
2.2 Rare-earth-doped Fibres and Fibre Fabrications	14
2.2.1 Rare-earth-doped fibres	14
2.2.2 Fabrication of rare-earth doped fibres	18
2.3 Rare-earth-doped Fibre Lasers	24
2.4 Applications of Rare-earth-doped Fibre Lasers	30
2.5 Summary	35
References	36
<b>3 Fabrication of Thulium- and Thulium/Ytterbium-doped Optical Fibres</b>	41
Abstract	41
3.1 Introduction	41
3.2 Fabrication Process	43
3.2.1 MCVD process	43

3.2.2	Solution doping technique	45
3.3	Experimental Work	46
3.3.1	MCVD set-up used	46
3.3.2	Fabrication of Thulium-and Thulium/Ytterbium-doped preforms	48
3.3.2.1	Deposition	50
3.3.2.2	Solution doping	51
3.3.2.3	Consolidating and collapsing	52
3.3.3	Characterization of preform	53
3.3.3.1	Refractive Index and geometric profile analysis	53
3.3.3.2	Rare-earth concentration	54
3.3.4	Fibre drawing	56
3.3.5	Fibre characterization	58
3.3.5.1	Refractive Index and geometric profile	58
3.3.5.2	Spectral attenuation	59
3.4	Summary	61
	References	63
<b>4</b>	<b>Spectroscopic Analysis of Thulium and Ytterbium to Thulium</b>	
	<b>Energy-transfer</b>	67
	Abstract	67
4.1	Introduction	67
4.2	Absorption and Emission Spectral Analysis of Thulium	70
4.2.1	Energy levels	70
4.2.2	Absorption and emission cross-sections	72
4.2.3	Judd-Ofelt analysis	74
4.2.4	Fluorescence measurement	77
4.3	Absorption Spectral Analysis of Ytterbium	79
4.4	Ytterbium to Thulium Energy-transfer	80
4.4.1	First step Energy-transfer	80

4.4.2	Second step Energy-transfer	85
4.4.3	Third step Energy-transfer	88
4.5	Optimization of Yb:Tm Proportion	89
4.6	Summary	92
	References	93
<b>5</b>	<b>'All-fibre' Tuneable Laser at 2 <math>\mu</math>m Region</b>	<b>96</b>
	Abstract	96
5.1	Introduction	96
5.2	Pumping Scheme	98
5.3	Experimental Work	101
5.3.1	Design of a laser resonator	101
5.3.1.1	Pump laser at 1.6 $\mu$ m	101
5.3.1.2	Laser resonator at $\sim$ 2 $\mu$ m	102
5.3.2	Performance of laser at $\sim$ 2 $\mu$ m	108
5.3.2.1	Effect of host composition	108
5.3.2.2	Effect of Yb:Tm proportion	111
5.3.2.3	Effect of Tm-ion concentration	113
5.3.3	Tuning of laser resonator	115
5.4	Summary	119
	References	120
<b>6</b>	<b>Thulium-doped Microsphere Laser</b>	<b>123</b>
	Abstract	123
6.1	Introduction	123
6.2	Basic Principle of Operation	126
6.3	Experimental Work	129
6.3.1	Fabrication of tapered-optical fibre	129
6.3.2	Fabrication of Tm-doped silica microspheres	132

6.3.3	Formation of a laser resonator	135
6.4	Laser Performance	136
6.5	Summary	140
	References	141
<b>7</b>	<b>Detection of CO<sub>2</sub> Using a Novel Tuneable Thulium-doped ‘All-fibre’</b>	
	<b>Laser</b>	144
	Abstract	144
7.1	Introduction	144
7.2	Sensor Principle	147
7.3	Experimental Work	149
	7.3.1 Selection of laser wavelength	149
	7.3.2 Experimental set-up	150
	7.3.3 Laser characteristics	153
	7.3.4 CO <sub>2</sub> detection	157
7.4	Summary	162
	References	163
<b>8</b>	<b>Conclusion and Future Work</b>	165
8.1	Conclusion	165
8.2	Future Work	166
	References	168
	<b>List of Publications</b>	169

# List of Figures

- 2.1 Lanthanide series of the elements
- 2.2 Schematic of MCVD fabrication process
- 2.3 Schematic of OVD fabrication process
- 2.4 Schematic of VAD Preform fabrication Process
- 2.5 Schematic diagram of a basic laser
- 2.6 A three-level laser pumping system
- 2.7 Tuneable laser using Littrow prism to select a single wavelength
- 2.8 Schematics of various fibre resonators (a) Fabry–Perot with dielectric reflectors (b) Fabry–Perot with fibre Bragg gratings (c) ring and (d) Fox–Smith
- 3.1 Schematic diagram of the MCVD setup at CSIR-CGCRI, India
- 3.2 Schematic diagram of MCVD process coupled with solution doping technique
- 3.3 Refractive Index profile of a Thulium-doped alumino-silicate preform
- 3.4 (a) Thulium and Ytterbium ion distribution in fibre core (b) Aluminium ion distribution in fibre core
- 3.5 Schematic representation of a fibre drawing tower
- 3.6 Refractive Index profile of a Thulium-doped alumino-silicate fibre
- 3.7 Absorption spectrum of a Tm-Yb doped fibre
- 4.1 Energy level diagram of Tm-doped in alumino-silicate glass fibre; Absorption and emission wavelengths are mentioned in ‘nm’
- 4.2 Absorption and Emission cross sections of Tm/Yb-doped fibre (Fibre ID: TYDF A-5) in the 2  $\mu\text{m}$  wavelength range

- 4.3 Fluorescence spectrum of TYDF-A-3 under excitation at 0.976  $\mu\text{m}$
- 4.4 Absorption and emission cross-sections of Yb in Tm/Yb doped fibre (Fibre ID: TYDF-A-3)
- 4.5 First energy-transfer (ET1) processes in Tm/Yb-co-doped system
- 4.6  ${}^2F_{7/2} \rightarrow {}^2F_{5/2}$  absorption and emission spectra of  $\text{Yb}^{3+}$  and  ${}^3H_6 \rightarrow {}^3H_5$  absorption spectrum of  $\text{Tm}^{3+}$  used to calculate the first step energy-transfer microparameters
- 4.7 Variation of the energy-transfer probability  $K_1$  for the first step energy-transfer as a function of the product of  $N_{\text{Tm}}$  and  $N_{\text{Yb}}$
- 4.8 Second energy-transfer (ET2) processes in Tm/Yb-co-doped system
- 4.9 Variation of the second step energy-transfer parameter,  $W_2$ , as a function of the  $\text{Yb}^{3+}$  concentration
- 4.10 Normalized decay curves for  ${}^2F_{5/2}$  level in TYDF-A-4 considering first step energy-transfer (theoretical) and second step energy-transfer (experimental)
- 4.11 Third energy-transfer (ET3) processes in Tm/Yb-co-doped system
- 4.12 Fluorescence intensity variations with Yb:Tm proportion for fixed pump power at 976 nm
- 4.13 Saturated ASE spectra of Tm/Yb-doped fibre, pumping at 0.98  $\mu\text{m}$
- 5.1 Energy level of  $\text{Tm}^{3+}/\text{Yb}^{3+}$  doped in silica using Russell-Saunders Coupling. All transition wavelengths are in nm
- 5.2 Schematic of a 1.6  $\mu\text{m}$  Er-doped fibre laser set-up to be used as a pump source for a Tm-doped fibre laser
- 5.3 (a) Variation of laser output power with pump power (b) Spectrum of laser source
- 5.4 Schematic of the laser resonator (a) at 1.997  $\mu\text{m}$  under pumping at 1.6  $\mu\text{m}$  (b) at

- 1.874  $\mu\text{m}$  under dual pump combination of 1.6  $\mu\text{m}$  and 0.98  $\mu\text{m}$
- 5.5 Variation of the Tm-doped laser output power with pump power at 1.6  $\mu\text{m}$
  - 5.6 Variation of Tm/Yb-doped fibre laser output power with pump power at 0.98  $\mu\text{m}$
  - 5.7 Reflection spectrum of a mirror fabricated at the fibre end face
  - 5.8 Schematic of laser resonator by using a HR FBG and a broadband mirror fabricated at fibre end face
  - 5.9 Variation of the Tm-doped fibre laser (FBG-Mirror) output power with pump power at 1.6  $\mu\text{m}$
  - 5.10 Tm-doped fibre laser output power at 1.874  $\mu\text{m}$  against 1.6  $\mu\text{m}$  pump
  - 5.11 Tm-doped fibre laser output power at 1.874  $\mu\text{m}$  against 0.98  $\mu\text{m}$  pump
  - 5.12 Laser output power at 1.874  $\mu\text{m}$  against 0.98  $\mu\text{m}$  pump (480 mW) for fibres with different Yb<sup>3+</sup>:Tm<sup>3+</sup> ratio
  - 5.13 The variation of the maximum laser output power with Tm<sup>3+</sup> concentration  
Variation
  - 5.14 3-D trace of normalized laser spectrum (at  $\sim 1.997 \mu\text{m}$ ) as a function of negative strain or compression
  - 5.15 Variation of the laser wavelength (at  $\sim 1.997 \mu\text{m}$ ) with compression of FBG(s)
  - 5.16 Laser power, FWHM and  $1/e^2$  line width as a function of tuned lasing wavelength range of 1.997  $\mu\text{m}$  for both resonator configurations
  - 5.17 Wavelength variation of the reference FBG as a function of laser wavelength
  - 6.1 Schematic of WGM field components in a microsphere resonator (not to scale)
  - 6.2 Schematic of CO<sub>2</sub> laser based setup for tapered fibre fabrication; BBS: broadband source; OSA: optical spectrum analyzer

- 6.3 GUI with set parameter for tapered fibre fabrication process
- 6.4 GUI with set parameter for the spectral loss property during fabrication; elapsed time in second and taper diameter in  $\mu\text{m}$
- 6.5 Image of fabricated tapered fibre showing the smooth, symmetric taper
- 6.6 Schematic of CO<sub>2</sub> laser based setup for microsphere fabrication
- 6.7 Images of the (a) etched fibre end and (b) formed microsphere at the fibre tip
- 6.8 SEM image of the fabricated Tm-doped silica microsphere with a diameter 99  $\mu\text{m}$
- 6.9 Magnified image of Tm-doped microsphere with the tapered fibre. The divisions on the graticule are equivalent to a distance of 0.214  $\mu\text{m}$
- 6.10 Schematic of Tm-doped microsphere laser system (TLS: Tuneable Laser Source)
- 6.11 Resonances in the microsphere coupled with a tapered fibre
- 6.12 Spectral outputs showing multi-mode lasing in the Tm-doped microsphere laser
- 6.13 Spectral output showing single-mode lasing in the Tm-doped microsphere laser
- 6.14 Multi-mode lasing for different excitation wavelengths and identical coupling
- 6.15 Variation of laser output power with pump power
- 7.1 ASE spectrum from Tm-doped fibre overlapped with the absorption spectrum of CO<sub>2</sub>. Inset: Higher resolution spectra of CO<sub>2</sub> showing absorption line strength on the Y-axis
- 7.2 Schematic of the gas sensor system using the Tm-doped tuneable fibre laser (HR: High reflective FBG; LR: low reflective FBG; BBS: broadband source)
- 7.3 Images of Tm-doped tuneable fibre laser and gas cell used in sensor system
- 7.4 Laser output spectrum and variation of laser output power at 1.995  $\mu\text{m}$  with the set point voltage of the forward 0.98  $\mu\text{m}$  pump source laser diver

- 7.5 Transient behaviour of Tm-doped fibre laser
- 7.6 Modulated intensity of the Tm-doped fibre laser at 1.995  $\mu\text{m}$
- 7.7 Linear relationship between the centre wavelength of the tuneable laser at 1.995  $\mu\text{m}$  and the Bragg wavelength of reference FBG at 1.584  $\mu\text{m}$
- 7.8 Stability of the Tm-doped fibre laser based gas sensor system over time
- 7.9 Measured amplitudes  $A_m$  of the modulated tuneable Tm-doped fibre laser exposed in the gas cell
- 7.10 Measured amplitudes  $A_m$  of the modulated Tm-doped fibre laser (at 1.9975  $\mu\text{m}$  and 1.9979  $\mu\text{m}$ ) with  $\text{CO}_2$  gas concentration

# List of Tables

- 1.1 Summary of basic gas sensing methods
- 2.1 Emission of REs doped in oxide glass
- 2.2 Comparison of the optical preform fabrication processes
- 3.1 Standardized parameters during porous core layer deposition
- 3.2 RI and geometrical characterization data of a Thulium-doped fibre
- 3.3 List of fibres Fabricated and Characterized
- 4.1 Energy state position with respect to  $^3H_6$  level and energy gap to the next lower level for  $Tm^{3+}$
- 4.2 Experimental ( $f_{exp}$ ) and calculated ( $f_{cal}$ ) Oscillator strengths of absorption transition of  $Tm^{3+}$  in Tm/Yb doped silica fibre
- 4.3 Calculated radiative lifetimes, radiative transitions rates and branching ratios for Tm/Yb-doped fibre
- 4.4 Measured and calculated lifetimes for fabricated fibres having different Yb:Tm proportion
- 4.5 Parameters for First Step  $Yb^{3+}$  to  $Tm^{3+}$  Energy-transfer (ET1)
- 4.6 Parameters for Second Step  $Yb^{3+}$  to  $Tm^{3+}$  Energy-transfer (ET2)
- 5.1 Fibre parameters for TDF and TYDF having different host composition
- 5.2 Fibre parameters for TYDF having different Yb:Tm proportion
- 5.3 Fibre parameters for TYDF having different Tm concentration
- 7.1 Absorption bands of  $CO_2$  in IR region

# Glossary of Acronyms

<b>MCVD</b>	Modified chemical vapour deposition
<b>RE</b>	Rare-earth
<b>Tm</b>	Thulium
<b>Yb</b>	Ytterbium
<b>RI</b>	Refractive Index
<b>GSA</b>	Ground state absorption
<b>ASE</b>	Amplified spontaneous emission
<b>ET</b>	Energy-transfer
<b>FBG</b>	Fibre Bragg grating
<b>HR</b>	High reflective
<b>LR</b>	Low reflective
<b>OSA</b>	Optical spectrum analyzer
<b>WGM</b>	Whispering gallery mode



# Chapter 1

## Introduction

Gas sensors are of highly importance for a variety of environmental, industrial, medical, scientific and even domestic applications. Trace gases such as methane, acetylene, carbon monoxide and carbon dioxide were monitored in the past almost entirely for safety and pollution control. Lately, industrial sector creates high demand of sophisticated gas analysis as a vital control tool for manufacturing processes [1-2].

Gas detection methods may be classified into two groups, (i) direct methods such as Optical spectroscopy, Mass spectrometry and Gas chromatography, which monitor a physical parameter of the target gas and (ii) indirect methods through interaction with a chemical indicator, involving interaction with the surface of a semiconductor or ceramic layer, e.g. (CHEMFETS and other electrochemical sensors) and catalytically induced combustion and measurement of the heat change (Pellistor gas sensors) which use a chemical reaction or indicator to show the concentration of the gas being sensed [1]. Most sensor technologies that have been developed over the years utilizing indirect method, also classified as ‘reactive’; that is, the analyte chemically interacts with the sensor element, providing an electrical signal that is proportional to the gas concentration. Reactive sensors suffer from a variety of drawbacks inherent to their nature: a) the incomplete reversibility of the chemical changes at the end of the reaction, b) depletion of the chemicals in the sensor element over time, c) lack of specificity to the desired analyte d) interference from other environmental factors and e) lack of broad range selectivity due to a lack of sensitive materials for every gas and/or due to crosstalk. On the other hand, optical sensing techniques as a direct method, have some inherent advantages (a) immunity to electromagnetic interference since the optical components are highly electrically resistive materials, (b) insensitivity to environmental variations such as

temperature and pressure for carefully designed optical sensor and (c) capability of sensing without having the electronic components located at the measurement environment [3]. Table 1.1 gives an overall summary in advantages, disadvantages and application fields for the mentioned gas sensing methods.

Table 1.1 Summary of basic gas sensing methods

<b>Materials/ Methods</b>	<b>Advantages</b>	<b>Disadvantages</b>	<b>Target Gases and Application Fields</b>
Optical Methods	<ul style="list-style-type: none"> <li>• High sensitivity, selectivity and stability</li> <li>• Long lifetime</li> <li>• Insensitive to environment change</li> </ul>	<ul style="list-style-type: none"> <li>• Difficulty in miniaturization</li> <li>• High cost</li> </ul>	<ul style="list-style-type: none"> <li>• Remote air quality monitoring</li> <li>• Gas leak detection systems with high accuracy and safety</li> <li>• High-end market applications</li> </ul>
Mass Spectrometry (Acoustic Methods)	<ul style="list-style-type: none"> <li>• Long lifetime</li> <li>• Avoiding secondary pollution</li> <li>• Design flexibility</li> </ul>	<ul style="list-style-type: none"> <li>• Low sensitivity</li> <li>• Poor reversibility and slow response time</li> <li>• Sensitive to environmental change</li> </ul>	<ul style="list-style-type: none"> <li>• Components of Wireless Sensor</li> <li>• Networks</li> </ul>
Gas chromatography	<ul style="list-style-type: none"> <li>• Excellent separation performance</li> <li>• High sensitivity and selectivity</li> </ul>	<ul style="list-style-type: none"> <li>• High cost</li> <li>• Difficulty in miniaturization for</li> <li>• Portable applications</li> </ul>	<ul style="list-style-type: none"> <li>• Typical laboratory analysis</li> </ul>
Metal Oxide Semiconductor	<ul style="list-style-type: none"> <li>• Low cost</li> <li>• Short response time</li> <li>• Wide range of target</li> </ul>	<ul style="list-style-type: none"> <li>• Relatively low sensitivity and selectivity</li> </ul>	<ul style="list-style-type: none"> <li>• Industrial applications and civil use</li> </ul>

	gases <ul style="list-style-type: none"> <li>• Long lifetime</li> </ul>	<ul style="list-style-type: none"> <li>• Sensitive to environmental factors</li> <li>• High energy consumption</li> </ul>	
Calorimetric Methods (Pellistor gas sensor)	<ul style="list-style-type: none"> <li>• Stable at ambient temperature</li> <li>• Low cost</li> <li>• Adequate sensitivity for industrial detection (ppm range)</li> </ul>	<ul style="list-style-type: none"> <li>• Risk of catalyst poisoning and explosion</li> <li>• Intrinsic deficiencies in selectivity</li> </ul>	<ul style="list-style-type: none"> <li>• Most combustible gases under industrial environment</li> <li>• Petrochemical plants</li> <li>• Mine tunnels</li> <li>• Kitchens</li> </ul>
Electro-chemical (Polymer)	<ul style="list-style-type: none"> <li>• High sensitivity</li> <li>• Short response time</li> <li>• Low cost of fabrication</li> <li>• Simple and portable structure</li> <li>• Low energy consumption</li> </ul>	<ul style="list-style-type: none"> <li>• Long-time instability</li> <li>• Irreversibility</li> <li>• Poor selectivity</li> </ul>	<ul style="list-style-type: none"> <li>• Indoor air monitoring</li> <li>• Storage place of synthetic products as paints, wax or fuels</li> <li>• Workplaces like chemical industries</li> </ul>

In response to the demand for gas sensors with fast temporal response, high selectivity of particular species, long-term stability without maintenance and re-calibration and real-time measurement in few seconds, tuneable continuous-wave narrow line-width laser-based absorption spectroscopy methods are highly advantageous and are paid increasing attention for fast and selective on-line measurement of trace gases in situations such as industrial plants for environmental monitoring and process control. In particular, infrared (IR) absorption spectroscopy is a convenient and useful technique that is applied for many environmental trace gas species detection, since most environmental trace gas molecules have overtone and fundamental ro-vibrational absorption lines in the near-IR (NIR) and mid-IR (MIR) regions [4]. Furthermore, as IR spectroscopy-based sensors do

not rely on catalytic or electrochemical reactions, they are not prone to depletion or contamination of the sensor surface. The primary advantage of IR instruments is that the detector does not directly interact with the gas (or gases) to be detected. The major functional components of the analyzer are protected with optical parts. In other words, gas molecules interact only with a light beam. Only the sample cell and related components are directly exposed to the gas sample, therefore these components can be protected or pre-treated, making them resistant to corrosion and can be designed to be removable for maintenance or replacement. Having been well recognized for accurate identification of gases and reliable concentration measurements, this technology was previously used only in high-end instruments and was not a preferred choice for cost-effective gas detection applications due to its high cost. However, recent breakthroughs in sensor design have made it possible to apply this technology to cost sensitive applications.

Absorption spectroscopy is a technique used to measure the amount of light absorbed by a gas. The amount of light absorbed by a target gas at a specific wavelength is proportional to the amount of the gas in the path of the light. An IR gas sensor consists of a source (emitting at wavelength absorbed by the target gas) and a detector that are separated by a gas cell. If the frequency (or wavelength) of the IR light source matches the vibrational frequency of the molecule, then light will be absorbed. The Beer-Lambert law can be used to calculate molecule concentration (in parts per million-ppm) from the characteristic absorption a molecule exhibits. As a source, a laser is ideally suited for this as the light output is considered to be monochromatic. A tuneable laser with a narrow line-width (narrower than the Doppler widths of absorption lines) is necessary for targeting individual gas absorption lines in order to eliminate cross-sensitivity to other gases [5].

The NIR region, from 1  $\mu\text{m}$  to 2  $\mu\text{m}$ , usually belongs to the first and second overtone bands and the transition strength of which is one or two orders of magnitude weaker than that of the fundamental ro-vibrational absorption lines existing in the MIR region from 2

$\mu\text{m}$  -  $30 \mu\text{m}$ . The price of optical and optoelectronic components (laser and detector), however, increases significantly with wavelength, if at all available. Over the last decade there has been considerable research into the use of tuneable laser diodes in gas sensing applications [6]. Diode lasers, specifically DFB lasers, are attractive for molecular spectroscopy because their emission bands are narrower than the Doppler widths of absorption lines. In the NIR selected wavelengths from III-V devices are widely used in communication and consumer electronics and the lasing materials are already mature and highly efficient. In contrast, the availability of MIR diode lasers with the required output power and wavelength ranges is still limited and most of the MIR diode lasers are produced in small batches with high costs. Thus it is more practical and economical by creating a suite of compact and economic NIR gas sensors [7-9], taking full advantages of the availability and price of the optical components in the NIR region. Although the absorbance of molecules in the NIR are relatively weak compared with that in the MIR, the combination with sensitive detection methods can greatly increase the sensitivity of measurements in this wavelength range and make the detection of fractional absorbance to be in the order of  $10^{-6}$ . Within the NIR region, utilization of the  $2 \mu\text{m}$  wavelength region is preferred since the absorption of some targeted gases over this wavelength band is around hundred times stronger than that of the shorter wavelength region such as  $1.5 \mu\text{m}$  [HITRAN2008].

In absorption spectroscopy based sensing, tuning of laser wavelength to the absorption line of gas is essential. As DFB lasers typically have temperature tuning ranges of only several nanometers, it is necessary to specify the desired operational wavelength range to this tolerance before fabrication. DFB lasers have found limited applications in industrial process control due to both the complex instrumentation required and the lack of high-quality, high-power diode lasers with the required spectral profiles needed for detection.

An alternate approach to obtain wavelength tuneable laser emission in the  $2 \mu\text{m}$  spectral region is by use of rare-earth-doped fibre lasers. These active fibre devices combine the excellent properties of well-known laser materials and hosts with the high-energy confinement available in optical fibres. These fibre lasers have not just demonstrated

excellent conversion efficiencies of pump light to fibre laser emission but also the inherent compatibility with optical fibre based systems for remote monitoring of gases. The key feature of fibre lasers that shows the significance in their applications in gas sensing is their stable behavior coupled with narrow line-width wavelength tuneable operation at room temperature. A number of fibre laser configurations have been investigated to assess their suitability for narrow line-width, tuneable fibre laser operation emitting around 1.5  $\mu\text{m}$  and 2  $\mu\text{m}$  for hydrocarbon gas monitoring [10-12].

## 1.1 Aims and Objectives

The objective of the work presented here is to develop a compact ‘all-fibre’ laser system in the 2  $\mu\text{m}$  wavelength region with stable and tuneable output power as well as narrow line-width suitable for gas sensing. The previous lasers were built with bulk optical components which required alignment and adjustment limiting the development of compact system while an ‘all-fibre’ configuration can provide more rugged, maintenance-free stable system. The trivalent Thulium ( $\text{Tm}^{3+}$ ) ion is an attractive activator for solid-state lasers that emit in the 2  $\mu\text{m}$  wavelength region. The featureless emission in the region of 1.7 to 2.1  $\mu\text{m}$  gives the opportunity of achieving a broad tuning range with operating wavelengths being significant for hydrocarbon gas monitoring. The detailed aims and objectives of the work can thus be summarized as follows:

- Fabrication of a series of Thulium-doped silica optical fibres with modified host compositions and suitable dopant concentrations effective for laser development.
- Investigation on Ytterbium to Thulium energy-transfer mechanism, by means of co-doping of Ytterbium, is pursued thereby opening up the opportunity of using inexpensive pump laser diodes emitting at around 0.98  $\mu\text{m}$ .
- Understanding of  $\text{Yb}^{3+} \rightarrow \text{Tm}^{3+}$  energy-transfer mechanism is essential in designing and modelling (based on rate equations) of fibre amplifiers and lasers and therefore qualitative and quantitative spectroscopic investigation is undertaken and discussed in detail in the following chapters.

- Identification and optimization of suitable host composition, dopant concentration level in active fibres and effective pumping schemes are performed.
- Aiming at the identification of specific hydrocarbon absorption features, the tuneability of the fibre laser is taken into account in the laser design.
- Optimization of fibre laser parameters is performed with a view to produce a compact and efficient laser source for absorption spectroscopy based gas sensing.
- Investigation of a silica based microresonator system is also pursued to achieve a very low threshold and high-Q lasing in the 2  $\mu\text{m}$  wavelength region targeting gas sensing applications.
- Implementation of the designed fibre laser for the detection of carbon dioxide.

## 1.2 Structure and Design of the Thesis

The thesis is structured with a series of chapters describing the comprehensive work carried out to achieve the aims set out and meeting the objectives given.

**Chapter 1** begins with the brief introduction to NIR optical fibre lasers in the context of using spectroscopic technique for gas sensing applications. The aims and objectives of the work, followed by the structure of the thesis designed to meet the objectives at various stages of the work are put forward, outlining the whole work carried out.

**Chapter 2** provides a comprehensive review of rare-earth-doped fibre including the fabrication process of rare-earth-doped fibre, their suitability in fibre laser resonator and the application of rare-earth-doped fibre laser.

**Chapter 3** describes the fabrication process of Thulium-doped fibres and the experimental infrastructure at CSIR-CGCRI used for the preparation of optical preforms and drawing of optical fibres out of optical preforms. The experimental setup utilized for characterization of basic waveguide and transmission properties of the fabricated fibres is explained. The characterized results of the fabricated fibres such as core diameter, numerical aperture, rare-earth concentration, absorption are used throughout the thesis.

**Chapter 4** investigates the basic absorption and emission properties of fabricated Thulium-doped fibre. The calculation of the radiative emission and absorption parameters is explained. The major part of the chapter covers the estimation of the principal energy-transfer parameters for the Thulium/Ytterbium-doped silica fibre based on the spectroscopic measurements and the migration-assisted energy-transfer model.

**Chapter 5** presents the design and development of a tuneable Thulium-doped ‘all-fibre’ laser executed at City University London. The laser resonator is formed by using fabricated Thulium-as well as Thulium/Ytterbium-doped fibres as a gain medium and fibre Bragg grating pair under in-band pumping at 1.6  $\mu\text{m}$  and/or pumping by a laser diode at 0.98  $\mu\text{m}$  respectively. In order to utilize Ytterbium to Thulium energy transfer effect, unidirectional auxiliary pump at approximately 1.6  $\mu\text{m}$  in conjunction with a 0.98  $\mu\text{m}$  primary pump has been explained. The influence of the Tm/Yb concentration, their relative proportions and the host glass composition on the lasing efficiency has also been investigated to optimize the fibre parameters to achieve maximum laser output power. Tuning method of the designed laser has also been explained to make the laser system suitable for gas sensing system.

**Chapter 6** presents the details of a high-Q, narrow line-width and low threshold Thulium-doped microsphere laser. The chapter explains the fabrication of Thulium-doped silica microspheres out of fabricated Thulium-doped fibre and tapered fibre couplers carried out at City University London. Lasing operation under different coupling and pumping conditions has also been described.

**Chapter 7** describes the utilization of a designed ‘all-fibre’ tuneable laser in a gas sensor system at University of Limerick, Limerick, Ireland and at City University London. The laser system is tailored for detection of  $\text{CO}_2$ . The gas detection mechanism has been explained along with the modulation technique of the designed laser. The stability of laser performance has also been tested with a view to develop a prototype sensor system that meets the needs of practical ‘in-the-field’ applications.

**Chapter 8** describes the summary of the work and indicates the future scope of work related to the research.

## References

- [1] G Stewart 'Optical Fiber Sensors Technology', Chapter 5, Kluwer Academic Publishers, Dordrecht, Ed: K T V Grattan and B T Meggitt (1999)
- [2] R F Taylor 'Chemical and biological sensors: markets and commercialisation', Handbook of Chemical and Biological Sensors, IoP Publishing, Bristol, Ed: R. F. Taylor and J. S. Schultz (1996)
- [3] J Janata 'Principles of Chemical Sensors', Plenum Press, New York (1989)
- [4] B Stuart, B George and P McIntyre 'Modern Infrared Spectroscopy', John Wiley & Sons (1996)
- [5] J E Crooks 'The Spectrum in Chemistry', Academic Press Inc. London (1978)
- [6] G J Fetzer, A S Pittner, W L Ryder and D A Brown 'Tunable diode laser absorption spectroscopy in coiled hollow optical waveguides', Applied Optics, Vol. 41, pp. 3613 – 3621 (2002)
- [7] M E Webber, D S Baer and R K Hanson 'Ammonia monitoring near 1.5  $\mu\text{m}$  with diode-laser absorption sensors', Applied Optics, Vol. 40, pp. 2031-2042 (2001)
- [8] P Werle 'A review of recent advances in semiconductor laser based gas monitors', Spectrochimica Acta Part A, Vol. 54, pp. 197–236 (1998)
- [9] A Fried, B Henry, B Wert, S Sewell and J R Drummond 'Laboratory, ground-based, and airborne tunable diode laser systems: performance characteristics and applications in atmospheric studies', Applied Physics B, Vol. 67, pp. 317–330 (1998)
- [10] G Stewart, G Whitenett, P Shields, J Marshall and B Culshaw 'Industrial and highway sensors technology' in Design of Fiber Laser and Sensor Systems for Gas Spectroscopy in the Near-IR, Proceedings. SPIE 5272, pp.172–180 (2003)
- [11] K Chan, H Ito and H Inaba 'An optical-fiber-based gas sensor for remote absorption measurement of low-level CH<sub>4</sub> gas in the near-infrared region', Journal of Lightwave Technology, Vol. 2, pp. 234–237 (1984)

- [12] K Liu, W Jing, G Peng, J Zhang, Y Wang, T Liu, D Jia, H Zhang and Y. Zhang  
'Wavelength Sweep of Intracavity Fiber Laser for Low Concentration Gas  
Detection' IEEE Photonics Technology Letters, Vol. 20, pp.1515-1517 9 (2008)

# Chapter 2

## Rare-earth-doped Fibres, Fibre Lasers and Their Applications

### 2.1 Background

Optics and Photonics are technical enablers for many areas of the economy and their dramatic technical advances have made a significant impact on daily life; indeed, UNESCO has recently adopted a resolution declaring 2015 to be the “International Year of Light” [1]. In the introduction of his 2009 Nobel Prize lecture [2], Charles Kao remarked on his work in optical fibre communications, “the work has fundamentally transformed the way we live our daily lives” [2]. Such technologies are ubiquitous: in the displays of smart phones and computing devices, as the backbone of the Internet for high-speed high-volume data transfer, in advanced precision manufacturing, enhanced defence capabilities and a plethora of medical diagnostics tools. The opportunities arising from optics and photonics offer the potential for even greater societal impact in the coming decades, including solar power generation and efficient lighting that could transform the nation's energy landscape and novel optical capabilities that will be essential to support the continued exponential growth of the Internet.

The birth of laser (Light Amplification by Stimulated Emission of Radiation), stemming from Albert Einstein’s theory on “Stimulated emission”, by Theodore H. Maiman in 1960 at Hughes Research Laboratories in Malibu, California [3], triggered the biggest explosion of activities in optics. It also opened up several entirely new fields for scientists, such as nonlinear optics, fibre optics and opto-electronics, because of its ability to generate an intense and very narrow beam of light of a single wavelength. Numerous

researches, patents and businesses have been established capitalizing on the applications of lasers. Instead of being a branch of fundamental physics, the study of laser has evolved as mainstream science and technology, transforming other fields such as information technology, sensing, medicine treatment, biological study and entertainment. Many new lasers have been discovered so far, each with its own special properties and applications, and their cost, performance, and usability have all improved dramatically.

A significant development of mid-infrared (MIR) laser sources in the wavelength range from 2 to 30  $\mu\text{m}$  occurred since 1980s propelled by the extensive application in the area such as molecular fingerprinting [4], trace gas detection [5], frequency combs [6] and laser spectroscopy [7]. Within this range, 2 to 5  $\mu\text{m}$  lasers are of great interest due to their potential application in the telecommunications and molecular spectroscopy. A good spectral purity, continuous wave (CW) output powers at room temperature and a good tuning range are the requirements for high resolution gas detection. The III-V compound semiconductor material system (Al, Ga, In, As, Sb) forms an ideal basis for the realization of diode lasers emitting in this wavelength range. The most promising new development in the MIR region is the quantum cascade laser. These lasers operate near room temperature in quasi continuous wave mode (long pulse) with high optical powers (up to 100 mW). The lasers can be made with DFB structures so that they operate naturally on a single longitudinal mode. Quantum cascade lasers are made by the deposition of numerous layers of, for example, AlInAs and GaInAs by molecular beam epitaxy. When a voltage is applied across the semiconductor super lattice structure, lasing occurs between the different “quantum wells” (i.e., inter-subband transitions in the conduction band) rather than simply across the bandgap. This means that the lasing wavelength is determined by the quantum well structure rather than by the semiconductor composition. The nonlinearity of glass fibres can also be utilized to generate coherent broad band lasing via supercontinuum generation.

Recently a great deal of research effort has been invested in 2  $\mu\text{m}$  laser development including both solid-state laser and fibre laser field. The strong absorption by water and

the weak absorption by human tissues at 2  $\mu\text{m}$  nominate it as an ideal wavelength for biological and medical applications including laser angioplasty in the coronary arteries, ophthalmic procedures, arthroscopy, laparoscopic cholecystectomy and refractive surgeries [8-10]. In addition, other features of 2  $\mu\text{m}$  lasers such as the lower atmospheric absorption, smaller scattering and “eye-safe” property (radiation in this range will be absorbed by the cornea rather than the more sensitive retina) make the wavelength desirable for material processing, ranging, low altitude wind shear and remote sensing, which includes Doppler lidar wind sensing and water vapour profiling by differential absorption lidar (DIAL) [11-18]. Such wavelength is also a pump source for high power and high brightness mid-infrared generation required for spectroscopic and medical applications (such as in molecular composition detection and tissue ablation) [19]. In the wavelength range around 2  $\mu\text{m}$  the most interesting transitions for efficient laser operation exist in the trivalent rare-earth (RE) ions Thulium ( $\text{Tm}^{3+}$ ) and Holmium ( $\text{Ho}^{3+}$ ).

## 2.2 Rare-earth-doped Fibres and Fibre Fabrications

### 2.2.1 Rare-earth-doped fibres

The first application of REs found day of light in the late 19<sup>th</sup> century. The lanthanides class of REs is a group of elements as shown in Fig. 2.1.

57 La	58 Ce	59 Pr	60 Nd	61 Pm	62 Sm	63 Eu	64 Gd	65 Tb	66 Dy	67 Ho	68 Er	69 Tm	70 Yb	71 Lu
----------	----------	----------	----------	----------	----------	----------	----------	----------	----------	----------	----------	----------	----------	----------

Fig. 2.1 Lanthanide series of the elements

There are fifteen elements in this group starting with Lanthanum (La). The other fourteen elements, in order of increasing atomic weight, are Cerium (Ce), Praseodymium (Pr), Neodymium (Nd), Promethium (Pm), Samarium (Sm), Europium (Eu), Gadolinium (Gd), Terbium (Tb), Dysprosium (Dy), Holmium (Ho), Erbium (Er), Thulium (Tm), Ytterbium

(Yb) and Lutetium (Lu). They are characterized by the electronic filling of the inner  $4f$  shell within the  $[\text{Xe}] 4f^N 5s^2 5p^6 6s^2$  electronic shells where the superscript  $N$  represents the number of electrons in the  $4f$  shell; La has one electron while Lu has fifteen electrons. REs have interesting optical characteristics because of such electronic configurations that distinguish them from other optically active ions: they emit and absorb over narrow wavelength ranges, the wavelengths of the emission and absorption transitions are relatively insensitive to host material, the lifetimes of metastable states are long and the quantum efficiencies tend to be high, except in aqueous solutions. Electronic transitions within the  $4f$  shell occur at optical frequencies and the number of electrons occupying the  $4f$  shell determines their optical characteristics. REs are most stable when in their triply ionized configuration. This occurs when one electron is removed from the  $4f$  shell and two electrons are removed from the  $6s$  shell. Their electronic configuration is thus  $4f^{N-1} 5s^2 5p^6 6s^0$  and the ions are positively charged. The outer  $5s$  and  $5p$  shells remain filled. This has an effect of shielding the remaining electrons in the  $4f$  shell from perturbation due to external fields [20]. Consequently, electronic transitions within the  $4f$  shell are relatively insensitive to the host material and only weak perturbation occurs. The absorption and emission lines of RE ions are relatively sharp (in solid hosts) compared to most other elements because of the shielding phenomenon [21].

In spite of the shielding of the  $4f$  transitions, when the RE ions are introduced as dopants in condensed materials such as crystal or glasses, weak interactions with the electrostatic field of the atomic arrangement take place and as a consequence each transition level split into discrete sub-levels (called multiplet) because of the weak electrostatic interactions with the atoms of the material. This is called Stark effect and it is so weak that the sub-levels are spaced between  $10\text{-}100\text{ cm}^{-1}$ . The strength of the effect depends on the type of host material. Therefore the choice of suitable host glass matrix for RE ion dopants is the key factor to optical laser and amplifier, since the quantum efficiency of fluorescence emission and bandwidth strongly depend on the structural properties of host glass [22, 23, 24]. The most common hosts for RE-doped laser are crystal and glass. A crystal is a solid in which the constituent atoms, molecules, or ions are packed in a regularly ordered and

repeating pattern extending in all three spatial dimensions. In a crystal laser the active medium is composed of ionic species supported in a crystalline host. Glass is defined as ‘an inorganic product of fusion which has been cooled to a rigid condition without crystallization’. It forms an important host family for RE ions because of its good mechanical, thermal and optical properties. Compared with crystal, glass is of significant low cost to fabricate. RE ions can also be easily doped and uniformly distributed into the glass. The possibility for some glasses to be drawn into fibres has opened up plenty of opportunities for the development of fibre lasers and fibre amplifiers. In glass REs exhibit quite broad absorption and emission transitions, whose bandwidths range from tens to hundreds of nanometers. Such a broad line-width results from inhomogeneous broadening caused by the lack of regularity of structure in glass. The broad absorption band of glass material reduces the wavelength tolerance for pump source, while the broad emission band is favourable for a tuneable laser source. Furthermore, emission quantum efficiency from given levels depends strongly on the phonon energy of the glass hosts. The glass host should always have low phonon energy, like non-oxide glasses, such as fluoride and chalcogenide glass; however, these glasses suffer from poor mechanical strength and chemical durability. Although oxide glasses, such as silica glass, have a bit higher phonon energy but have shown a superior refractory nature, thermal shock resistance and high chemical durability compared to the non-oxide glasses. The oxide glass is also advantageous in terms of its crucial structural compatibility with readily available telecommunication optical fibres and the mature techniques available for mass production. Table 2.1 shows the transitions and emissions of the REs doped in oxide glass.

Table 2.1 Emission of REs doped in oxide glass

Dopant Ion	Transition	Operating Range (nm)
Tm <sup>3+</sup>	<sup>1</sup> G <sub>4</sub> → <sup>3</sup> H <sub>6</sub>	480
	<sup>3</sup> F <sub>4</sub> → <sup>3</sup> H <sub>6</sub>	1700–2015
Sm <sup>3+</sup>	<sup>4</sup> G <sub>5/2</sub> → <sup>6</sup> H <sub>9/2</sub>	651
Nd <sup>3+</sup>	<sup>4</sup> F <sub>3/2</sub> → <sup>4</sup> I <sub>9/2</sub>	900–950
	<sup>4</sup> F <sub>3/2</sub> → <sup>4</sup> I <sub>11/2</sub>	1000–1150
	<sup>4</sup> F <sub>3/2</sub> → <sup>4</sup> I <sub>13/2</sub>	1320–1400
Yb <sup>3+</sup>	<sup>5</sup> F <sub>5/2</sub> → <sup>5</sup> F <sub>7/2</sub>	970–1040
Pr <sup>3+</sup>	<sup>1</sup> D <sub>2</sub> → <sup>3</sup> F <sub>4</sub>	1060–1110
Er <sup>3+</sup>	<sup>4</sup> I <sub>13/2</sub> → <sup>4</sup> I <sub>15/2</sub>	1500–1600
Ho <sup>3+</sup>	<sup>5</sup> I <sub>7</sub> → <sup>5</sup> I <sub>8</sub>	2040–2080

Silica, which is pure SiO<sub>2</sub>, is a covalently bonded glass which can sustain phonons with maximum energies in the range of 1050–1100 cm<sup>-1</sup>. The covalent bonding creates the desirable mechanical properties of the glass but the large phonon energies result in large rates of nonradiative decay between the energy levels of excited RE ions which limits the number of fluorescence transitions that are useful for fibre lasers. Silica is a tightly bonded glass that has a rigid network comprising of few non-bridging Oxygen (NBOs) atoms sites which can allow the incorporation of large network modifiers such as the RE ions. To increase RE solubility in silica and decrease the negative effects of clustering, co-doping is most commonly used technique to incorporate REs in silica glass matrix and the most popular solubilizer is Aluminium (Al). Al can be incorporated in the silica network either in tetrahedral coordination as a network former or in octahedral coordination as a network modifier. The four coordinated Al shares NBO ions with RE ions, therefore reducing RE ion clustering. Similarly Phosphorus (P) is another popular codopant. Adding network former compounds e.g., Al<sub>2</sub>O<sub>3</sub> or P<sub>2</sub>O<sub>5</sub> has been shown to increase the solubility of RE cations significantly and minimise clustering [25]. Codopants also provide the index modification needed for creating a waveguiding

structure and are often used to alter spectroscopic properties, such as increasing the emission band width or shifting undesirable excited state absorption features.

The high intensities and long interaction lengths made possible by fibre waveguides make these devices vastly superior to their bulky glass counterparts in most applications. RE-doped fibre lasers have interesting properties which make them to be attractive alternatives to other solid state lasers: One being the simple setup because of the waveguide structure of the fibre like in a diode laser and the other the long interaction length of pump and laser field and the high surface to volume ratio for heat transfer, which result in very high efficiencies. Last but not least is the inherent high beam quality of single-mode fibre lasers, which is more or less independent of the output power, in contrast to laser diodes. The simplest setup of a fibre laser consists of a RE-doped fibre with a pair of fibre Bragg gratings written into the fibre at both ends as laser mirrors and a pigtailed pump diode spliced to one fibre end whereas the other end delivers the laser radiation. Such a simple setup does not require any specific alignment, in addition, the wide ranges of operating wavelengths of fibre lasers provide further flexibility for those applications where operation wavelength is vital, such as laser spectroscopy, remote sensing and coherent laser seeding application.

### **2.2.2 Fabrication of rare-earth doped fibres**

In order to fabricate low-loss fibres suitable for long-distance transmission, it is important to ensure low absorption, low scattering and weak waveguiding in fibres. The first two requirements are common to all-low-loss optical fibres, but the last applies uniquely to fibres used for long-distance lightwave transmission. In contrast, the requirements for the active fibre used in fibre lasers are not the same as those for fibres used for long-distance transmission. An optical fibre becomes active by doping its core with one or more atomic elements, usually REs. So the active fibres are usually designed with a greater variety of materials and structures in order to realize their superior characteristics of lasing and amplification over a wide range of operating wavelengths. The bias toward fibre communications has provided a strong incentive to consider active fibre designs and

compositions compatible with standard low-attenuation, silica-based fibre. Specifically, the ability to connect active fibre components to doped silica telecommunications fibres by fusion splicing, with low insertion loss and low reflectivity, allows the creation of reliable, low-noise, high-gain amplifiers and lasers. This same telecommunication bias has likewise directed RE-doped fibre fabrication towards variations in traditional doped silica processing.

The essential lasing properties of the RE-doped optical fibre depend strongly on the choice of RE ions and fibre materials. The key factors that influence the fabrication and characteristics of practical optical fibres for laser are summarized below.

- i. The homogeneous doping of active ions in host materials
- ii. The phonon energy properties of materials
- iii. The refractive index properties and the controllability of the refractive-index profile in fibres
- iv. Low intrinsic loss and potential for extrinsic loss reduction at operating wavelengths
- v. Precise control of the shape and size of the cross-section and along the axial direction of fibres
- vi. High chemical and mechanical durability of materials

The first five factors strongly affect the lasing characteristics of fibres. The clustering of RE ions shortens the lifetime of radiative transitions. The phonon energy of host materials determines the radiative quantum efficiency. The transmission loss and refractive index difference between the core and cladding of fibres, which are related to factors three and four, strongly influence the gain coefficient. Factor six is necessary for practical fibre fabrication and applications.

The simplest method for fabricating RE-doped fibre is using rod-in-tube technique, where a core rod containing the RE ions is inserted inside a tube which is converted into the cladding when the ensemble is drawn into the fibre [26]. Though this type of fibre can be used in laser applications, low loss RE-doped fibres are usually fabricated by using

modified chemical vapour deposition (MCVD), outside vapour deposition (OVD) or vapour-phase axial deposition (VAD) techniques coupled with some special processes such as vapour delivery process, solution doping process or sol-gel process for incorporating RE in the core of the preform. The main difficulty is the unavailability of suitable RE materials for MCVD, OVD or VAD, as these processes require high vapour pressure sources to introduce sufficient RE vapours during the formation of optical fibre core. Thus several modifications have been made in existing MCVD, OVD and VAD processes to make them suitable for the fabrication of low-loss RE-doped fibres.

**Modified Chemical Vapour Deposition (MCVD) process:** This process starts with a high purity quartz tube mounted on a special glass-working lathe [26]. A mixture of ultra-pure gases flows through the inside of the tube while a heat source (burner) is applied outside. The heat from the burner converts the gases into glass soot. As the burner traverses along the outside of the tube, it creates the fine soot particles and sinters them into a thin layer of doped glass on the inside of the tube. After the first layer is deposited, the mixture of reactive gases is changed and the burner is brought back to the starting position. This process is continued, layer by layer, to construct the complex core structure in the optical fibre. The schematic of the MCVD fabrication process is shown in Fig. 2.2.

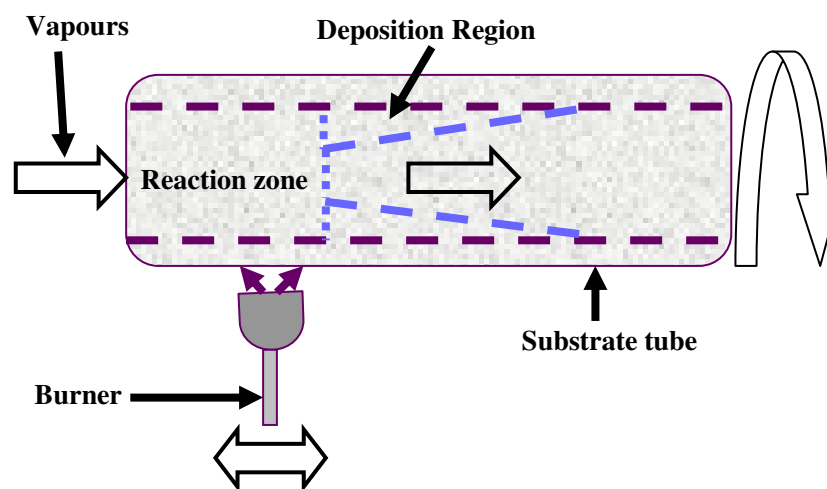


Fig. 2.2 Schematic of MCVD fabrication process

**Outside Vapour Deposition (OVD):** Basic OVD optical fibre manufacturing consists of three steps: laydown, consolidation and draw [26]. In the laydown step, a soot preform is made from ultra-pure vapours as they travel through a traversing burner and react in the flame to form fine soot particles of glass. These particles are deposited on the surface of a rotating target rod. The core material is deposited first, followed by the pure silica cladding. When deposition is complete, the bait rod is removed from the centre of the porous preform and the preform is placed into a consolidation furnace. During the consolidation process, the water vapour is removed from the preform. This high-temperature consolidation step sinters the preform into a solid, dense and transparent glass. The schematic of the OVD fabrication process is shown in Fig. 2.3.

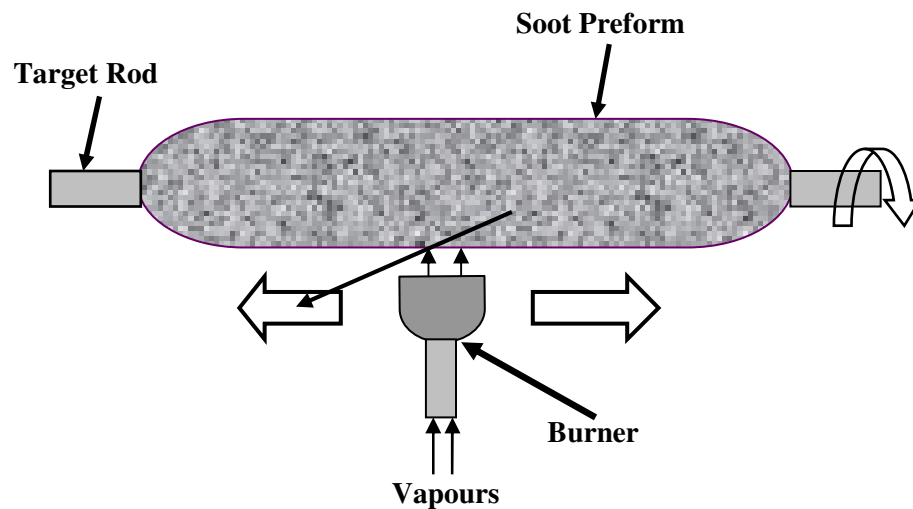


Fig. 2.3 Schematic of OVD fabrication process

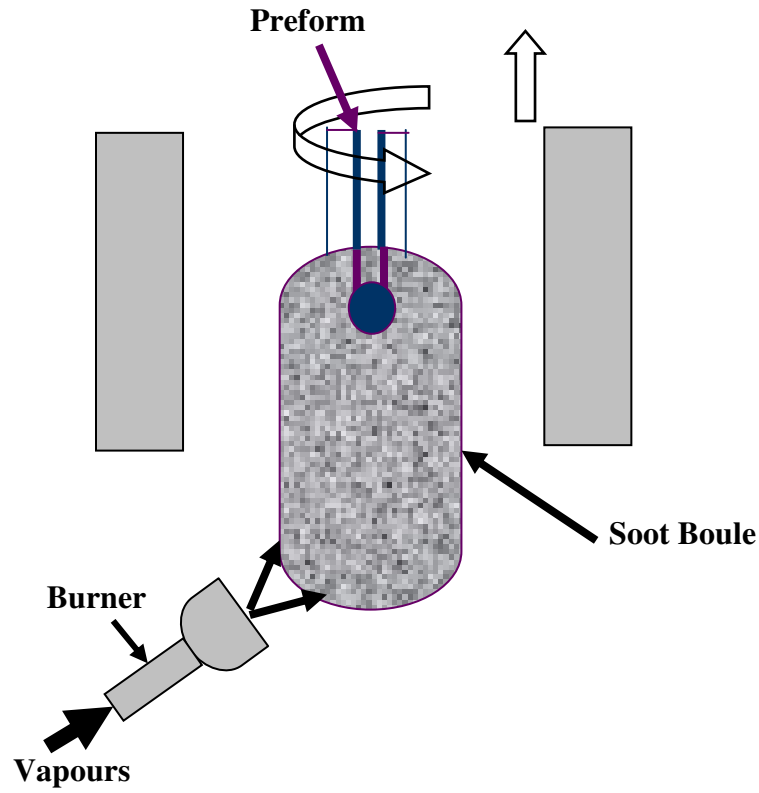


Fig. 2.4 Schematic of VAD Preform fabrication Process

**Vapour Axial Deposition (VAD):** The VAD process utilizes a very short glass target rod suspended by one end [26]. A computer-controlled mixture of gases is applied between the end of the rod and the heat source as shown in Fig. 2.4. The heat source is slowly backed off as the preform lengthens due to tile soot build-up caused by gases reacting to the heat and fusing to the end of the rod. After sufficient length is formed, the target rod is removed from the end, leaving the soot preform followed by collapsing steps to obtain transparent glass preform.

Comparison of the three fabrication processes is summarized in Table 2.2.

Table.2.2 Comparison of the optical preform fabrication processes

Parameter	MCVD	OVD	VAD
Chemical Reaction	Oxidation	Hydrolysis	Hydrolysis
Deposition rate, gm/min	5	Core: 5-10 Clad: 20-100	Core: 5-10 Clad: 20-100
Deposition Efficiency, %	40 - 60	50 - 70	50 - 70
Size of preform rod (fibre Km)	200-400	> 1000	> 1000
Profile control	Very good	Good	Good for SM fiber
Invented at	AT & T	Corning	NTT

As indicated earlier only the MCVD, OVD or VAD technique is not enough to incorporate RE in core region. In an intermediate step of those preform fabrication processes, RE ions can be incorporated into the preform core coupled with one of the following routes: vapour delivery process, solution doping process and sol-gel process.

**Vapour delivery process:** Methods to deliver RE vapour species to the reaction/deposition zone of a preform process can be devised for both MCVD, VAD or OVD techniques [26]. In MCVD system, RE dopants are delivered to an oxidation reaction region along with other index-controlling dopants. The low vapour pressure RE reactant (RE chelated compounds having higher vapour pressure or chlorides having lower vapour pressure) is accommodated either by taking the vapour source close to the reaction zone and immediately diluting it with other reactants or by delivering the material as an aerosol or higher vapour pressure organic compound.

**Solution doping method:** In the solution-doping technique an unsintered (porous) layer of silica is first deposited inside a silica tube by the MCVD process [26]. This layer is doped by filling the tube with an aqueous RE chloride solution; this solution is allowed to

soak for nearly 1 hour, and then the solution is drained. The impregnated layer is dried at high temperatures in the presence of flowing chlorine/oxygen mixture. Index-raising dopants such as Al have also been incorporated by this method. This general method has also been extended by replacing aqueous solutions with ethyl alcohol, ethyl ether, or acetone solvents for Al and RE halides. Solubility varies widely among the RE nitrates, bromides and chlorides and all are useful.

**Sol-Gel Method:** The process coats the inside of an MCVD substrate tube with a RE-containing sol, which subsequently gels, leaving a thin dopant layer [26]. Both RE and index-raising dopants may be combined. The coating sol is formed by hydrolyzing a mixture of a soluble RE compound with  $\text{Si}(\text{OC}_2\text{H}_5)_4$  (TEOS). The viscosity of the gel slowly increases with time as hydrolysis polymerizes the reactants. Deposition of the film then proceeds by filling the inside of the MCVD support tube with the gel, followed by draining. The gel layer thickness is controlled by the viscosity of the gel which, in turn, is determined by its age and the rate at which the gel liquid is drained. Film thickness of a fraction of a micrometer is typical, thereby allowing a well-confined dopant region. The coated tube is returned to the glass-working lathe for subsequent collapse.

The transparent glass preform prepared by using MCVD, OVD or VAD technique coupled with RE incorporation through vapour delivery process, solution doping process or sol-gel process is then taken to the drawing tower to be heated and pulled into the required fibre length.

## 2.3 Rare-earth-doped Fibre Lasers

Lasers are devices that produce intense beams of light which are monochromatic, coherent and highly collimated. The wavelength of laser light is extremely pure (monochromatic) when compared to other sources of light and all of the photons (energy) that make up the laser beam have a fixed phase relationship (coherence) with respect to one another. Light from a laser typically has very low divergence. It can travel over great

distances or can be focused to a very small spot with a brightness which exceeds that of the sun. Schematic diagram of a basic laser setup is shown in Fig. 2.5.

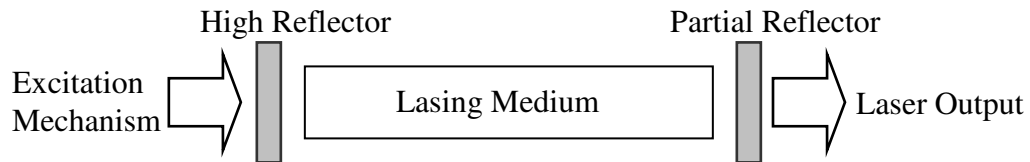


Fig. 2.5 Schematic diagram of a basic laser

A laser is constructed from three principal parts: i) an energy source (usually referred to as the pump or pump source) - the pump source is the part that provides energy to the laser system [27]. The type of pump source used principally depends on the gain medium and this also determines how the energy is transmitted to the medium; ii) a gain medium or laser medium - the gain medium is the major determining factor of the wavelength of operation and other properties of the laser. Gain media in different materials have linear spectra or wide spectra which allow tuning of the laser frequency. The medium is excited by the pump source to produce a population inversion and it is in the gain medium that spontaneous and stimulated emission of photons takes place, leading to the phenomenon of optical gain or amplification; and iii) two or more mirrors that form an optical resonator - the optical resonator or optical cavity in its simplest form is two parallel mirrors placed around the gain medium which provide feedback of the light. Typically one will be a high reflector and the other will be a partial reflector. The latter is called the output coupler, because it allows some of the light to leave the cavity to produce output beam of the laser.

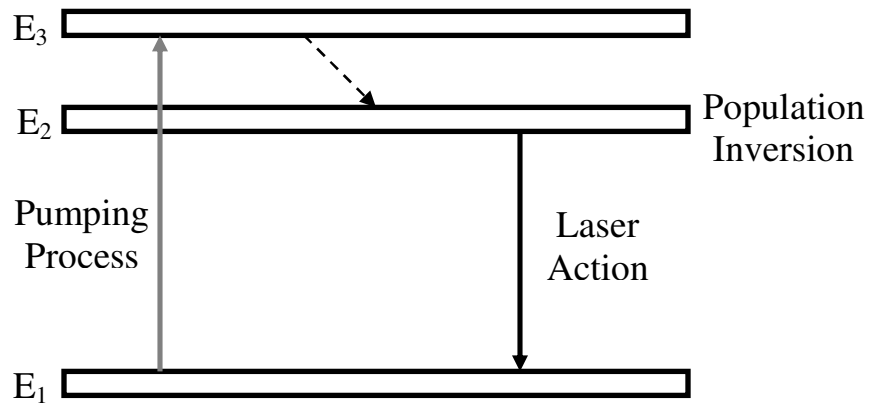


Fig. 2.6 A three-level laser pumping system

A typical three level laser pumping scheme is shown in Fig. 2.6, where the lasing medium (or gain medium) is pumped continuously to create a population inversion at the lasing wavelength. As the excited atoms start to decay, they emit photons spontaneously in all directions. Some of the photons travel along the axis of the lasing medium, but most of the photons are directed out the sides. The photons travelling along the axis have an opportunity to stimulate atoms they encounter to emit more photons, but the ones radiating out the sides do not. Furthermore, the photons travelling parallel to the axis will be reflected back into the lasing medium by the reflectors shown in Fig. 2.5 and given the opportunity to stimulate more excited atoms. As the on-axis photons are reflected back and forth interacting with more and more atoms, spontaneous emission decreases, stimulated emission along the axis predominates and laser output can be obtained.

To create a tuneable laser, the wavelength-selective reflector(s) must be sufficiently broadband to accommodate the entire tuning range and a variable wavelength tuning element must be introduced into the cavity, either between the cavity optics or replacing the high-reflecting optics, to introduce loss at undesired wavelengths. Three tuning mechanisms are in general use: Littrow prisms, diffraction gratings, and birefringent filters. Schematic of a tuneable laser using Littrow prisms is shown in Fig. 2.7.

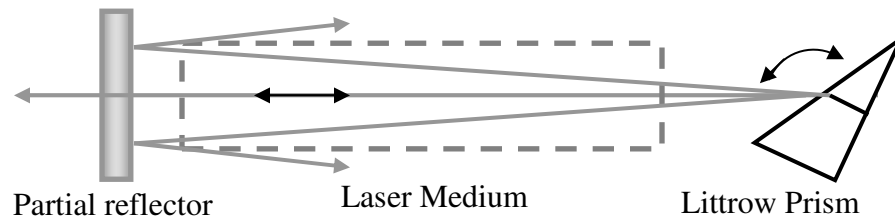


Fig. 2.7 Tuneable laser using Littrow prism to select a single wavelength

RE-doped glass and crystal fibre lasers were first investigated experimentally as early as the 1960s [24], then in the 1970s [28] and early 1980s [29]. However, following the development of the Erbium-Doped Fibre Amplifier (EDFA) in the late 1980s, fibre lasers drew serious attentions. The optical confinement provided by the fibre, combined with the excellent laser properties of trivalent RE ions, make this type of laser extremely efficient. They can operate with extremely low thresholds, as low as few microwatts, and yet can be pumped extremely hard to produce output powers in the excess of several watts with optical conversion efficiencies greater than 50%.

To date, laser transition has been demonstrated for a wide spectrum of wavelengths, Samarium has produced the shortest wavelength (650 nm) [30] and Thulium-sensitized Holmium the longest (2260 nm) [31]. The first reported RE-doped glass fibre device fabricated with MCVD technology was a Neodymium (Nd)-doped fibre laser operated at 1.088  $\mu\text{m}$  in 1985 [32]. After the first demonstration, Erbium-doped fibre lasers have been studied extensively for their potential use as source in the communication system operating in the third communication window [33]. The first Tm-doped fibre laser, demonstrated by Southampton in 1988 [34].  $\text{Tm}_2\text{O}_3$  was doped into a single-mode silica fibre with a doping concentration of 884 ppm ( $6.5 \times 10^8$ ). A Nd:YAG solid state laser at 1.064  $\mu\text{m}$  was used as pumping source. In the following 20 years, various glasses, such as ZBLAN [35] and lead-germanate glasses [36], were investigated as the host material for Tm-doped fibre laser. The motivation was to find a material with low phonon energy that helps to increase the quantum efficiency by reducing the multi-phonon decay rate of the

laser transition. During that time, all kinds of pumping sources, such as Ti:sapphire laser at 0.793  $\mu\text{m}$  [37], Er-doped fibre laser at 1.57  $\mu\text{m}$  [38], InGaAs/InP at 1.6  $\mu\text{m}$  [39], GaAs laser diode at 0.790  $\mu\text{m}$  [36], and NaCl color-center laser at 1.58  $\mu\text{m}$  [40] have been explored. Different pumping schemes have also been studied, such as in-band pump, two-photon pump, and direct  $^3\text{H}_4$  state pump. Recently, Ytterbium-sensitization was developed for Thulium-doped fibres for operation at around 2  $\mu\text{m}$ . In these, pump energy at 0.91 – 0.98  $\mu\text{m}$  is absorbed by the Yb-ions, and then transferred non-radiatively to the lasing Tm-ions. This is similar to the operation of the more widespread erbium-ytterbium co-doped fibres. Ytterbium-sensitization takes advantage of (i) broad energy level can absorb strongly in the region covered by the output of high power GaAs laser diodes around 980 nm (ii) presence of only two levels eliminates any unwanted up-conversion losses, and (iii) broad excited state overlaps with a range of energy levels in other RE ions where direct diode pumping is not feasible. Additionally, the strong overlap of absorption and emission spectra enhances the energy migration among the Yb ions. This migration assisted energy-transfer significantly increases the probability of interaction between sensitizer and activator [41].

Several types of optical resonators have been used in RE-doped fibre lasers in continuous wave (CW) mode; such as Fabry-Perot (FP) resonator [42], ring resonator [43] and Fox-Smith resonator [44]. Schematic of a set of different RE-doped fibre laser resonators is shown in Fig. 2.8.

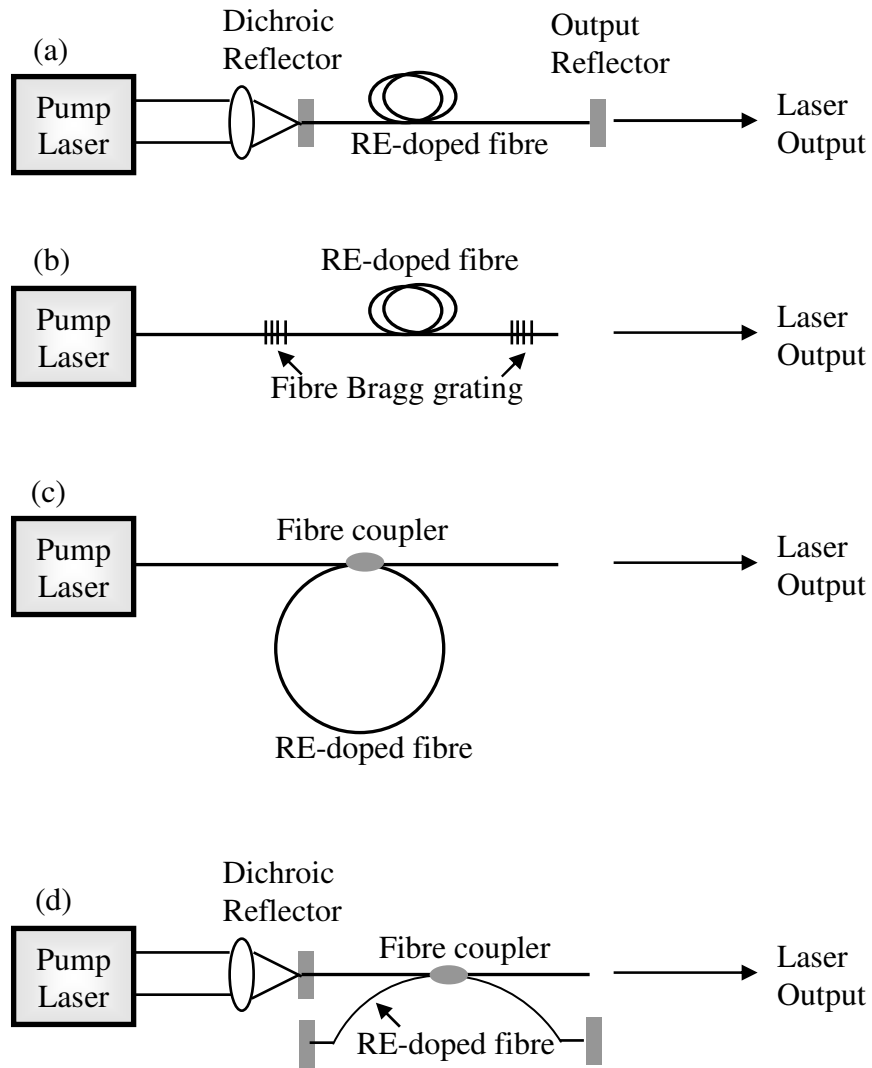


Fig. 2.8 Schematics of various fibre resonators (a) Fabry-Perot with dielectric reflectors (b) Fabry-Perot with fibre Bragg gratings (c) ring and (d) Fox-Smith

Among them, the most commonly used resonator is the FP resonator where two mirrors are separated by an amplifying medium with an inverted population. It is typically formed by placing miniature planar dielectric reflectors in the intimate contact with the ends of the doped fibre, which are either polished or cleaved perpendicular to the fibre axis. The pump beam is usually focused into the fibre through high reflective mirror, which must be dichroic to transmit the pump. The main drawback of this approach is the

bulk pumping system, bulk optical components and end-buttet fibre-mirror interface, which result in poor pump efficiency, consequently, a low slope efficiency. Furthermore, a mirror with dielectric coatings could be damaged by focused, high-power pump radiation. Modern fibre devices-fibre Bragg grating (FBG), which is fabricated by the transverse writing of feedback elements directly into the fibre core with UV radiation [45], provides a perfect solution to avoid pumping the light through dielectric mirrors. FBG is a reflective type of filter with a much narrower bandwidth than a dielectric mirror. In 1991, G. A. Ball [46] first utilized two FBG to form an Er-doped fibre laser. The FBG allow reflecting the laser light and transmitting the pump. It can be either spliced to the fibre ends or, when compatible with the fibre composition, written directly in the RE-doped fibre, which reduces the number of splices and hence the loss. The practical benefit of this configuration is that a fibre-pigtailed laser diode pump source can be spliced directly to the fibre laser, thereby reducing pump coupling loss. Such 'all-fibre' configuration is superior in terms of key laser parameters such as output power, line-width and stable tuning range, important for application in absorption spectroscopy based sensing.

## **2.4 Applications of Rare-earth-doped Fibre Lasers**

Lasers have become an integral part of daily life that many people may not realize how ubiquitous they are. Although fibre lasers are a relatively new type of laser, they have begun to compete for applications with many other types of lasers having active materials such as solid rods, gases or semiconductors. Many of these other lasers have reached a state of relative maturity. However, the applications of fibre lasers are still in a state of rapid development but already have become important in materials processing, communications, spectroscopy, medicine and military [47].

### **Manufacturing**

*Laser Welding:* The use of fibre lasers is effective in welding applications. Most of the welding applications of fibre lasers have involved Yb-doped fibres operating near 1  $\mu\text{m}$ ,

because these lasers can emit the highest values of power. Fibre lasers have been used in the conduction mode for welding razor blades, diaphragms for medical devices, cases for pacemakers and other thin samples. The power needed for such welding has usually been in the range of some hundreds of watts. Fibre lasers with multi-kilowatt output power have been used to make deeper welds in the penetration mode. Materials that have been welded with Yb-doped fibre lasers include stainless steel and other types of steel, titanium and aluminum alloys, and Inconel (a nickel alloy). Applications include butt welding titanium panels, conduction welding of diaphragms, full penetration welding of transmission gears and shaft assemblies and welding of thick steels. The reason that single-mode fibre lasers produce excellent results for welding when compared to other high power lasers is their excellent beam quality and ease of control and handling. This allows the beam to be focused to a very small spot size producing high irradiance at the target surface.

*Laser Material Removal - Drilling, Cutting and Marking:* The fibre laser cut relatively thin samples (1 - 2 mm) at speeds about 5 times faster than the carbon dioxide laser. For greater thickness (10 mm) the fibre laser cut about 1.3 times faster. These results indicated that fibre lasers are valid candidates for sheet metal cutting applications. Effective cutting with fibre lasers has also been demonstrated for non-metals, including plastics, acrylics, polycarbonate and leather. Practical examples of cutting with pulsed fibre lasers include cutting silicon wafers for solar panels and stencil cutting. High power multimode fibre lasers have been used for CW cutting of metals ranging from thin sheets to heavy plate for a variety of applications. The large depth of field and small spot size of fibre lasers lead to small kerfs and straight walls - even in thick metals. Common applications with high power multimode fibre lasers include cutting automotive body parts like hydroform tubes.

Lasers have found many applications in micromachining. They have been used for applications such as producing medical devices like stents, drilling holes for microvias in circuit boards, patterning of thin films and repair of semiconductor memories. The

properties that are needed for these applications include high peak power for rapid material removal, short pulse length (nanosecond regime) for vaporization without producing a large heat-affected zone, good beam quality for focusing to a small spot, and high pulse repetition rate for high volume production. Reasonably high average power is also desirable. Frequency-doubled or tripled Nd:YAG lasers have dominated these applications for many years. But fibre lasers have all the properties listed above and are now competing for these applications.

Marking by Q-switched fibre lasers with nanosecond pulse duration has been demonstrated for many materials, including glassy carbon, copper, silver, plastics and polymeric materials. The high values of peak power available are important for such marking. As an example of using fibre laser marking, a fibre laser with a beam scanning system included is being sold for applications in bar code marking of metal tools and parts and plastic components [47]. The 24" x 12" area covered by the scanning system can contain one large part for processing or could hold many smaller parts to treat simultaneously. The cost of this commercial system is claimed to be about 30% less than that of a Nd:YAG laser system with comparable capabilities.

Fibre lasers can also be used in the semiconductor processing industry, particularly for cutting and dicing silicon or other crystalline wafers on which integrated circuits have been fabricated. Cutting of silicon using a diamond saw has been common in the semiconductor industry. But diamond saws can cut only in straight lines and there can be problems with breakage. Other methods tend to be slow or expensive. The cutting of silicon wafers can be accomplished with 200 watts of CW power from a 1  $\mu\text{m}$  wavelength fibre laser.

### **Telecommunication**

Laser based fibre telecommunications systems using fibre optic links have been in widespread use since the 1970s. The laser source has most often been a semiconductor laser diode. Now the fibre laser offers an alternative choice that has advantages. For Instance:

- Erbium-doped fibres emit at a wavelength near 1.55  $\mu\text{m}$ , the wavelength which is most favourable for well-developed glass transmission fibres. Such fibres have the lowest loss near that wavelength. Thus the erbium-doped fibre lasers have a very desirable wavelength.
- The emission from a fibre laser comes out of a fibre, so it is relatively easy to couple the light into a fibre for long distance transmission. It is simple to join the laser fibre and the transmission fibre by fusion coupling. This is in contrast to the use of semiconductor diode lasers as sources, from which the light is emitted over a broader angle and which is more difficult to couple into a fibre.
- For communication applications, a passively Q-switched fibre laser offers high pulse repetition rates, up to at least 100 MHz. This is compatible with high data transmission rates.
- Fibre lasers are very reliable and maintenance free. With all these advantages, fibre lasers are becoming popular in the telecommunications industry and their use will continue to grow

### **Spectroscopy**

Fibre lasers have been used in a variety of scientific investigations involving spectroscopic studies of atoms and molecules and more macroscopic objects including solids, liquids and gases. Fibre lasers offer many advantages, including small size, portability, low maintenance and reliability. Tuneable titanium-doped sapphire lasers have been widely used for laser spectroscopy, but because of the same advantages mentioned for telecommunications, fibre lasers are becoming popular alternatives. This popularity in spectroscopy has spawned from the fibre lasers ability to generate very short pulse lengths in the femtosecond range that allows for high speed studies of the dynamics of atoms and molecules.

### **Medicine and Surgery**

Fibre lasers have a variety of applications in the medical field, including marking and

manufacturing of medical devices and direct irradiation of the body for diagnosis or treatment.

*Fractional Resurfacing:* An erbium-doped fibre laser emitting infrared radiation at 1.55  $\mu\text{m}$  is useful for treating age spots, freckles, wrinkles and acne scars. Tiny spots are heat treated by the laser. In the treated areas the old skin is replaced by new, healthy tissue. The laser radiation is delivered through a specially designed scanner to the skin which is to be resurfaced.

*Marking Implants:* Medical implants must be clearly marked for both tracking and identification. Methods like using ink or dye are unsuitable to mark these devices because they may cause contamination or allergic reaction. Lasers are used to create permanent, contaminant-free marks. There is no distortion to the surface. Fibre lasers with a beam that can be focused to a very small spot size accurately engrave characters as small as 0.3 mm. Fibre lasers can be used to inscribe areas which could not be marked by other methods. The fibre lasers that have been used in medical marking have been Q-switched Yb-doped devices emitting laser radiation at a wavelength near 1  $\mu\text{m}$ . Typically these lasers operate at 1mJ with a pulse repetition rate of 20 kHz and pulse duration around 400 ns.

*Microsurgery:* Fibre lasers are being considered for use in microsurgery. For such potential applications they offer advantages such as lower cost, low maintenance, high efficiency and compactness. As compared to other lasers they do not need an additional delivery fibre. In one experimental study researchers used a 110 watt Tm-doped fibre laser to vaporize prostate tissue. Another group of researchers is using Yb, Er and Tm-doped fibre lasers for studies of soft tissue surgery in the areas of urology, dermatology and ophthalmology.

## **Military**

*Ranging:* Fibre lasers, which are compact and portable, can emit femtosecond duration pulses with very high peak power. As a result, fibre lasers are now being seriously considered as replacements for the military's current ranging systems.

*Remote sensing:* Thulium-doped fibre lasers have been developed for remote gas sensing. Thulium-doped fibre lasers operate at wavelengths in the 1.8 to 2.2  $\mu\text{m}$  region. This wavelength region contains spectral absorption lines for many gases of interest, both for military applications and for industrial emission monitoring. In one application, the laser beam is transmitted to a fixed reflecting target and the strength of the reflected return signal is monitored. The laser is tuned over a spectral range containing absorption lines of the gases of interest. A reduction in the return signal at a specific wavelength can identify the presence of a given gas and its concentration.

## **Security**

Fibre lasers have been studied for their ability to detect and locate disturbances over long paths. This can provide enhanced security for military installations or for homeland security applications. The laser, operating CW, was frequency modulated and part of the output sent via fibre to a nearby fixed reflector. The reflected return serves as a local oscillator. The rest of the laser light is sent through a long fibre which acts as the sensing element and is deployed over the area to be monitored. The light reflected from the sensing fibre and the light from the local oscillator are mixed and generate a beat frequency. The beat frequency is proportional to the difference in time delay between the two signals.

## **2.5 Summary**

Lasers have become important devices for variety of applications. Particularly, laser in the 2  $\mu\text{m}$  spectral region is proved to be very effective for gas detection, long-range LIDAR, free-space optical communication, medical diagnostics, laser surgery and optical

pumping of longer wavelength solid-state lasers. Rare-earth-doped materials are effective to be used as a gain medium in laser resonator for emission in the wavelength range of UV-Vis-IR. Fibre lasers offer significant advantages like compactness, low maintenance and efficiency over traditionally used semiconductor or bulk glass lasers in the said spectral region. Emission near 2  $\mu\text{m}$  from trivalent Thulium generates unique opportunity to build Thulium-doped fibre laser. Silica glass with suitable network modifier is good host for Thulium in terms of chemical durability, stability and compatibility with standard telecommunication optical fibre. Thulium-doped silica fibre can be fabricated through MCVD, OVD or VAD technique and in an intermediate step RE ions can be incorporated into the preform core using one of the following routes: vapour delivery process, solution doping process and sol-gel process. An 'all-fibre' laser has the advantage of being more robust than many other systems, as well as showing a low loss, making it more rugged and reliable for installation and thereby reducing maintenance needs.

## References

- [1] <http://www.eps.org/news/106324/>
- [2] C K Kao 'Sand from Centuries Past: Send Future Voices Fast' Nobel Lecture 2009  
[http://www.nobelprize.org/nobel\\_prizes/physics/lectures/2009/kao\\_lecture.pdf](http://www.nobelprize.org/nobel_prizes/physics/lectures/2009/kao_lecture.pdf)
- [3] H H Maiman 'Stimulated optical radiation in ruby' Nature, Vol. 187, pp.493 (1960)
- [4] S A Diddams, L Hollberg and V Mbele 'Molecular fingerprinting with the resolved modes of a femtosecond laser frequency comb', Nature, Vol. 445, pp. 627-630 (2007)
- [5] M J Thorpe, D Balslev-Clausen, M S Kirchner and J Ye 'Cavity-enhanced optical frequency comb spectroscopy: application to human breath analysis', Optics Express, Vol. 16, pp. 2387–2397 (2008)
- [6] A Schliesser, N Picqué and T W Hänsch 'Mid-infrared frequency combs', Nature Photonics, Vol. 6, pp. 440-449 (2012)

- [7] F K Tittel, D Richter and A Fried 'Mid-Infrared Laser Applications in Spectroscopy', Solid-State Mid-Infrared Laser Sources, edited by I T Sorokina and K L Vodopyanov, Berlin, Springer, 2003, pp. 445-516
- [8] B Ropoulos 'Medical lasers: new wavelengths, new designs enhance cost effectiveness', Photon. Spectra, June, pp.116–120 (1996)
- [9] J G Manni 'High powered delivery: fiber optic laser surgery', Optics and Photonics News, July, pp. 23–28 (1996)
- [10] J G Manni 'Solid-state lasers in medicine today', Lasers Optronics, April, pp. 17–20 (1992)
- [11] L Esterowitz 'Diode-pumped holmium, thulium, and erbium lasers between 2 and 3  $\mu\text{m}$  operating at room temperature', Optical Engineering, Vol. 29, pp.676-680 (1990)
- [12] R C Stoeman and L Esterowitz 'Efficient, broadly tunable, laser-pumped Tm:YAG and Tm:YSGG CW lasers', Optics Letters, Vol. 15, 486-488 (1980)
- [13] S W Henderson, P J M Suni, C P Hale, S M Hannon, J R Magee, D L Bruns and E H Yuen 'Coherent laser radar at 2  $\mu\text{m}$  using solid-state lasers', IEEE Transactions on geoscience and remote sensing, Vol. 31, pp. 4-15 (1993)
- [14] K Miazato, D F De sousa, A Delben, J R. Delben, S L de Oliveira and L A Nunes 'Upconversion mechanisms in Tm<sup>3+</sup> doped lead fluoroindogallate glasses', Journal of non-crystalline solids, Vol. 273, pp. 246-251 (2000)
- [15] M Storm 'Coherent 2  $\mu\text{m}$  sources burst into wind-shear detection,' Laser Focus World, pp. 117–122 (1991)
- [16] R Targ, B C Steakley, J G Hawley, L L Ames, P Forney, D Swanson, R Stone, R G Otto, V Zarifis, P Brockman, R S Calloway, S H Klein and P Robinson 'Coherent lidar airborne wind sensor II: Flight-Test results at 2 and 10  $\mu\text{m}$ ', Applied Optics, Vol. 35, pp.7117–7127 (1996)
- [17] D Theisen, V Ott, H W Bernd, V Danicke, R Keller and R. Brinkmann 'CW high-power IR-laser at 2  $\mu\text{m}$  for minimally invasive surgery', in Proc. SPIE, Vol. 5142, pp. 96–100 (2003)

- [18] R C Stoneman and L Esterowitz ‘Efficient, broadly tunable, laser-pumped Tm-YAG and Tm-YSGG CW lasers’, *Optics Letters*, Vol. 29, pp. 486–488 (1990)
- [19] P A Budni, L A Pomeranz, M L Lemons, C A Miller, J R Mosto and E P Chicklis, ‘Efficient midinfrared laser using 1.9  $\mu\text{m}$ -pumped Ho:YAG and ZnGeP optical parametric oscillators’, *Journal of Optical Society of America B*, Vol. 17, pp. 723–728 (2000)
- [20] P C Becker, N A Olsson and J R Simpson ‘Erbium-Doped Fiber Amplifiers: Fundamentals and Technology (Optics and Photonics)’, Academic Press; 1st edition (1999)
- [21] E Desurvire ‘Erbium-Doped Fiber Amplifiers, 2 Volume Set (Wiley Series in Telecommunications and Signal Processing)’ Wiley-Interscience; 2<sup>nd</sup> edition (2002)
- [22] G Liu and B Jacquier ‘Spectroscopic Properties of Rare Earths in Optical Materials’, (Springer Series in Materials Science) Springer; 2005 edition (2005)
- [23] C Y Chen, R R Petrin, D C Yeh, W A Sibley and J L Adam ‘Concentration-dependent energy-transfer processes in  $\text{Er}^{3+}$ - and  $\text{Tm}^{3+}$ -doped heavy-metal fluoride glass’, *Optics Letters*, Vol.14, pp. 432 (1989)
- [24] M Naftaly, S Shen and A Jha ‘ $\text{Tm}^{3+}$ -doped tellurite glass for a broadband amplifier at 1.47  $\mu\text{m}$ ’, *Applied Optics*, Vol. 39, pp. 4979 (2000)
- [25] S Q Xu, Z M Yang, G N Wang, S X Dai, J J Zhang, L L Hu and Z H Jiang ‘Spectroscopic properties and Judd-Ofelt theory analysis of  $\text{Er}^{3+}$ -doped heavy metal oxyfluoride silicate glass’, *Journal of Rare Earths*, Vol. 22, pp. 375 (2004)
- [26] A Mendez and T F Morse ‘Specialty Optical Fibers Handbook: Chapter 7.4 Fabrication of Rare Earth-Doped Fibers’, Academic Press (2006)
- [27] E Snitzer ‘Proposed Fiber cavities for optical masers’, *Journal of Applied Physics* , Vol. 32, pp. 36-39 (1961)
- [28] J Stone, C A Burus ‘Neodymium-doped silica lasers in end-pumped fiber geometry’, *Applied Physics Letters*, Vol. 23, pp. 388-389 (1973)
- [29] M J F Digonnet, C J Gaeta, H J Shaw ‘1.064 and 1.32  $\mu\text{m}$  Nd:YAG single crystal fiber lasers’, *Journal of Lightwave Technology*, Vol. 4, pp. 454-460 (1986)

- [30] M C Ferries, P R Morkel, J E Townsend ‘Sumarium<sup>3+</sup> doped glass laser operating at 651 nm’, *Electronics Letters*, Vol. 24, pp. 709-711 (1988)
- [31] C Ghisler, W Lüthy, H P Weber, J Morel, A Woodtli, R Dändliker, V Neuman, H Berthou, G Kotrotsios ‘A Tm<sup>3+</sup> sensitized Ho<sup>3+</sup> silica fibre laser at 2.04  $\mu\text{m}$  pumped at 809 nm’, *Optics Communication*, Vol. 109, pp. 279-281 (1994)
- [32] R J Mears, L Reekie, S B Poole and D N Payne ‘Neodymium-doped silica single-mode fibre lasers’, *Electronics Letters*, Vol. 21, pp. 738-740 (1985)
- [33] R Wyatt, B J Ainslie, S P Craig ‘Efficient operation of array-pumped Er<sup>3+</sup> doped silica fibre laser at 1.5  $\mu\text{m}$ ’, *Electronics Letters*, Vol. 24, pp.1362–1363 (1988)
- [34] D C Hanna, I M Jauncey, R M Percival, I R Perry, R G Smart, P J Suni, J E Townsend and A C Tropper ‘Continuous-wave oscillation of a monomode thulium-doped fibre laser’, *Electronics Letters*, Vol. 24, pp.1222 – 1223 (1988)
- [35] R M Percival, D Szebesta and S T Davey ‘Highly efficient and tunable operation of two colour Tm-doped fluoride fibre laser’, *Electronics Letters*, Vol. 28, pp.671-673 (1992)
- [36] J R Lincoln, C J Mackechnie, J Wang, W S Brocklesby, R S Deol, A Pearson, D C Hanna, D N Payne ‘New class of fibre laser based on lead-germanate glass’ *Electronics Letters*, Vol. 28, pp.1021-1022 (1992)
- [37] R L Shubochkin, V A Kozlov, A L G Carter, T F Morse ‘Tunable thulium-doped all-fiber laser’, *IEEE Photonics Technology Letters*, Vol. 10, pp. 944-945 (1998)
- [38] T Yamamoto, Y Miyajima, T Komukai ‘1.9- $\mu\text{m}$  Tm-doped silica fiber laser pumped at 1.57- $\mu\text{m}$ ’, *Electronics Letters*, Vol. 30, pp. 220-221 (1994)
- [39] R M Percival, D Szebesta, C P Seltzer, S D Perrin, S T Davey, M Louka ‘1.6  $\mu\text{m}$  semiconductor diode pumped thulium doped fluoride fibre laser and amplifier of very high efficiency’, *Electronics Letters*, Vol. 29, 1993, p. 2110 – 2112 (1993)
- [40] T Yamamoto, Y Miyajima, T Komukai and T Sugawa ‘1.9  $\mu\text{m}$  Tm-doped fluoride fibre amplifier and laser pumped at 1.58  $\mu\text{m}$ ’, *Electronics Letters*, Vol. 29, pp. 986-987 (1993)
- [41] K Arai, H Namikawa, K Kumata, T Honda, Y Ishii and T Handa ‘Aluminum or phosphorus co-doping effects on the fluorescence and structural properties of

- neodymium doped silica glass' Journal of Applied Physics, Vol. 59, pp. 3430-3437 (1986)
- [42] M Shimizu, H Suda and M Horiguchi 'High efficiency Nd-doped fibre lasers using direct coated dielectric mirrors', Electronics Letters, Vol. 23, pp. 768-769 (1987)
- [43] Y Chaoyu, P Jiangde and Z Bingkun 'Tunable Nd<sup>3+</sup> doped fiber ring resonator', Electronics Letters, Vol. 25, pp.101-102 (1989)
- [44] P Barnsley, P Urquhart, C Millar and M Brierley 'Fiber Fox-Smith resonators: application to single-longitudinal-mode operation of fiber lasers', Journal of Optical Society of America. A, Vol. 5, pp. 1339-1346 (1988)
- [45] R Kashyap 'Fiber Bragg Gratings', Academic Press; 2 edition (November 18, 2009)
- [46] G A Ball, W W Morey and W H Glenn 'Standing-wave monomode erbium fiber laser' IEEE Photonics Technology Letters, Vol.3 613-615 (1991)
- [47] K Thyagarajan and A Ajoy 'Lasers: Fundamentals and Applications' Springer (2010)

# Chapter 3

## Fabrication of Thulium- and Thulium/Ytterbium-doped Optical Fibres

*Abstract: In this chapter both Thulium- and Thulium/Ytterbium-doped single-mode single-clad silica optical fibres are designed and fabricated for a systematic analysis before being used as laser gain media for the development of fibre lasers at 2  $\mu\text{m}$  wavelength region. The optical preforms are fabricated by using the modified chemical vapour deposition technique coupled with solution doping to enable the incorporation of rare-earth into the core of the preforms. As a result a set of optical fibres having different host compositions, Thulium-ion concentrations and proportions of Ytterbium to Thulium is fabricated successfully to allow further evaluation and cross-comparison. This effort is aimed to identify the most suitable fibre for the fibre laser configuration with improved lasing efficiency through an appropriate control and optimization of the preform fabrication process both in terms of host composition and dopant concentration in order to achieve enhanced process reproducibility. The waveguide and transmission properties of these Thulium- and Thulium/Ytterbium-doped optical fibres are characterized for further spectroscopic analysis and design of fibre lasers.*

### 3.1 Introduction

The fundamental difference between traditional solid-state lasers and fibre lasers lies in the form of the gain medium, with the former being bulk crystals/glasses in rod or slab geometries and the latter with active ions being doped into the core of a length of an optical fibre. The rare-earth (RE) elements such as Erbium (Er), Neodymium (Nd),

Ytterbium (Yb), Samarium (Sm), Holmium (Ho) and Thulium (Tm) can be doped into the core of such fibres to act as the active medium for the fibre laser, thus producing wide range of wavelengths ranging from visible to near-infrared (NIR) [1]. The broad emission spectrum of  $\text{Tm}^{3+}$  in the range of 1.7  $\mu\text{m}$  to 2.1  $\mu\text{m}$  makes it a prominent candidate for the development of a fibre laser in the 2  $\mu\text{m}$  wavelength region [2]. Pure silica is generally less preferred to non-oxide glasses as a host for REs due to (a) rigid structure resulting in low solubility of REs and (b) high phonon energy ( $E_p \sim 1100 \text{ cm}^{-1}$ ) leading to reduced quantum efficiency [2]. As a result, spectroscopic properties and laser/amplifier performance of Tm-doped fibres with different hosts, such as fluoride, telluride, tellurite, germanate, aluminate and phosphate glass fibre were studied extensively over the last decade [3-9]. However, these Tm-doped glass fibres have shown limited potential for practical implementation and applications largely due to their host material instability, low pump power damage threshold, complex fabrication process and less compatibility with silica fibre based systems. This leads to the further development of modified Tm-doped silica fibres and local modification of the Tm-ion environment by co-doping the fibre core with oxides of Bismuth (Bi) and Gallium (Ga) or Germanium (Ge) [10-12]. In doing so significant improvement in solubility of REs in silica glass can be achieved by incorporating network modifiers such as Aluminium (Al) and Phosphorus (P) [13-14]. Thus modified silica glass offers advantages over the other host materials for the incorporation of Tm- ions in terms of high mechanical strength, chemical durability, high threshold for optical damage ensuring a low tendency for laser-induced breakdown, non-hygroscopic property, fabrication with standard and mature technology and overall compatibility with existing optical fibre systems [15].

This work focuses on the fabrication of Tm-doped silica optical fibres with modified host composition and suitable dopant concentration effective for laser development. Co-doping of Yb is explored to investigate the energy-transfer mechanism from Yb to Tm and thereby opening up the opportunity of using economic pump laser diodes emitting at around 0.98  $\mu\text{m}$ . The specialty Tm- and Tm/Yb-doped fibres were fabricated at CSIR-CGCRI by using modified chemical vapour deposition (MCVD) technique, coupled with

solution doping of REs in the core glass. The objective of this chapter is to determine and optimize the key process parameters by using the MCVD-solution doping technique to enable the fabrication of Tm- and Tm/Yb-doped fibres, with required host composition, dopant concentration as well as their proportion, to obtain improved fibre properties and enhanced process reproducibility. Basic fibre parameters are characterized for further spectroscopic analysis and design of laser resonator.

## **3.2 Fabrication Process**

Optical fibre fabrication process involves realisation of a glass composition with an appropriate core-clad guiding structure, through the production of an intermediate, called preform, which has the same structure of the final optical fibre. The preforms are heated and softened in a furnace then pulled into a thin filament to produce the optical fibre [16]. Laboratories around the world are in continuous effort to develop improved fabrication technology with refined process parameters. Efficient fabrication of fibres requires a standard and optimized process with good repeatability which generally varies with chosen process and differs from machine to machine. There have been a number of different preform fabrication processes which includes Outside Vapor Deposition (OVD, invented by Corning Glass Works) [17], Vapor phase Axial Deposition (VAD, invented by NTT Corp. Japan) [18], Modified Chemical Vapor Deposition (MCVD, invented by AT&T Bell lab) [19] and Plasma Chemical Vapor Deposition (PCVD, invented by Philips Research Ltd) [20]. MCVD is considered as one of the most versatile and flexible processes for fabrication of specialty optical fibre preform [21-22].

### **3.2.1 MCVD process**

MCVD process developed at Bell Labs in 1974 has been widely used to fabricate competitive telecommunication optical fibres as well as specialty optical fibres. Though the process of deposition in MCVD is not very efficient (70% for silica and 10-20% for Germania), and the deposition rates are very low (~5 g/min), the MCVD technique has been widely used by most of the research laboratories, due to the great versatility of this

method especially for manufacturing specialty optical fibre [23]. The primary advantage of this technique is that it involves the process of inside vapour phase oxidation (IVPO) of starting materials and this avoids both unwanted atmospheric contaminant and restricts the incorporation of OH in deposited glass from burner, compared to the outside vapour phase oxidation (OVPO) process. Additionally, precise control in waveguide design and composition is possible through the control of gas flow and temperature instead of optimizing complex burner design and burner distance essential for OVD process. In order to utilize solution doping technique for RE incorporation inside the core of the preforms, precise control of porous core layer structure is also possible and this leads to the control of RE concentration and distribution inside fibres.

In MCVD process, the reactant halide precursors along with oxidizing and inert gasses are flown in a controlled quantity by Mass Flow Controllers (MFCs) through a high purity rotating silica tube or substrate tube which is externally heated by an oxy-hydrogen burner, moving in the direction of gas flow and oxidised in proximity of the heated zone. Sub-micrometer soot particles are produced as a result of high temperature oxidation of reactant halide and deposited downstream of the hot zone according to thermophoretic mechanism [24]. Burner movement causes the hot zone to be shifted into the zones where silica has been deposited as soot by thermophoresis: the deposited particle gets consolidated to clear glass layer by subsequent cooling. At the end of each cycle, the burner returns quickly to its initial position to initiate another layer of glass deposition. The required amount of carrier gas flowing through the halide precursor in order to obtain desired soot composition can be estimated by Equation 3.1.

$$Q_i = \frac{(P_i \times P)}{(P - P_i)} \times \frac{V \times \eta_i}{R \times T}; \quad i = \text{specific halide precursor} \quad (3.1)$$

where  $Q_i$  = flow of a material as a function of O<sub>2</sub> flow mole/min

$P$  = 760 torr

$P_i$  = Vapour pressure of halide

$R$  = Universal gas constant (0.082 lit atm mol<sup>-1</sup> K<sup>-1</sup>)

$V$  = Standard litres per minute

$\eta_i$  = Evaporation efficiency

$T$  = Bubbler temperature in Kelvin

Both the composition of the input gas mixture and the fabrication process conditions are required to be altered to produce different types of glass layers thus to manufacture different types of fibres. After the completion of the glass deposition process, a collapse phase is started: the internal hole of tube is progressively reduced by successive slower burner passes (typically 5-10 passes) at a temperature more than 2050°C, due to the action of surface tension when the high temperature lowers the viscosity of the glass, until a solid cylindrical rod is produced, with a refractive index profile corresponding to the final optical fibre profile.

### **3.2.2 Solution doping technique**

Doping of RE inside a preform core is not possible through conventional MCVD process due to the low vapour pressure of the RE precursors at room temperature. Solution doping method [25], sol-gel process [26] and direct nano-particle deposition (DND) [27] have been developed to overcome this problem and have been successfully implemented for fabrication of RE-doped preforms/fibres. Additionally, there exists different vapour phase delivery techniques namely heated frit source delivery [28], heated source delivery [29], heated source injector delivery [30], aerosol delivery [31], chelate delivery [32] method which require relatively complex set-ups and have not yet been standardized for commercial production of RE-doped optical fibre. MCVD-solution doping process owing to its process simplicity and low implementation cost has been well accepted since its invention in 1987 [22].

MCVD process coupled with solution doping technique comprises of two major steps, namely

- I. deposition of porous core layer within a silica tube by using the MCVD process
- II. soaking of the porous deposit in a solution containing salts of RE (or combination of REs) and a co-dopant, mostly Al

It is essential to optimize and control the deposition temperature based on the selected vapour phase composition in order to achieve uniform soot porosity [33-34]. Through a careful selection of solution composition, it is also possible to control the material properties such as viscosity, surface tension etc. and for adjusting dopant incorporation levels [35-36]. Soaked RE- and Al-salts are usually oxidized prior to dehydration in the presence of chlorine ( $\text{Cl}_2$ ) to eliminate the OH-ion, adsorbed in the soot during solution doping. The dehydration temperature is optimized in between 800-1200°C for a fixed time span based on the thickness of the porous soot layer. Stepwise sintering process is carried out through the gradual increment of burner temperature to avoid formation of imperfections within the sintered RE-doped core glass. The tube containing the RE-doped core layer is finally collapsed to produce the preform employing soft-collapsing process to avoid loss of RE and Al-oxides from the core, particularly from the innermost region, as well as formation of central dip in the core.

### **3.3 Experimental Work**

Tm- and Tm/Yb-doped optical preforms have been fabricated by using MCVD and solution doping techniques. Although this process is widely used for routine production of commercial fibre by many fibre manufacturers, it still suffers from problems such as poor control over RE incorporation and repeatability. Judicious selection of starting raw materials and optimization of process parameters as well as conditions are important for fabrication of fibres with desired properties. The experiments discussed in the following sections are designed to investigate into these key process parameters in a systematic way.

#### **3.3.1 MCVD set-up used**

A typical MCVD setup consists of a glass working lathe, vapour delivery and control systems together with some supporting equipments. Fig. 3.1 shows the schematic of the MCVD system used at CSIR-CGCRI in India.

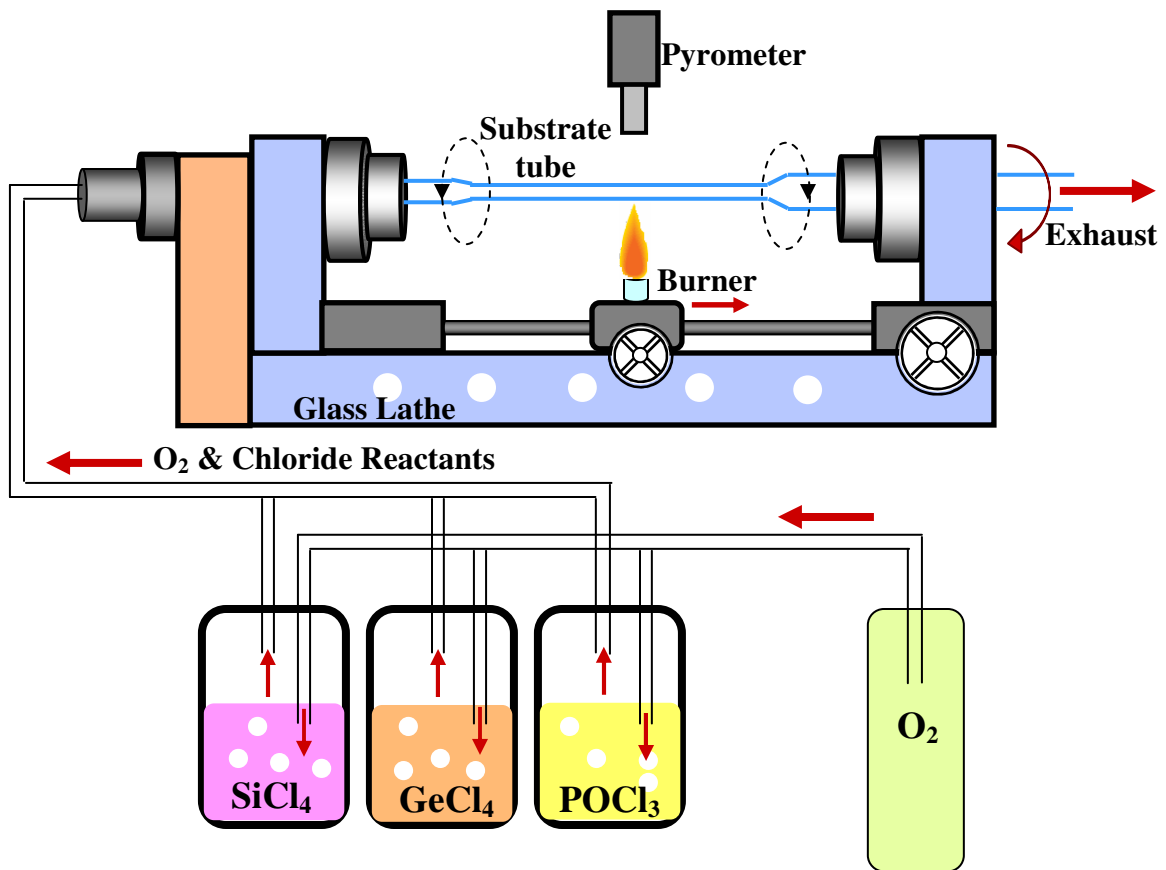


Fig. 3.1 Schematic diagram of the MCVD setup at CSIR-CGCRI, India

The glass working lathe (Litton, USA), comprising two synchronous chucks with three gripping jaws, is capable of processing long tubes with lengths up to one meter. A quartz oxy-hydrogen burner is fixed on the lathe bed and its 'to and fro' motion is controlled by a microprocessor controller. The burner temperature can be well adjusted by changing the flow of H<sub>2</sub>-O<sub>2</sub> gas, which is supplied through two separate mass flow controllers (MFCs) with capacity of 0-200 lit and 0-100 lit respectively. An infrared (IR) pyrometer (Williamson Corporation, USA) with temperature range of 800-2500°C is attached to the lathe which is also moving synchronously with the burner to monitor the hot zone temperature of the rotating silica tube during the preform fabrication process. A continuous flow of Nitrogen (N<sub>2</sub>) is maintained through this pyrometer to keep it cool. The bubbler chamber consists of three pyrex glass bubblers with various capacities

ranging from 1-2 liter containing liquid halide precursors of Silicon, Germanium and Phosphorous. The bubblers are immersed in an oil bath to maintain constant temperature in the range of 15-30°C resulting in a consistent vapour flow during fabrication. Each bubbler has input line for the carrier gas connected through check valves and MFCs for precise control. The outlet is connected to either vent or run manifold. The outlet of the run manifold is connected to the rotating silica tube mounted in a lathe through a separate rotary seal for supply of the input gas mixture. The flow rates of different carrier gases are controlled according to a pre-calculated program and controlled through the MFCs. High purity O<sub>2</sub> (99.9998%) used as the carrier gas for the halide precursors (SiCl<sub>4</sub>, GeCl<sub>4</sub>, POCl<sub>3</sub>) is dried further by passing through special driers (Aeronox, USA) to maintain the moisture below ppb level. The moisture level in the gas is monitored through a sensor unit attached to the MCVD control panel. The effluent gases from the collecting tubes are fed to the scrubber to absorb the effluent gasses. An air exhaust blower is placed just above the glass working lathe which helps to remove the hot air and fine particles produced during processing of preforms.

### **3.3.2 Fabrication of Thulium and Thulium/Ytterbium-doped preforms**

Fabrication of Tm- and Tm/Yb-doped optical preforms using MCVD coupled with solution doping technique involves the following procedures below and shown in Fig.3.2.

1. Deposition
2. Solution doping
3. Consolidating and collapsing

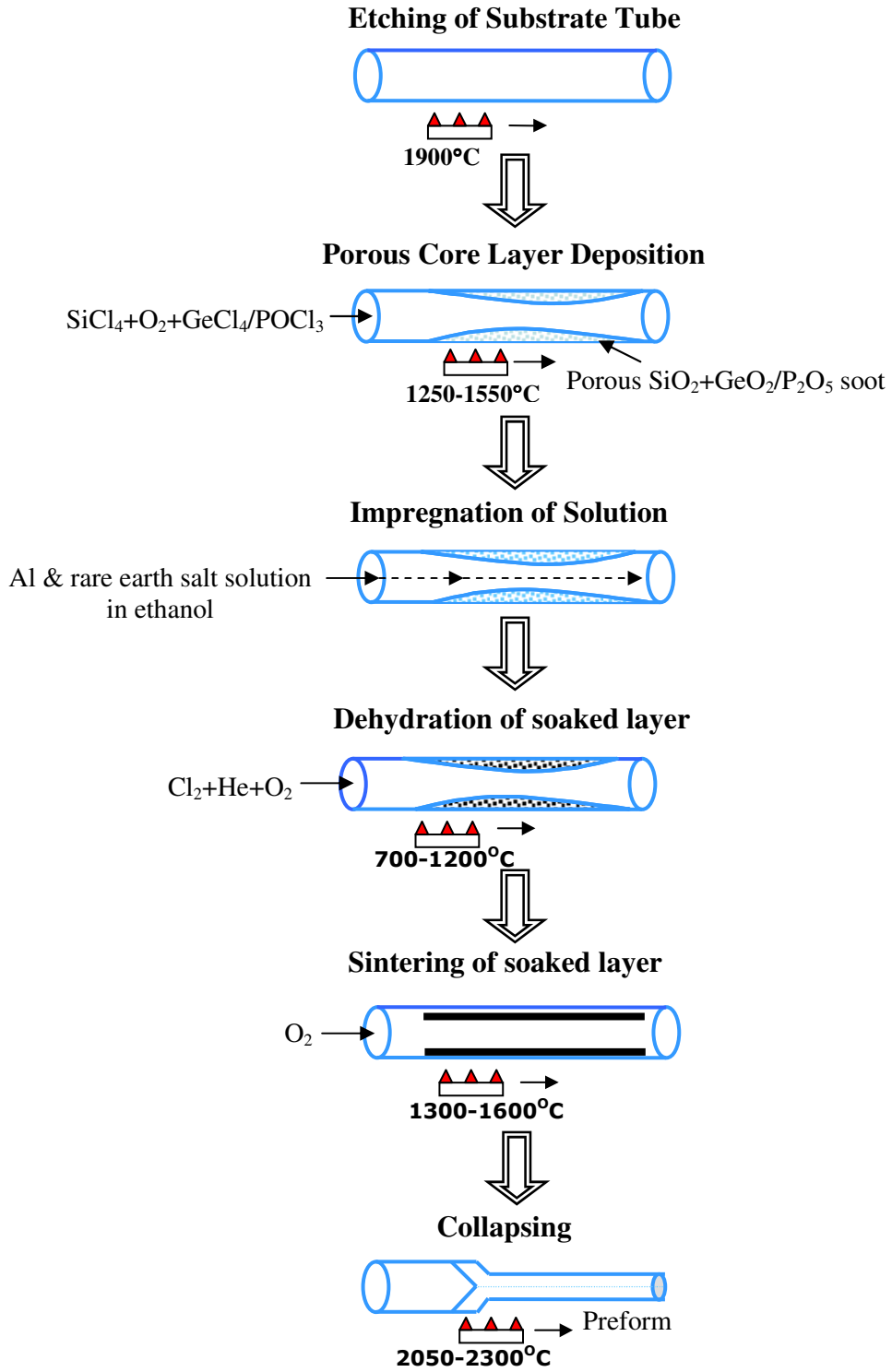


Fig. 3.2 Schematic diagram of MCVD process coupled with solution doping technique

### 3.3.2.1 Deposition

The deposition process started with etching of the inner surface of a substrate tube having outer diameter of 20 mm and wall thickness of 1.5 mm using a mixture of O<sub>2</sub> and freon (CCl<sub>2</sub>F<sub>2</sub>) at a temperature around 1900°C in order to remove impurities. In the next step, about three to five layers of pure silica sintered cladding were deposited on the inner surface of the tube at around 1850°C. Finally unsintered core layer of SiO<sub>2</sub> was deposited in the form of porous structure to allow absorption of Al, Tm and Tm/Yb into the core layer during the solution doping stage. In order to incorporate Germanium (Ge) and P oxide in the core to increase the refractive index of the core layers and to modify the host composition for Tm and Yb, a mixture of SiCl<sub>4</sub> and GeCl<sub>4</sub>/POCl<sub>3</sub> was used to deposit oxide soot layers (in porous form) inside the tube. Proper care was taken to maintain the variation of deposition temperature within  $\pm 5^\circ\text{C}$  and this was monitored by the IR pyrometer, synchronously moving with the burner in a forward direction at a speed of 125 mm/min. A total flow of 1 litre/min was maintained during deposition while all the bubbler temperatures were kept at 25°C. In the context of the present work, it was critical to maintain desired porosity over the entire core area and along the length of the preform to obtain uniform incorporation of REs and the other dopants. Thus a suitable reaction temperature is required for a selected vapour phase flow rate during the deposition of core layers with different types of soot composition. Corresponding optimization was carried out for different soot compositions: temperature in the range of  $1560\pm 20^\circ\text{C}$  for pure SiO<sub>2</sub> soot,  $1290\pm 20^\circ\text{C}$  for GeO<sub>2</sub>-doped soot and  $1100\pm 10^\circ\text{C}$  for P<sub>2</sub>O<sub>5</sub>-doped soot layer were found to be optimum to achieve similar porosity. The slight variation in porosity at the optimum deposition temperature for different soot composition is usually caused by the change in glass viscosity. Higher deposition temperature results in partial sintering of soot layers leading to inhomogeneous impregnation of solution. Since Phosphorous reduces viscosity in a greater extent, P<sub>2</sub>O<sub>5</sub> doped soot requires a lower deposition temperature compared to that of GeO<sub>2</sub>-doped soot which in turn requires a lower temperature than that of pure silica soot. The deposited core layers are porous in nature with white appearance. The soot structure morphology was studied through

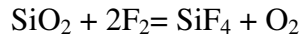
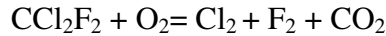
scanning electron microscope (SEM) analysis. Optimized deposition parameters are listed in Table 3.1.

Table 3.1 Standardized parameters during porous core layer deposition

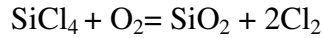
	Host/Soot composition		
	Pure SiO <sub>2</sub>	GeO <sub>2</sub> -doped SiO <sub>2</sub>	P <sub>2</sub> O <sub>5</sub> -doped SiO <sub>2</sub>
<b>Deposition temperature</b>	1560±20°C	1290±20°C	1100±10°C
<b>Vapour phase flow rate</b>	40 sccm SiCl <sub>4</sub>	40 sccm SiCl <sub>4</sub> 340 sccm GeCl <sub>4</sub>	40 sccm SiCl <sub>4</sub> 245 sccm POCl <sub>3</sub>

The chemical reactions involved in the deposition stage are:

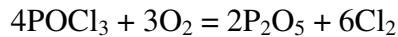
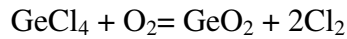
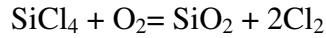
**Etching:**



**Cladding layer deposition:**



**Core layer deposition:**



### 3.3.2.2 Solution doping

Once the cladding and porous core layers were deposited, the substrate tube with the deposit was removed from glass working lathe and soaked with ethanol solution containing the required amount of precursor salts of Al, REs (Tm as well as combination of Tm and Yb). Suitable amount of Al(NO<sub>3</sub>)<sub>3</sub>·9H<sub>2</sub>O (99.9995%, Alfa Aesar, Germany), TmCl<sub>3</sub>·6H<sub>2</sub>O (99.99%, Alfa Aesar, Germany) and YbCl<sub>3</sub>·6H<sub>2</sub>O (99.99%, Alfa Aesar, Germany) were utilized to obtain Tm concentration in the range of 0.01-0.4 mol% and proportion of Yb:Tm in the range of 1-13 in the preform core glass. In order to achieve a

number of preforms with different Yb:Tm ratio, the concentration of YbCl<sub>3</sub> salt was varied from 0.0075 to 0.15 (M) while for TmCl<sub>3</sub> the variation was from 0.008 to 0.04 (M). Addition of Al works as network modifier through breaking up the rigid silica structure thereby improving RE solubility. Thus the incorporation of high level of REs is possible without causing clustering effect. The concentration of Al was adjusted according to the selected Tm and Tm/Yb concentrations. Thus Al(NO<sub>3</sub>)<sub>3</sub> concentration was varied in the range of 0.3 to 1.25 (M) in different soaking solutions to maintain the suitable Al dopant level in the soot structure. Al also acts to increase the refractive index of the core and reduces the phonon energy of silica glass resulting in the increase of fluorescent lifetime of Tm at different energy levels. The soaking period was maintained in the range of 30 min to 60 min for precise control of dopant level within the preform core.

After the absorption of solution by the soot layer, the remaining solution was carefully drained out of the substrate tube. The doped deposit was then rigorously dried by passing inert gases such as Argon (Ar) or N<sub>2</sub> to remove any remaining solvent. This is a necessary procedure in the solution doping process as incomplete drying can result in the formation of air bubbles during the consolidation stage and increase in OH level in the preform.

### **3.3.2.3 Consolidating and collapsing**

The tube containing doped soot layers was remounted on to the lathe for further processing. The first step was oxidation followed by dehydration for one hour in presence of O<sub>2</sub>/He/Cl<sub>2</sub> gas mixture. Both the oxidation and dehydration temperatures were optimized to avoid unwanted phase separation within preform core region and evaporation of dopants, specially Tm-ion. Thus oxidation temperature was fixed to 900°C while dehydration temperature was adjusted to around 800 to 850°C. At a higher dehydration temperature, strong red vaporization from soot surface was observed resulting in a significant reduction of Tm-ion concentration in preform. The dehydration step was also standardized to reduce the OH level to the maximum extent. The tube was

then heated gradually from 1200°C to 1850°C in the presence of O<sub>2</sub> to sinter the core layers to form a transparent. The increment of temperature was controlled stepwise in order to avoid phase-separation of Al-rich glass and to ensure better homogeneity in glass structure thus minimizing scattering loss of the fibre. The substrate tube was then heated further stepwise to 2200°C to collapse into a solid rod known as a preform. The collapsing of sintered glass was carried out using the burner moving at a slow speed and maintaining a pressurized condition to ensure core-clad circularity. For alumina-germano-silicate core composition, during collapsing, additional GeCl<sub>4</sub> flow was maintained to avoid the central dip in refractive index profile due to GeO<sub>2</sub> evaporation from the core.

### **3.3.3 Characterization of preform**

#### **3.3.3.1 Refractive Index and geometric profile analysis**

Prior to the fibre drawing, the Refractive Index (RI) and geometrical properties of the fabricated preform both along the length and at different angular positions were characterized by using Preform Analyzer (PK2600). The instrument is capable of measuring the RI with an accuracy of the 4<sup>th</sup> decimal point by employing deflection function technique to compute the RI profile [37].

The preform to be measured was mounted vertically and immersed in the tank filled with index-matching fluid. The preform was then scanned with a laser (at a wavelength of 630 nm) and the refraction of the beam was analyzed to determine the RI and geometry of the layers of the preform. Thus a complete analysis of the RI, diameter, non-circularity, layer concentricity for each rotational angle and for each longitudinal position was performed to predict the property of the fibre. The measured RI profile of a typical Tm-doped alumino-silicate core preform is shown in Fig. 3.3.

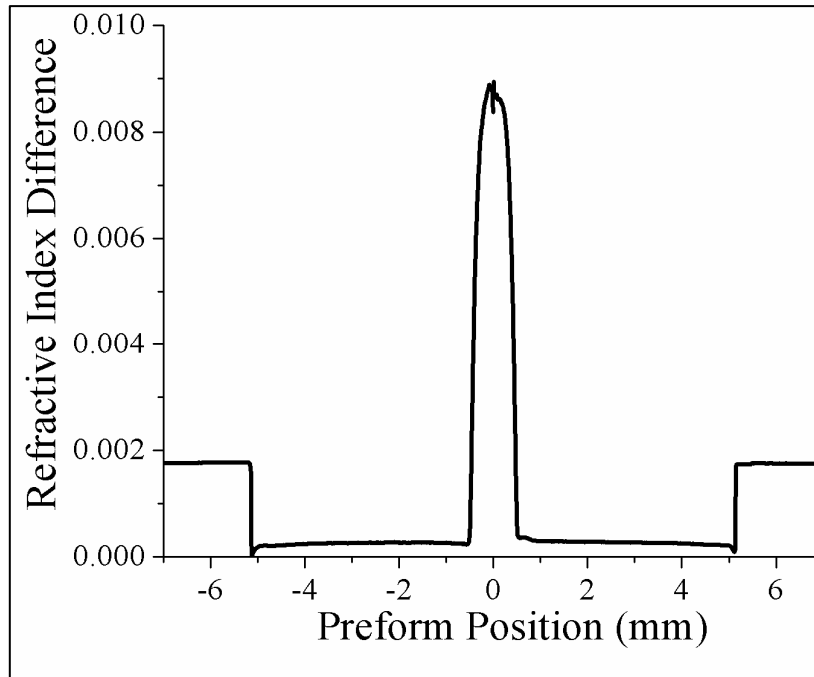


Fig. 3.3 Refractive Index profile of a Thulium-doped alumino-silicate core preform

### 3.3.3.2 Rare-earth concentration

The absolute concentration and distribution profiles of the dopants i.e. Tm, Yb, Al, Ge and P ions were evaluated by Electron Probe Microanalysis (EPMA) at University of Minnesota, Mexico using a polished preform section with thickness of 1.5 mm. The step size of the analysis was 5  $\mu\text{m}$ . Fig. 3.4(a) represents the distribution of Tm and Yb ions and Fig. 3.4(b) indicates distribution of Al ion in one of the fabricated preform. Both the radial homogeneity and flat distribution of REs and Al were observed throughout the core region.

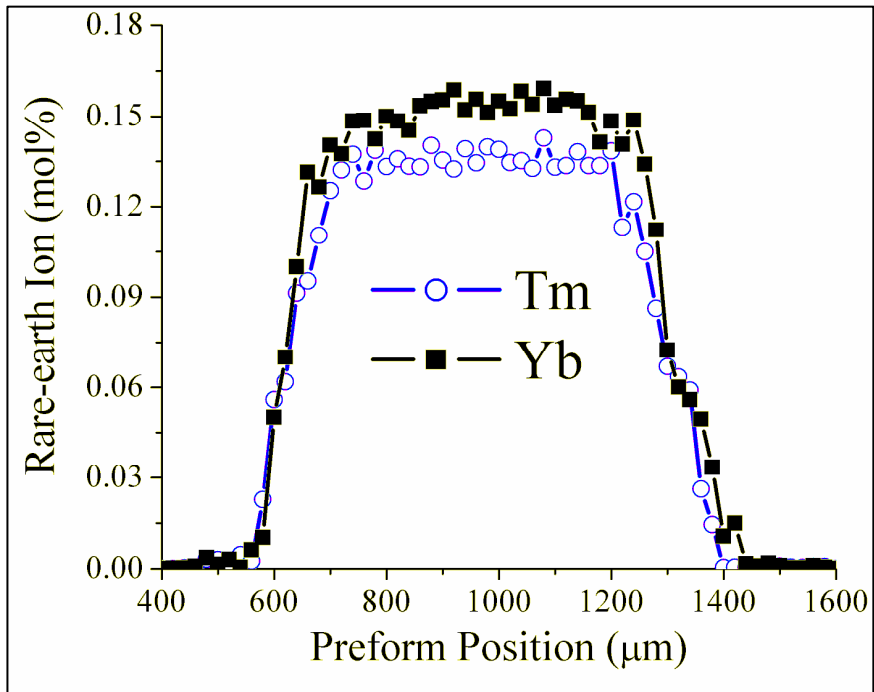


Fig. 3.4(a) Thulium and Ytterbium ion distribution in the fibre core

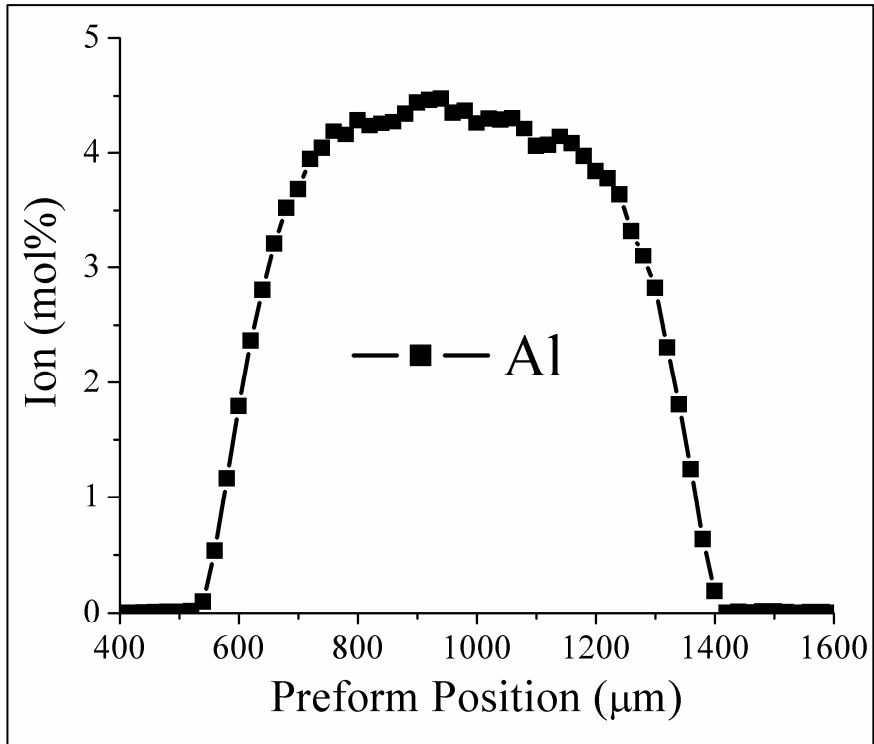


Fig. 3.4(b) Aluminium ion distribution in the fibre core

### 3.3.4 Fibre drawing

After the fabrication and characterization of the preforms, a drawing tower (Heathway), as shown in Fig. 3.5, at CSIR-CGCRI was used to draw single-clad fibres from these preforms. The preform was held above the furnace in a mount that feeds the preform into the furnace at a predetermined speed. The preform was initially lowered into the resistive heating furnace such that the end of the preform was just below the hot zone of the furnace. As the furnace heats up to 2050°C, the preform softens at the hot zone and begins to neck and elongate. The resulting 'neck-down' falls under gravity and further elongates the neck to the desired fibre diameter. The 'neck-down' was then cut off and the fibre was fed into the capstan and the fibre take-up drum. Below the furnace, there is a non-contact diameter monitor that measures the diameter of the drawn fibre. This measured diameter was compared with a set value, or a desired diameter, and the difference was used to control the speed of the capstan at the bottom of the tower.

The capstan was sped up to reduce the diameter or was slowed down to increase the diameter. Immediately below the diameter monitor is the coating applicator followed by a ultra-violet (UV) curing oven. Both primary and secondary coating were applied and the thickness of primary coating as well as secondary coating and their uniformity were maintained properly through adjusting the pressure of the flow of the inlet gases into the vessel of primary and secondary coating resin during the drawing of the fibre. The coated fibre then passed through the capstan and finally onto a take-up drum. Dual coated fibres of overall diameter of  $250\pm 2$   $\mu\text{m}$  were drawn at a drawing speed in the range of 50-75 meter/minute maintaining the fibre diameter of  $125\pm 0.5$   $\mu\text{m}$ .

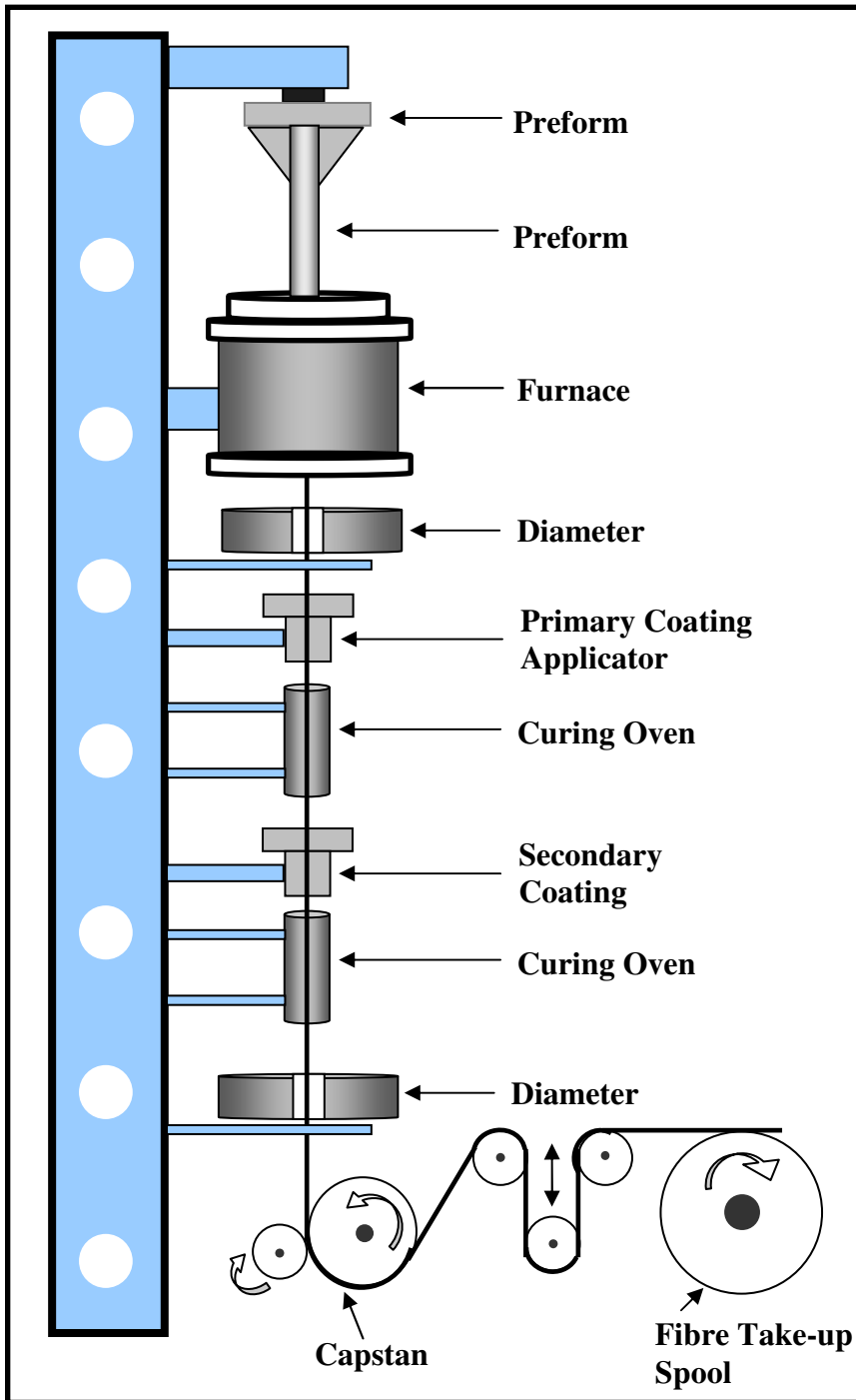


Fig. 3.5 Schematic representation of a fibre drawing tower

### 3.3.5 Fibre characterization

In order to identify suitable fibres for further spectroscopic investigation and laser experimentation, basic waveguide and transmission properties of the fabricated fibres were characterized. The characterization data are useful both for spectroscopic analysis and for an optimum design of fibre laser resonators.

#### 3.3.5.1 Refractive Index and geometric profile

The Refractive Index (RI), geometric and mode field profile of the fabricated fibres were characterized through Optical Fibre Analyzer (NR-9200, EXFO). The instrument uses both the refracted near-field (RNF) and transmitted near-field (TNF) techniques [37]. The RNF provides the RI profile (RIP) as well as geometrical parameters (core and cladding diameter, concentricity, circularity etc.). The TNF produces the mode-field diameter (MFD) at 1.31  $\mu\text{m}$  and 1.55  $\mu\text{m}$  according to Petermann II and Gaussian definitions. The basic waveguide characteristic of the fabricated fibre was estimated from the distribution of RI while coupling and splicing losses were determined from the mode profile of the fibre. The characterized waveguide parameters are listed in Table 3.2 and measured RI profile of a Tm-doped alumina-silicate core optical fibre is shown in Fig. 3.6.

Table.3.2 RI and geometrical characterization data of a Thulium-doped fibre

Parameter	Unit	Measured Value
Numerical Aperture (NA)		0.16
Core Diameter	$\mu\text{m}$	8.8
Clad Diameter	$\mu\text{m}$	125.5
Non-circularity (core)	%	1.2
Concentric error	%	0.19
MFD @ 1.55 $\mu\text{m}$	$\mu\text{m}$	10

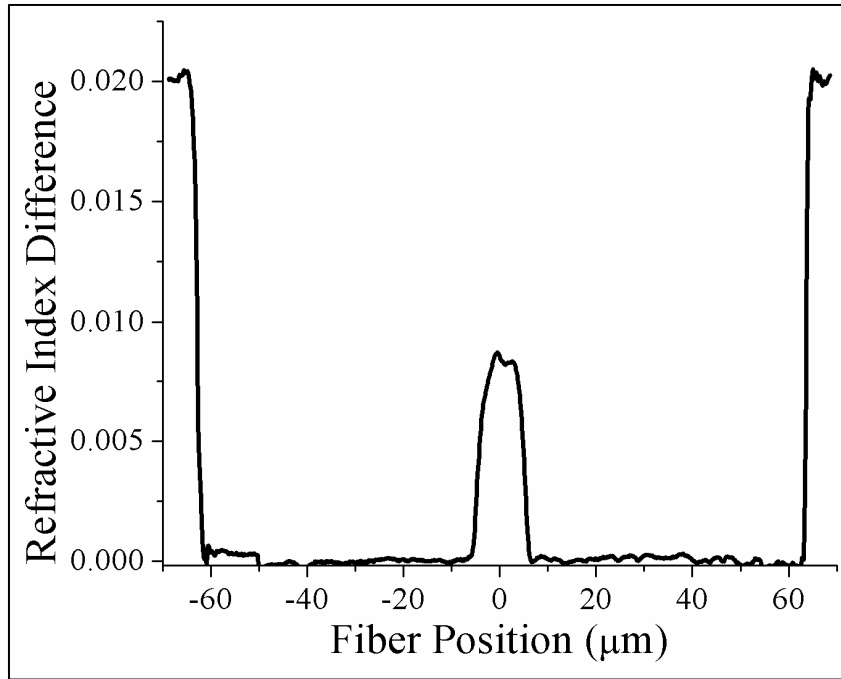


Fig. 3.6 Refractive Index profile of a Thulium-doped alumino-silicate core fibre

### 3.3.5.2 Spectral attenuation

Spectral absorption measurements for Tm- and Tm/Yb-doped optical fibres were performed differently, depending upon the RE doping levels. For lightly RE-doped fibres, a conventional ‘cut-back’ (or differential) method was utilized as follows. One end of the fibre under test was inserted into the measuring system (a white light source with scanning double-monochromator providing the input for the fibre), and the transmitted power,  $P_1$ , was measured at other end as a function of wavelength using either a Si (for wavelength range 0.35-1.0  $\mu\text{m}$ ) or peltier cooled InGaAs detector (for wavelength range 1.0-2.4  $\mu\text{m}$ ). Then the fibre was cut back by a few tens of centimetres (depending on the RE doping level) and the transmitted power,  $P_2$ , was measured again keeping the similar launching condition at the input end. The absorption of the fibre in decibel per unit length (dB/m) can be obtained from the measured transmitted power ratio,  $P_2/P_1$ , of the two measurements by using Equation 3.2

$$\alpha(\text{dB}/\text{m}) = \frac{10 \log_{10}(P_2/P_1)}{L_1 - L_2} \quad (3.2)$$

where  $L_1$  and  $L_2$  are the original fibre length and the ‘cut-back’ fibre length ( in meter) respectively.

For highly Tm- and Tm/Yb-doped fibres, on the other hand, a much shorter fibre length is required to obtain accurate absorption spectra. To overcome the limitation of limited dynamic range of the measurement system, the doped fibre under test was spliced between a launched fibre and a receiving fibre (passive fibre) and the transmitted power,  $P_1$ , was measured while transmitted power,  $P_2$ , was measured by splicing only the launched and receiving fibre end, without the doped fibre. Here the ‘cut-back’ fibre length is the length of the doped fibre only. The length of RE-doped fibre under test was standardized for each fibre according to the concentration level of Tm and Yb in the fibre core. The absorption spectrum of a Tm/Yb-doped optical fibre measured through multiple ‘cut-back’ method is shown in Fig.3.7. The benefit of this technique is that it allows measurement of the fibre characteristics without introducing errors due to the variation in the input light launching conditions.

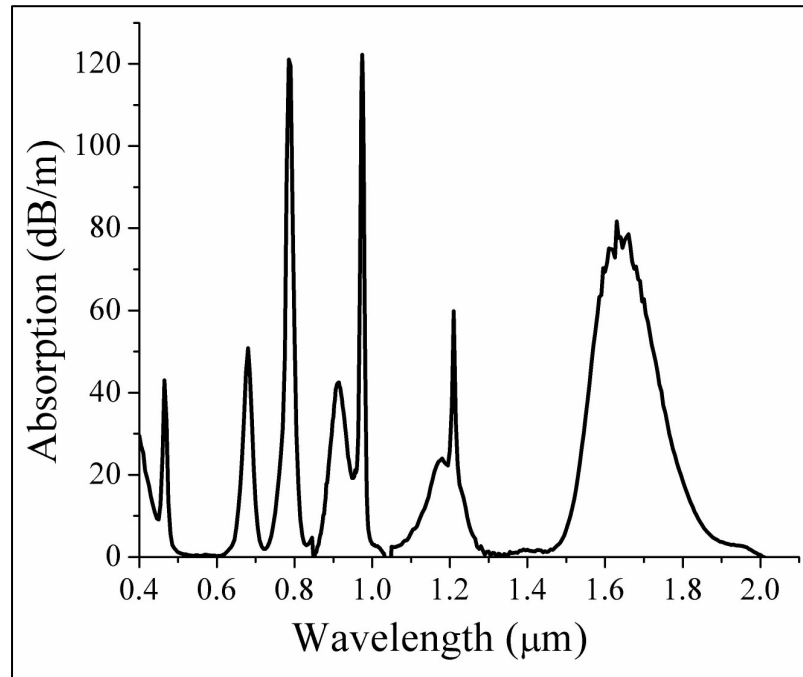


Fig.3.7 Absorption spectrum of a Tm/Yb-doped aluminosilicate fibre

The absorption spectrum provides necessary information about the position (in wavelength) and strength of ground state absorption (GSA) of Tm and Yb in fabricated fibre. The spectrum also reflects the effect of host composition on the GSA. The Tm<sup>3+</sup> and Yb<sup>3+</sup> concentrations were deduced from the 0.785  $\mu\text{m}$  ( $^3\text{H}_6 \rightarrow ^3\text{H}_4$ ) and 0.915  $\mu\text{m}$  ( $^2\text{F}_{7/2} \rightarrow ^2\text{F}_{5/2}$ ) absorption peaks respectively and showed a good agreement with results obtained from the EPMA performed in preform samples.

### **3.4 Summary**

This chapter has summarized the standardization process for the fabrication of Tm- and Tm/Yb-doped optical fibres through a series of systematic experiments using MCVD-solution doping technique to achieve the desired characteristics and good repeatability. A total of twenty-four preforms and their fibres are selected for further spectroscopic investigations and laser experiments based on their fibre quality and their spectral characteristics. The details of the selected fibres are listed in Table 3.3. The waveguide and ground state absorption data will also be used extensively for investigations and experiments presented in subsequent chapters.

Table 3.3 List of fibres fabricated and characterized

Sl. No	Fibre ID	NA	Core Dia ( $\mu\text{m}$ )	Dopant Ion Concentration (mol%)						Absorption at 0.78 $\mu\text{m}$ (dB/m)	Absorption at 0.92 $\mu\text{m}$ (dB/m)
				Tm	Yb	Al	Ge	P	Yb:Tm		
<b>A. Thulium Doped Fibre</b>											
1	TDF-1	0.15	8	0.024	----	0.91	7	----	----	26.08	----
2	TDF-2	0.14	8.6	0.030	----	4	----	----	----	34.60	----
3	TDF-3	0.15	8	0.031	----	9	----	6.3	----	33.64	----
4	TDF-4	0.16	8	0.290	----	5	----	----	----	267.23	----
5	TDF-5	0.16	8	0.350	----	5.5	----	----	----	660.77	----
<b>B. Thulium-Ytterbium Doped Alumino-silicate Fibre</b>											
6	TYDF-A-1	0.14	8.6	0.030	0.028	4	----	----	0.93	34.60	12.98
7	TYDF-A-2	0.15	8.4	0.090	0.095	5.2	----	----	1.05	56.77	22.41
8	TYDF-A-3	0.15	8.5	0.080	0.070	5.5	----	----	0.88	98.56	38.09
9	TYDF-A-4	0.15	8.4	0.082	0.490	6	----	----	5.98	89.52	167.51
10	TYDF-A-5	0.15	8.2	0.072	0.680	5.7	----	----	9.44	87.07	386.10
11	TYDF-A-6	0.16	8	0.066	0.960	5	----	----	14.55	71.47	545.60
12	TYDF-A-7	0.15	8.5	0.081	0.15	4.9	----	----	1.85	121.06	42.43
13	TYDF-A-8	0.16	8	0.070	0.210	5.8	----	----	3.00	227.85	160.11
14	TYDF-A-9	0.17	7.5	0.056	0.059	6	----	----	1.05	311.10	153.71
15	TYDF-A-10	0.17	7.5	0.106	0.150	6	----	----	1.4	226.23	160.11
16	TYDF-A-11	0.16	8	0.08	0.960	5	----	----	12.1	71.47	545.60
17	TYDF-A-12	0.17	7.5	0.181	0.250	6	----	----	1.38	226.23	160.11
<b>C. Thulium-Ytterbium Doped Alumino-germeno-silicate Fibre</b>											
18	TYDF-AG-1	0.14	8.5	0.022	0.069	0.560	9.53	----	3.10	24.08	27.42
19	TYDF-AG-2	0.16	8.0	0.024	0.023	0.910	7.94	----	0.96	26.08	91.78
20	TYDF-AG-3	0.13	9.0	0.048	0.131	1.500	2.62	----	2.72	52.29	52.20
21	TYDF-AG-4	0.14	8.5	0.081	0.153	1.560	2.62	----	1.88	88.77	61.15
<b>D. Thulium-Ytterbium Doped Alumino-phospho-silicate Fibre</b>											
22	TYDF-AP-1	0.13	8.5	0.021	0.024	9.10	----	6.0	1.14	21.55	9.73
23	TYDF-AP-2	0.14	8.0	0.031	0.041	9.86	----	6.3	1.33	33.64	16.48
24	TYDF-AP-3	0.14	9.0	0.055	0.073	9.50	----	6.1	1.33	60.39	29.51

## References

- [1] S Sudo, Editor 'Optical fiber amplifiers: materials, devices, and applications', Artech House (1997)
- [2] G Liu and B Jacquier, Editors 'Spectroscopic Properties of Rare Earths in Optical Materials', Springer Series in Materials Science, Vol. 83, 2005
- [3] B G Aitken, M J Dejneka and M L Powley 'Tm-doped alkaline earth aluminate glass for optical amplification at 1460 nm', Journal of Non-Crystalline Solids, Vol. 349, pp. 115-119 (2004)
- [4] T Komukai, T Sugawa and Y Miyajima 'Upconversion pumped thulium-doped fluoride fiber amplifier and laser operating at 1.47  $\mu\text{m}$ ', IEEE Journal of Quantum Electronics, Vol. 31, pp. 1880 – 1889 (1995)
- [5] R M Percival, D Szebesta and J R William 'Highly efficient 1.064  $\mu\text{m}$  upconversion pumped 1.47  $\mu\text{m}$  thulium doped fluoride fibre laser', Electronics Letters, Vol. 30, pp. 1057-1058 (1994)
- [6] T Kasamatsu, Y Yano and H Sekita '1.50- $\mu\text{m}$ -band gain-shifted thulium-doped fiber amplifier with 1.05- and 1.56- $\mu\text{m}$  dual-wavelength pumping', Optics Letters, Vol. 24, pp.1684-1686 (1999)
- [7] S D Jackson 'Tm-doped silicate glass fibre lasers: The foundation technology for high-power mid-infrared light generation', Proc. of SPIE Vol. 7914, 79140M-1-9 (2011)
- [8] E R M Taylor, L N Ng, J Nilsson, R Caponi, A Pagano, M Potenza and B Sordo 'Thulium-doped tellurite fiber amplifier', IEEE Photonics Technology Letters, Vol. 16, pp. 777 - 779 (2004)
- [9] S Tanabe and T Tamaoka 'Gain characteristics of Tm-doped fiber amplifier by dual-wavelength pumping with a tunable L-band source', Optical Materials, Vol. 25, pp. 165-169 (2004)
- [10] S Ohara, N Sugimoto, Y Kondo, K Ochiai, Y Kuroiwa, Y Fukasawa, T Hirose, H Hayashi and S Tanabe 'Bi<sub>2</sub>O<sub>3</sub>-based glass for S-band amplification', Proc. SPIE 4645, pp.8–15 (2002)

- [11] M L Dennis and B Cole 'Amplification device utilizing thulium doped modified silicate optical fiber', US patent No. 6,924,928 B2, August 2 (2005)
- [12] P R Watekar, S Ju and W T Hu 'A Nd-YAG laser-pumped Tm-doped silica glass optical fiber amplifier at 840 nm', IEEE Photonics Technology Letters, Vol. 18, pp. 1651–1653 (2006)
- [13] K Arai, H Namikawa, K Kumata and T Honda 'Aluminum or phosphorus co-doping effects on the fluorescence and structural properties of neodymium-doped silica glass', Journal of Applied Physics, Vol. 59, pp. 3430-3436 (1986)
- [14] J Laegsgaard 'Dissolution of rare-earth clusters in SiO<sub>2</sub> by Al codoping: A microscopic model', Physical Review B. Condense Matter, Vol. 65, pp. 174114-1-174114-10 (2002)
- [15] A Bjarklev 'Optical Fiber Amplifiers: Design and System Applications', Artech House Inc., MA (1993)
- [16] Technical Staff of CSELT, Ed. F Tosco 'Fiber Optic Communication Handbook', Blue Ridge, Pennsylvania, (1990)
- [17] T Izawa, T Miyashita and F Manawa 'Continuous fabrication of high silica fibre preform', Proc. 1st IOOC, Tokio, Japan, pp. 375 (1977)
- [18] J F Hyde 'Method of making a transparent article of silica', U.S. patent 2272342 (February 10, 1942), filed August 27 (1934)
- [19] J B MacChesney 'Preparation of low loss optical fibres using simultaneous vapour phase deposition and fusion', Proc. 10<sup>th</sup> Int. Congr. Glass, Columbus, Ohio, pp. 640-644 (1974)
- [20] K Nassau and J W Shiever 'Plasma torch preparation of high purity, low OH content fused silica', Cerarnic Bulletin, Vol. 54, pp. 1004-1011 (1975)
- [21] S R Nagel, J B McChesney and K L Walker 'An overview of the modified chemical vapour deposition process and performance', IEEE, Journal of Quantum Electronics, Vol. QE-18, pp. 459-477 (1982)
- [22] J E Townsend, S B Poole and D N Payne 'Solution doping technique for fabrication of rare earth doped optical fibers', Electronics Letters, Vol. 23, pp. 329-331 (1987)

- [23] L Cognolato 'Chemical Vapour Deposition for Optical Fibre Technology' J.de Physique IV Colloque C5, supplkment au Journal de Physique 11, Vol.5, pp. C5-975-987 (1995)
- [24] K L Walker, F T Geyling and S R Nagel 'Thermophoretic Deposition of Small Particles in the Modified Chemical Vapor Deposition (MCVD) Process', Journal of American Ceramic Society, Vol. 63, pp. 552-558 (1980)
- [25] J Stone and C A Burrus 'Nd<sup>3+</sup> doped SiO<sub>2</sub> lasers in end pumped fiber geometry', Applied Physics Letters, Vol. 23, pp. 388-389, ISSN 1077-3118 (1973)
- [26] V Matejec, M Hayer, M Pospisilova and I. Kasik 'Preparation of optical cores of silica optical fiber by the sol-gel method', Journal of Sol-Gel Science Technology, Vol.8, pp. 889-893, ISSN 1573-4846 (1997)
- [27] S Tammela, P Kiiveri, S Sarkilahti, M Hotoleanu, H Vaikonen, M Rajala, J Kurki, and K. Janka 'Direct Nanoparticle Deposition process for manufacturing very short high gain Er-doped silica glass fibers', Proceedings of ECOC 2002, ISBN 8790974638, Copenhagen (2002).
- [28] B J Ainslie, R Armitage, S P Craig and B Wakefield 'Fabrication and optimization of the erbium distribution in silica based doped fibres', Proceedings of ECOC, pp. 62, Brighton, UK, September (1988)
- [29] S B Poole, D N Payne and M E Fermann 'Fabrication of low-loss optical fibres containing rare earth ions', Electronics Letter, Vol. 21, pp. 737-738, ISSN 0013-5194 (1985)
- [30] J B MacChesney and J R Simpson 'Optical waveguides with novel compositions', Proceedings of Optical Fibre Communication Conference, Paper WH5, p. 100, Technical Digest, San Diego, CA, USA, February (1985)
- [31] R Laoulacine, T F Morse, P Charilaou and J W Cipolla 'Aerosol delivery of non-volatile dopants in the MCVD System', Extended Abstracts of the AIChE Annual Meeting, Washington, DC, USA (1988)
- [32] D A Thompson, P L Bocko and J R Gannon 'New source compounds for fabrication of doped optical waveguide fibres', Proceedings of Fibre Optics adverse Environment II, SPIE, Vol. 506, ISBN 9780892525416 (1984)

- [33] T Li 'Optical Fiber Communications Volume 1 Fiber Fabrication' Academic Press, Inc., Orlando, Florida, Chap. 1 (1985)
- [34] A Dhar, M C Paul, M Pal, A K Mondal, S Sen, H S Maiti and R. Sen 'Characterization of porous core layer for controlling rare earth incorporation in optical fiber', Optics Express, Vol. 14, pp. 9006-9015 (2006)
- [35] K L Walker, J W Harvey, F T Geyling and S R Nagel 'Consolidation of particulate layers in the fabrication of optical fibre preforms', Journal of American Ceramic Society, Vol. 63, pp. 96-102 (1980)
- [36] A Dhar, M C Paul, M Pal, S K Bhadra, H S Maiti and R Sen 'An improved method of controlling rare earth incorporation in optical fiber', Optics Communication, Vol. 277, pp. 329-334 (2007)
- [37] D Marcuse 'Principles of Optical Fibre Measurement' Academic Press, New York, (1981)

# Chapter 4

## Spectroscopic Analysis of Thulium and Ytterbium to Thulium Energy-transfer

*Abstract:* In this chapter a thorough investigation of the basic emission and absorption characteristics of Thulium, doped in silica fibres, has been performed with an objective to achieve a better analysis of the laser performance when the doped fibre is used as a gain medium. In addition to this, the step-wise energy-transfer from Ytterbium to Thulium in Thulium/Ytterbium-doped silica fibres has been determined quantitatively. As a result several principal energy-transfer parameters are obtained both from spectroscopic measurements and from the migration-assisted energy-transfer model. The linear dependence of energy-transfer probability on the product of co-dopant concentrations confirms the accuracy of the implementation of migration-assisted energy-transfer model. It has been found that the step-wise energy-transfer process as well as emission at wavelength ranges of 0.475  $\mu\text{m}$ , 0.8  $\mu\text{m}$  and 2  $\mu\text{m}$  with pumping at 0.98  $\mu\text{m}$  is closely related to the level of Ytterbium concentration with respect to Thulium. The proportion has been optimized on the basis of emission at the mentioned wavelength ranges and amplified spontaneous emission experiment performed at 2  $\mu\text{m}$  shows a good agreement with the optimization result.

### 4.1 Introduction

The spectroscopic investigations play a prominent role in characterizing the rare-earth (RE)-doped glasses as well as in comprehending nature of interactions involving radiation and matter. Fundamental knowledge of RE spectroscopy, especially using

precise spectroscopic parameters such as fluorescence lifetimes, absorption and emission cross-sections, is the key to analyzing the laser and amplifier performance. Thulium (Tm), when doped in glass, shows a complex energy level diagram. In silica glass host having high phonon energy, the energy gap between the two levels of Tm-ion is not sufficient for dominating radiative transitions. It is worth noting that both the host glass and the composition significantly affect the position, line-width, strength and lifetime of a particular transition. Hence the selection of the host glass as well as active ion concentration is an important step in order to develop efficient Tm-doped optical devices. Spectroscopy of Tm in various glass hosts has been investigated and the laser operation involving Tm has been demonstrated in several non-oxide and oxide glasses [1-4]. Due to the advantages offered by silica glass in terms of chemical durability and compatibility with existing silica based components, the spectroscopic analysis of Tm-doped silica glass and fibre with modified host composition has been studied extensively, in particular in the improvement of the quantum efficiency and fluorescence life time of  $^3\text{H}_4$  level of Tm-ion for S-Band (1.47-1.52  $\mu\text{m}$ ) emissions [5-7].

Emission of  $^3\text{F}_4$  level of Tm-ion in the 2  $\mu\text{m}$  wavelength range occurs under excitation at around 0.8  $\mu\text{m}$ , 1.2  $\mu\text{m}$  and 1.6  $\mu\text{m}$ . To take advantage of diode pumping in compact laser system, co-doping of Tm-doped fibre with Ytterbium (Yb) is considered to be an effective route as, through the appropriate combination of sensitizer (Yb) with the activator (Tm), it would enable the exploration of pumping possibility over the wavelength region from 0.91 to 0.98  $\mu\text{m}$  for emission in the range of 2  $\mu\text{m}$ . In the past,  $\text{Pr}^{3+}$ ,  $\text{Ho}^{3+}$ ,  $\text{Er}^{3+}$  and  $\text{Tm}^{3+}$  ions were successfully excited via energy-transfer processes with  $\text{Yb}^{3+}$  as the sensitizer [8-10]. The sensitization of  $\text{Tm}^{3+}$  by  $\text{Yb}^{3+}$  was studied primarily in low phonon energy glass/fibre due to its high quantum efficiency [11-13]. Earlier, utilizing a modified silica host and an Yb-co-doped Tm-doped fibre, a fibre laser at 2  $\mu\text{m}$  [14], fibre amplifiers for the telecommunications S-band (1.45-1.52  $\mu\text{m}$ ) [15] and amplification in the first telecommunication window around 0.8  $\mu\text{m}$  [16] were reported.

In the Tm/Yb-doped silica glass, the quasi-resonant energy levels of  $\text{Tm}^{3+}$  with the excited  $\text{Yb}^{3+}$  level ( $^2\text{F}_{5/2}$ ) allow multistep  $\text{Yb}^{3+} \rightarrow \text{Tm}^{3+}$  energy-transfer, controlling the emission in the three major wavelength bands centred at around 0.475, 0.8 and 2  $\mu\text{m}$ . Due to the non-resonant energy-transfer, the possibility of  $\text{Tm}^{3+} \rightarrow \text{Yb}^{3+}$  back-transfer is very low. Such step-wise energy-transfer mechanism is strongly determined by the proportion of Yb to Tm and therefore the proportion needs to be optimized to achieve the emission at a desired wavelength. It is important to note that the coefficients describing the energy-transfer from  $\text{Yb}^{3+}$  to  $\text{Tm}^{3+}$  in silica fibre are required to be determined quantitatively instead of a range [17] in order to optimize Tm/Yb-doped silica fibre based devices. It is expected that the energy-transfer parameters for silica glass would be different from those of evaluated for Tm/Yb-doped fluoride based crystals, generally used [18] to model silica fibre laser and amplifier devices. In silica based materials, the energy-transfer coefficients are expected to be higher as the spectral line widths are much larger in amorphous materials like glasses.

The objective of this chapter is to generate spectroscopic parameters for Tm-doped in silica fibres from the measured ground state absorption (GSA) spectra and fluorescence lifetime, coupled with the theoretical analysis. From the measured absorption spectra, radiative parameters such as radiative transition probabilities, lifetimes and branching ratios has been predicted by using the Judd–Ofelt (JO) theory. In this chapter, a rigorous spectroscopic investigation has also been carried out to analyze, both in a qualitative and quantitative manner, the  $\text{Yb}^{3+} \rightarrow \text{Tm}^{3+}$  energy-transfer mechanism. The principal  $\text{Yb}^{3+} \rightarrow \text{Tm}^{3+}$  energy-transfer parameters, essential in designing and modelling (based on rate equations) of ‘all-fibre’ amplifier and lasers, have been estimated on the basis of migration-assisted energy-transfer model and luminescent decay measurements. Tm/Yb-doped fibres having different  $\text{Yb}^{3+}$  concentrations have been considered for the evaluation of the dependence of energy-transfer parameters on the sensitizer concentration. The proportion of Yb to Tm has been further optimized on the basis of emission at wavelengths centred at around 0.475  $\mu\text{m}$ , 0.8  $\mu\text{m}$  and 2  $\mu\text{m}$  with pumping at

0.98  $\mu\text{m}$ . Amplified spontaneous emission (ASE) under pumping at 0.98  $\mu\text{m}$  was measured at 2  $\mu\text{m}$  in Tm/Yb-doped fibre.

## 4.2 Absorption and Emission Spectral Analysis of Thulium

### 4.2.1 Energy levels

In silica glass, trivalent Tm-ion exhibits multiple energy levels that may cause photon emissions ranging from the near-infrared to the near-ultraviolet. An energy-level diagram was constructed from the GSA spectrum (measured using ‘cut-back’ method as explained in Chapter 3; Section 3.3.5.2) and is shown in Fig. 4.1. Each energy level is broad due to the ‘Stark-splitting’ but represented by a single line in the figure. The levels  $^3\text{F}_2$  and  $^3\text{F}_3$  are considered single as the identification of those is not possible, due to the small energy gap as well as broadening of the absorption line in silica glass.

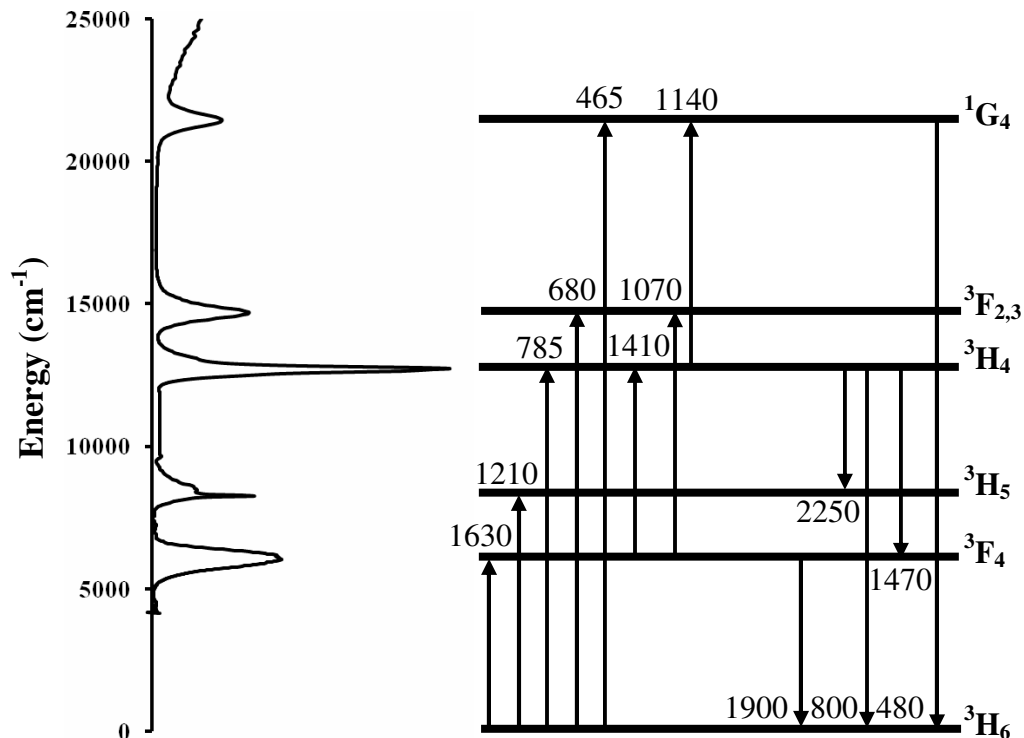


Fig. 4.1 Energy level diagram of Tm-doped in alumino-silicate glass fibre; Absorption and emission wavelengths are mentioned in ‘nm’

The excited states for the  $\text{Tm}^{3+}$  and the corresponding effective energy gaps separating each level from the next lower level are given in Table 4.1.

Table 4.1 Energy state position with respect to  ${}^3\text{H}_6$  level and energy gap to the next lower level for  $\text{Tm}^{3+}$

Energy State	Position ( $\text{cm}^{-1}$ )	Energy gap to next lower level ( $\text{cm}^{-1}$ )
${}^3\text{F}_4$	6175	6175
${}^3\text{H}_5$	8283	2108
${}^3\text{H}_4$	12743	4460
${}^3\text{F}_{2,3}$	14714	1971
${}^1\text{G}_4$	21517	6803

The characteristics of each excited manifold in silica glass host are explained below.

***${}^3\text{F}_4$  manifold:***

The  ${}^3\text{F}_4$  manifold is the first excited state of  $\text{Tm}^{3+}$  and is located around  $6100 \text{ cm}^{-1}$  above the ground state. The  ${}^3\text{H}_6 \rightarrow {}^3\text{F}_4$  absorption is broad in the range of  $1.55$  to  $1.8 \mu\text{m}$  while the  ${}^3\text{F}_4 \rightarrow {}^3\text{H}_6$  transition produces an extremely wide featureless emission band spanning  $1.6 - 2.0 \mu\text{m}$ . The energy gap between the  ${}^3\text{F}_4$  and  ${}^3\text{H}_6$  is in the critical interval at which the radiative and non-radiative rates are of the same order of magnitude in silica glass. The  ${}^3\text{F}_4$  manifold can be pumped directly at around  $1.6 \mu\text{m}$ , or excited through the decay of higher energy manifolds such as the  ${}^3\text{H}_5$  and  ${}^3\text{H}_4$  manifolds.

***${}^3\text{H}_5$  manifold:***

The  ${}^3\text{H}_5$  manifold is located at around  $8200 \text{ cm}^{-1}$  from the ground state and around  $2100 \text{ cm}^{-1}$  above the  ${}^3\text{F}_4$  manifold. The close energy spacing between the  ${}^3\text{H}_5$  and  ${}^3\text{F}_4$  manifolds results in decaying almost all of the excited state ions in the  ${}^3\text{H}_5$  manifold non-radiatively to the  ${}^3\text{F}_4$  manifold. The peak absorption wavelength of the  ${}^3\text{H}_5$  manifold is around  $1.2 \mu\text{m}$ . However, the broad absorption band also shows reasonable absorption at shorter wavelengths in the range of  $1 \mu\text{m}$ .

### ***<sup>3</sup>H<sub>4</sub> manifold:***

The <sup>3</sup>H<sub>4</sub> manifold is the third excited state of Tm<sup>3+</sup> and is located at around 12700 cm<sup>-1</sup> from the ground state and around 4460 cm<sup>-1</sup> above the <sup>3</sup>H<sub>5</sub> manifold. When ions are excited to the <sup>3</sup>H<sub>4</sub> manifold they may relax via several different routes. The radiative transitions from the <sup>3</sup>H<sub>4</sub> manifold, <sup>3</sup>H<sub>4</sub> → <sup>3</sup>F<sub>4</sub> and <sup>3</sup>H<sub>4</sub> → <sup>3</sup>H<sub>6</sub>, result in emission bands spanning 1.46 – 1.53 μm and 0.77 – 0.82 μm respectively where <sup>3</sup>H<sub>4</sub> → <sup>3</sup>H<sub>6</sub> radiative transition is the dominant.

### ***<sup>3</sup>F<sub>2,3</sub> manifolds:***

In silica glass, inhomogeneous broadening masks the absorption peaks from both excited state manifolds resulting in a single broad featureless absorption peak centred at around 0.68 μm and considered as a single level. The <sup>3</sup>F<sub>2,3</sub> manifold is located at around 14700 cm<sup>-1</sup> above the ground state manifold and around 1970 cm<sup>-1</sup> above the <sup>3</sup>H<sub>4</sub> manifold. The close energy spacing between the <sup>3</sup>F<sub>2</sub> and <sup>3</sup>F<sub>3</sub> manifolds and the next lower <sup>3</sup>H<sub>4</sub> manifold prevents any radiative emission from these manifolds.

### ***<sup>1</sup>G<sub>4</sub> manifold:***

The <sup>1</sup>G<sub>4</sub> manifold of Tm<sup>3+</sup> is located at around 21500 cm<sup>-1</sup> from the ground state and around 6800 cm<sup>-1</sup> above the <sup>3</sup>F<sub>2,3</sub> manifold. Radiative emission from the <sup>1</sup>G<sub>4</sub> manifold can occur through a number of possible transitions: <sup>1</sup>G<sub>4</sub> → <sup>3</sup>F<sub>2,3</sub>, <sup>1</sup>G<sub>4</sub> → <sup>3</sup>H<sub>4</sub> (1.175 μm), <sup>1</sup>G<sub>4</sub> → <sup>3</sup>H<sub>5</sub> (0.78 μm), <sup>1</sup>G<sub>4</sub> → <sup>3</sup>F<sub>4</sub> (0.65 μm) and <sup>1</sup>G<sub>4</sub> → <sup>3</sup>H<sub>6</sub> (0.475 μm) while <sup>1</sup>G<sub>4</sub> → <sup>3</sup>H<sub>6</sub> radiative transition is the dominant.

## **4.2.2 Absorption and emission cross-sections**

The absorption cross-section of a particular transition between two states of an ion represents the probabilities for that transition to occur with the concurrent absorption of light. The transition probability for the absorption of a photon is proportional to the absorption cross-section. The measured spectral attenuation is related to GSA cross-section by factor of overlap integral between the optical mode and the dopants distribution, and the simplified relationship is given by [19]

$$\sigma_a(\lambda) = \frac{\alpha(\lambda)}{\Gamma N} \quad (4.1)$$

where  $\sigma_a$  is GSA cross-section in meter square ( $\text{m}^2$ ),  $\alpha$  is spectral attenuation in  $\text{m}^{-1}$ ,  $\Gamma$  is overlap factor between signal mode and RE distribution; the assumption is made that the total core is uniformly doped by RE,  $N$  is Tm-ion concentration in  $\text{ions}/\text{m}^3$  and  $\lambda$  is operating wavelength. The GSA cross-section spectra allowed the prediction of the emission cross-section of the fibre through the McCumber equation as [19]

$$\sigma_e(\lambda) = \sigma_a(\lambda) \exp\left[\left(\varepsilon - \frac{hc}{\lambda}\right) / KT\right] \quad (4.2)$$

where  $\sigma_e$  is the emission cross-section in  $\text{m}^2$ ,  $\varepsilon$  is the energy required to lift an ion from ground state to the excited state,  $K$  is Boltzman's constant,  $T$  is the absolute temperature in Kelvin,  $h$  is Plank's constant and  $c$  is velocity of light. The calculated GSA and emission cross-sections of one fabricated Tm/Yb-doped fibre (Fibre ID: TYDF-A-5) in the 2  $\mu\text{m}$  wavelength range (involving transition between  $^3\text{H}_6$  and  $^3\text{F}_4$  level) are shown in Fig. 4.2.

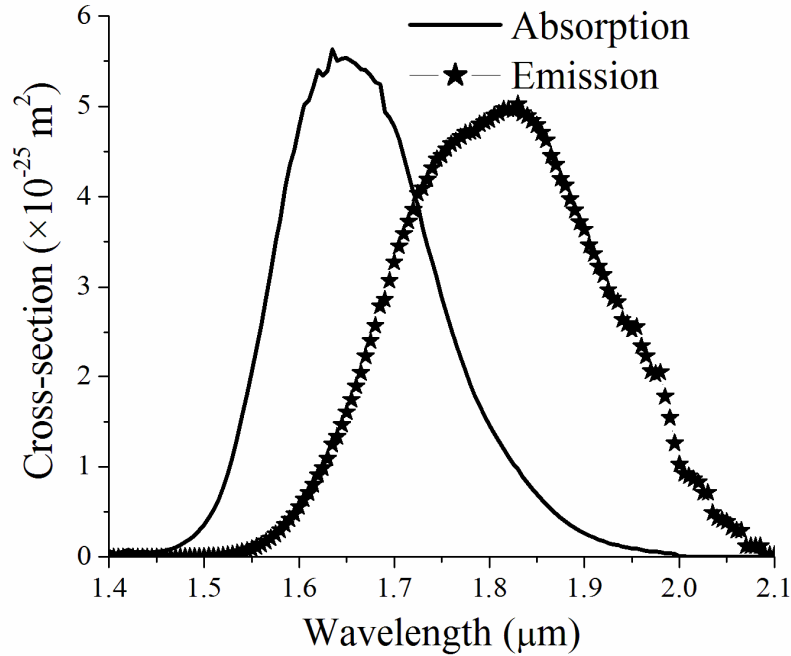


Fig. 4.2 Absorption and Emission cross-sections of Tm/Yb-doped fibre (Fibre ID: TYDF-A-5) in the 2  $\mu\text{m}$  wavelength range

The emission cross-section allows the calculation of the radiative lifetime through the relation given in Equation 4.3 and the calculated lifetime of  ${}^3F_4$  level for different fibres are presented in Table 4.4.

$$\frac{1}{\tau_r} = 8\pi n^2 c \int \frac{\sigma_e(\lambda)}{\lambda^4} d\lambda \quad (4.3)$$

### 4.2.3 Judd-Ofelt analysis

The Judd-Ofelt (JO) approximations were used to calculate  $4f$  transition intensities of Tm-ions in fabricated Tm-doped fibres. According to the JO theory, the spectral intensity,  $f$ , of the absorption band corresponding to transition  $J \rightarrow J'$  depending on JO parameters ( $\Omega_2, \Omega_4, \Omega_6$ ) is given as [19]

$$f_{cal} = \frac{8\pi^2 mc(n^2 + 2)}{2h\bar{\lambda}(2J + 1)9n} \sum_{t=2,4,6} \Omega_t \left| \left\langle \Psi_J \parallel U^{(t)} \parallel \Psi_{J'} \right\rangle \right|^2 \quad (4.4)$$

where  $J$  and  $J'$  are the total angular momentum quantum numbers of initial and final states respectively,  $\bar{\lambda}$  is the mean wavelength of the specific absorption band,  $c$  is the velocity of light,  $m$  is the electronic mass,  $n$  is the refractive index of the host glass at the mean wavelength and the elements  $\langle J \parallel U^{(t)} \parallel \Psi_{J'} \rangle$  are the reduced matrix elements of unit tensor operator  $U^{(t)}$  of rank  $t$ . The tensor operator  $U^{(t)}$  is a quantum mechanical operator for an electric dipole transition from state  $J \rightarrow J'$ . Since the  $4f$  electrons are well shielded by other layers in trivalent RE-ions,  $\langle J \parallel U^{(t)} \parallel \Psi_{J'} \rangle$  elements are virtually independent of the Ligand species surrounding the RE-ions, i.e. the host materials and are taken from the reference [20]. Since the effect of magnetic dipole interaction is very small compared to electric dipole interaction, the calculations here were done only using the latter.

The experimental oscillator strength of a transition is proportional to the area below the appropriate absorption line as given by Equation 4.5.

$$f_{exp} = \frac{4\pi\epsilon_0}{e^2} \frac{mc^2}{\pi} \int_{band} \sigma(k) dk \quad (4.5)$$

with dielectric constant  $\epsilon_0$ , mass of electron  $m$ , the speed of light in vacuum  $c$ , charge of electron  $e$  and  $\sigma$  is the measured absorption cross-section at frequency  $k$  in  $\text{cm}^{-1}$ .

From the measured absorption spectrum, well defined absorption bands such as  ${}^3\text{H}_6 \rightarrow {}^3\text{H}_4$ ,  ${}^3\text{F}_{2,3}$ ,  ${}^1\text{G}_4$  were selected in the computation of the JO intensity ( $\Omega_2$ ,  $\Omega_4$ ,  $\Omega_6$ ) parameters by using the least-squares fit method from Equations 4.4 and 4.5. Measured oscillator strengths of the absorption transitions in  $\text{Tm}^{3+}$  were derived by integrating each absorption bands area. The best-fit JO parameters along with the measured and calculated oscillator strengths as well as their root mean square (RMS) deviation for one Tm/Yb-doped fibre are listed out in Table 4.2.

Table 4.2 Experimental ( $f_{\text{exp}}$ ) and calculated ( $f_{\text{cal}}$ ) Oscillator strengths of absorption transition of  $\text{Tm}^{3+}$  in Tm/Yb-doped silica fibre

Energy Level	Fibre ID: TYDF-A-3	
	$f_{\text{cal}} \times 10^{-7}$	$f_{\text{exp}} \times 10^{-7}$
${}^3\text{H}_6 \rightarrow {}^3\text{F}_4$	2.418	3.259
${}^3\text{H}_6 \rightarrow {}^3\text{H}_5$	1.165	1.440
${}^3\text{H}_6 \rightarrow {}^3\text{H}_4$	2.783	3.697
${}^3\text{H}_6 \rightarrow {}^3\text{F}_3$	1.260	1.745
${}^3\text{H}_6 \rightarrow {}^3\text{F}_2$	0.346	0.206
${}^3\text{H}_6 \rightarrow {}^1\text{G}_4$	0.790	--
RMS deviation	$9.677 \times 10^{-8}$	
$\Omega_2 \times 10^{-20} \text{ cm}^2$	6.2659	
$\Omega_4 \times 10^{-20} \text{ cm}^2$	0.3588	
$\Omega_6 \times 10^{-20} \text{ cm}^2$	0.8137	

The small value of the RMS deviation between the experimental and calculated oscillator strengths describes the quality of the fit. The JO parameters can provide a view of the field strength of hosts. The characteristic feature of the larger  $\Omega_2$  parameter is that, it is

sensitive to the local environment of the RE-ions and is often related to the asymmetry of the coordination structure, polarizability of ligand ions or the bonding nature.

Considering only the electric-dipole probability, the radiative transition probability between state  $J$  and  $J'$  is given as

$$A = \frac{64\pi^4 e^2 n(n^2 + 2)^2}{3h\lambda_{mean}^3 (2J + 1)9n} \sum_{t=2,4,6} \Omega_t \left[ \langle J \| U^{(t)} \| \Psi' J' \rangle \right]^2 \quad (4.6)$$

where  $\lambda_{mean}$  is the mean (average) wavelength of transition. The line strength for the induced electric-dipole transition is given as

$$S_{ed} = e^2 \sum_{t=2,4,6} \Omega_t \left[ \langle J \| U^{(t)} \| \Psi' J' \rangle \right]^2 \quad (4.7)$$

The radiative transition rates or the total transition probability of the emitted levels are obtained by summing transition probabilities from that level to all lower levels as

$$A_T = \sum A(J, J') \quad (4.8)$$

and the reciprocal of the radiative rates gives radiative lifetimes of emitting level

$$\tau_R = 1/A_T \quad (4.9)$$

The branching ratio of the emission transitions is the fraction of the total photon flux from the emitting manifold  $J$  to the lower manifold  $J'$  given by the expression

$$\beta = A(J, J')/A_T \quad (4.10)$$

The calculated radiative lifetimes, radiative transitions rates, and branching ratios for one Tm/Yb-doped fibre are shown in Table 4.3.

Table 4.3 Calculated radiative lifetimes, radiative transitions rates and branching ratios for one Tm/Yb-doped fibre

Spontaneous emission transition	Fibre ID: TYDF-A-3				
	$S_{ed} \times 10^{-20}$	A	$\beta\%$	$A_T$	$\tau_R (\mu s)$
$^1D_2 \rightarrow ^1G_4$	1.217	150	1	21747.5	46
$^1D_2 \rightarrow ^3F_2$	0.513	441	2		
$^1D_2 \rightarrow ^3F_3$	1.057	1035	4.8		
$^1D_2 \rightarrow ^3H_4$	0.787	1411	6.5		
$^1D_2 \rightarrow ^3H_5$	0.014	44	-		
$^1D_2 \rightarrow ^3F_4$	3.821	16986	78		
$^1D_2 \rightarrow ^3H_6$	0.188	1680	7.7		
$^1G_4 \rightarrow ^3F_2$	0.099	5.1	-	3593	278
$^1G_4 \rightarrow ^3F_3$	0.332	22	1		
$^1G_4 \rightarrow ^3H_4$	1.281	177	5		
$^1G_4 \rightarrow ^3H_5$	4.993	2529	70		
$^1G_4 \rightarrow ^3F_4$	0.015	126	4		
$^1G_4 \rightarrow ^3H_6$	0.338	733	20		
$^3F_2 \rightarrow ^3F_3$	0.051	0.004	--	1078	928
$^3F_2 \rightarrow ^3H_4$	2.105	11	1		
$^3F_2 \rightarrow ^3H_5$	0.583	81	8		
$^3F_2 \rightarrow ^3F_4$	2.120	703	65		
$^3F_2 \rightarrow ^3H_6$	0.020	283	26		
$^3H_4 \rightarrow ^3H_5$	0.261	5.8	--	1022.5	978
$^3H_4 \rightarrow ^3F_4$	1.023	78	8		
$^3H_4 \rightarrow ^3H_6$	2.006	938	92		
$^3H_5 \rightarrow ^3F_4$	1.373	3	3	131	7629
$^3H_5 \rightarrow ^3H_6$	1.275	128	97		
$^3F_4 \rightarrow ^3H_6$	3.821	167.5	100	167.5	5969

#### 4.2.4 Fluorescence measurement

The fluorescence spectrum of Tm/Yb-doped fibre/preform was measured (at IPHT, Jena, Germany) over the wavelength range from 0.35 to 2.5  $\mu m$  by employing a 2 mm polished preform section as well as fibre with an excitation power of 3 mW at 0.976  $\mu m$ . Significant emission bands centred at 0.475, 0.65, 0.79 and 1.8  $\mu m$  were observed as

shown in Fig. 4.3. The fluorescence lifetime of  $\text{Yb}^{3+}$  ( $^2\text{F}_{5/2}$ ) was measured using excitation at  $0.976 \mu\text{m}$  and the  $^3\text{F}_4$  level life-time of  $\text{Tm}^{3+}$  was measured with excitation at  $0.8 \mu\text{m}$ .

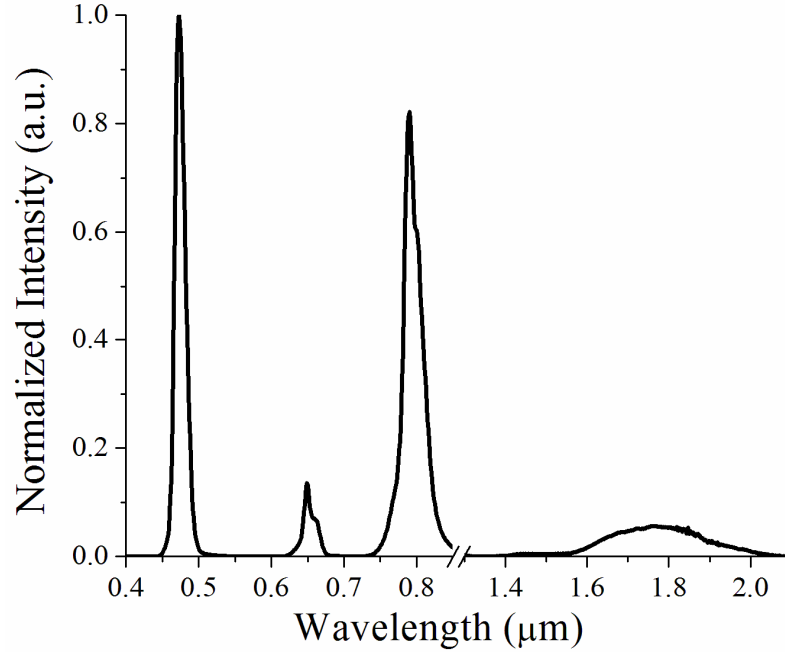


Fig. 4.3 Fluorescence spectrum of TYDF-A-3 under excitation at  $0.976 \mu\text{m}$

The measured and calculated lifetimes for fabricated fibres having different Yb:Tm proportions are listed in Table 4.4.

It is clear from the data given in this table that the measured radiative life-time ( $\tau_r$ ) for Tm-ion is similar for all the fibres having a similar Tm-ion concentration. The same phenomenon has been observed for Yb and its radiative lifetime decreases with the increment of the Yb-ion concentration. That indicates that Yb to Tm energy-transfer increases with the increment of Yb-ion concentration.

Table 4.4 Measured and calculated lifetimes for fabricated fibres having different Yb:Tm proportion

	TYDF-A-3	TYDF-A-4	TYDF-A-5	TYDF-A-6
<i>Concentration of dopants (EPMA)</i>				
Tm ion (mol %)	0.08	0.082	0.072	0.066
Yb ion (mol %)	0.07	0.49	0.68	0.96
<i>Yb:Tm proportion</i>	0.88	5.98	9.44	14.55
<i>Radiative life-time <math>\tau_r</math> (JO)</i>				
$^3F_4$ (ms)	5.969	5.49	7.361	8.868
$^3H_4$ ( $\mu$ s)	978	986	1146	1370
$^1G_4$ ( $\mu$ s)	278	272	332	398
<i>Radiative life-time <math>\tau_r</math> (McCumber)</i>				
$^3F_4$ (ms)	6.5	4.5	6.5	7.6
<i>Radiative life-time <math>\tau_r</math> (measured)</i>				
$^3F_4$ ( $\mu$ s)	579	609	595	657
<i>Radiative life-time <math>\tau_r</math> (measured)</i>				
$^2F_{5/2}$ ( $\mu$ s) for Yb	688	580	544	500

### 4.3 Absorption Spectral Analysis of Ytterbium

Yb-ion has the simplest energy level structure of all the RE-ions, with an excited state located at around  $10000 \text{ cm}^{-1}$  from the ground state; all other levels involve transitions in the ultraviolet region. The GSA cross-section was estimated from measured absorption spectrum and emission cross-section was calculated using McCumber equation (shown in Fig. 4.4). Due to the large energy gap between the  $^2F_{7/2}$  and  $^2F_{5/2}$  excited state, radiative transition from the  $^2F_{5/2}$  manifold is dominant. The radiative lifetime of this state was measured and given in Table 4.4.

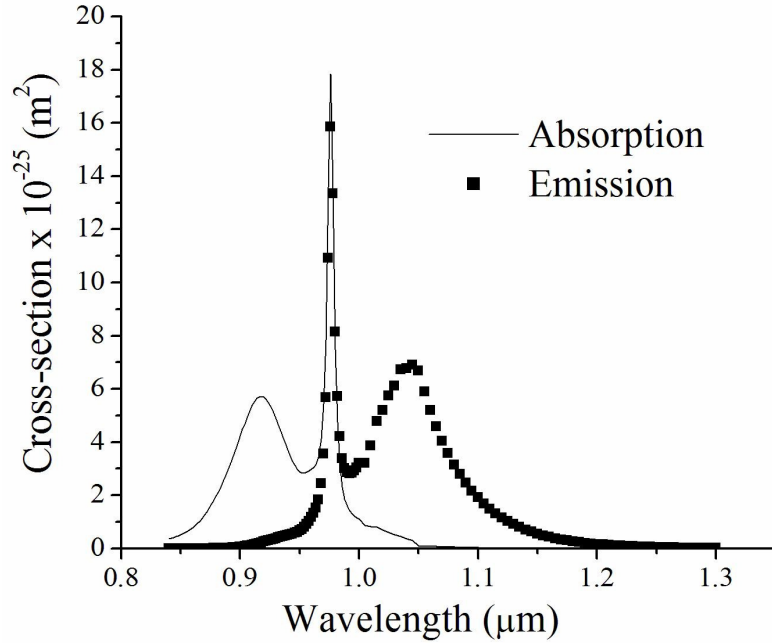


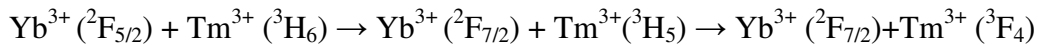
Fig. 4.4 Absorption and emission cross-sections of Yb in Tm/Yb-doped fibre (Fibre ID: TYDF-A-3)

## 4.4 Ytterbium to Thulium Energy-transfer

The Tm/Yb-doped system in silica glass host considers three possible energy-transfer paths under pumping at 0.98 μm. The step-wise energy-transfer process is explained in detail below and the related parameters are determined in the following section for the Tm/Yb-doped fibres having different Yb:Tm proportions.

### 4.4.1 First step energy-transfer

The first energy-transfer (ET1, indicated as path K<sub>1</sub> in Fig. 4.5) mechanism is involved in the 2 μm emission in silica fibre and can be summarized as



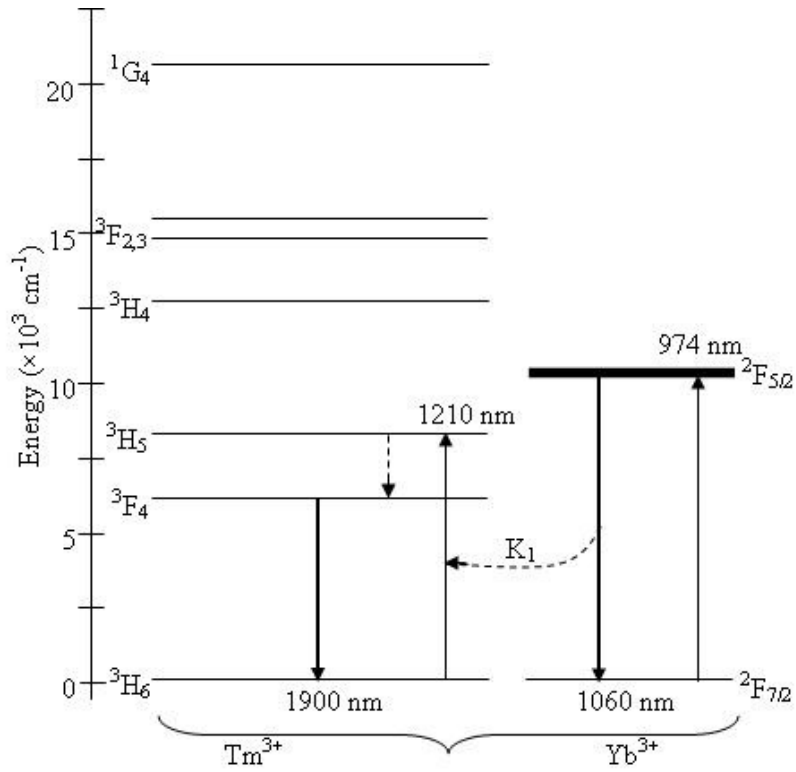


Fig. 4.5 First energy-transfer (ET1) processes in Tm/Yb-co-doped system

After being excited into  ${}^2F_{5/2}$  level,  $\text{Yb}^{3+}$  transfers its energy to the nearby  $\text{Tm}^{3+}$  via multipolar interactions. It is immediately followed by a fast multi-phonon relaxation from level  ${}^3H_5$  down to the metastable level  ${}^3F_4$ . The transition  ${}^3F_4 \rightarrow {}^3H_6$  is responsible for the laser emission near 2  $\mu\text{m}$ . ET1 is far from being resonant; the energy mismatch is nearly equal to  $\Delta E_1 \sim 1170 \text{ cm}^{-1}$  and necessitates the emission of at least two phonons in silica glass to conserve energy. Being qualified as exoenergetic, the energy-transfer has relatively high probability compared to endoenergetic process. As absorption and emission spectra of  $\text{Yb}^{3+}$  overlap very strongly,  $\text{Yb}^{3+}$  to  $\text{Tm}^{3+}$  direct energy-transfer occurs following an initial energy migration among  $\text{Yb}^{3+}$  ions. Considering the dipole-dipole interaction between a donor (Yb) and an acceptor (Tm) ion for migration assisted energy-transfer, the fluorescence decay of  $\text{Yb}^{3+}$  follows the relation [21]

$$I_{yb}(t) = I_0 \exp\left(-\frac{t}{\tau_{yb}} - \gamma^{1/2} - Kt\right) \quad (4.11)$$

$\tau_{Yb}$  is the  $Yb^{3+}$  ( ${}^2F_{5/2}$  level) fluorescence life-time in the absence of energy-transfer ( $\tau_{Yb} = 830 \mu m$ , recorded in a single Yb doped alumino-silicate fibre),  $K$  is the migration assisted energy-transfer probability and  $\gamma$  is the direct donor-acceptor energy-transfer probability. The migration assisted and direct energy-transfer probability parameters are related to the energy-transfer microscopic parameters, which are proportional to the overlap integral between the related absorption and emission spectra of acceptor and donor respectively. The donor-to-acceptor ( $C_{Yb-Tm}$ ) and the donor-to-donor ( $C_{Yb-Yb}$ ) microscopic energy-transfer parameters can be obtained from the relation [21]

$$C_{Yb-X} = \frac{3c}{8\pi^4 n^2} \int \sigma_{Yb}^{em}(\lambda) \sigma_X^{abs}(\lambda) d\lambda \quad (4.12)$$

$X$  represents either Tm or Yb.

The micro-parameters related to the first  $Yb^{3+} \rightarrow Tm^{3+}$  energy-transfer was calculated by using emission cross-section of the  ${}^2F_{5/2}$  ( $Yb^{3+}$ ) level of Yb and the corresponding absorption cross-section of  $Tm^{3+}$  ( ${}^3H_5$  level). The spectra of absorption cross-section and emission cross-section of  $Yb^{3+}$  as well as corresponding absorption cross-section of  $Tm^{3+}$  ( ${}^3H_5$  level) for one Tm/Yb-doped fibre (Fibre ID: TYDF-A-3) are shown in Fig. 4.6.

The direct donor-acceptor energy-transfer probability is given by

$$\gamma = \frac{4\pi^{3/2}}{3} N_{Tm} C_{Yb-Tm}^{1/2} \quad (4.13)$$

$N_{Tm}$  is  $Tm^{3+}$  concentration.

Due to the non-resonance between the  ${}^3H_5(Tm^{3+})$  and  ${}^2F_{5/2}(Yb^{3+})$  levels, the probability of energy migration among the  $Yb^{3+}$  sensitizers is much higher than the probability for  $Yb^{3+} \rightarrow Tm^{3+}$  direct energy-transfer on the microscopic scale,  $C_{Yb-Yb} \gg C_{Yb-Tm}$ . Hence the 'hopping model' is considered to predict the energy-transfer probability, thus  $K=K_H$  where

$$K_H = \pi \left( \frac{2\pi}{3} \right)^{5/2} C_{Yb-Tm}^{1/2} C_{Yb-Yb}^{1/2} N_{Tm} N_{Yb} \quad (4.14)$$

$N_{Yb}$  is the  $Yb^{3+}$  concentration.

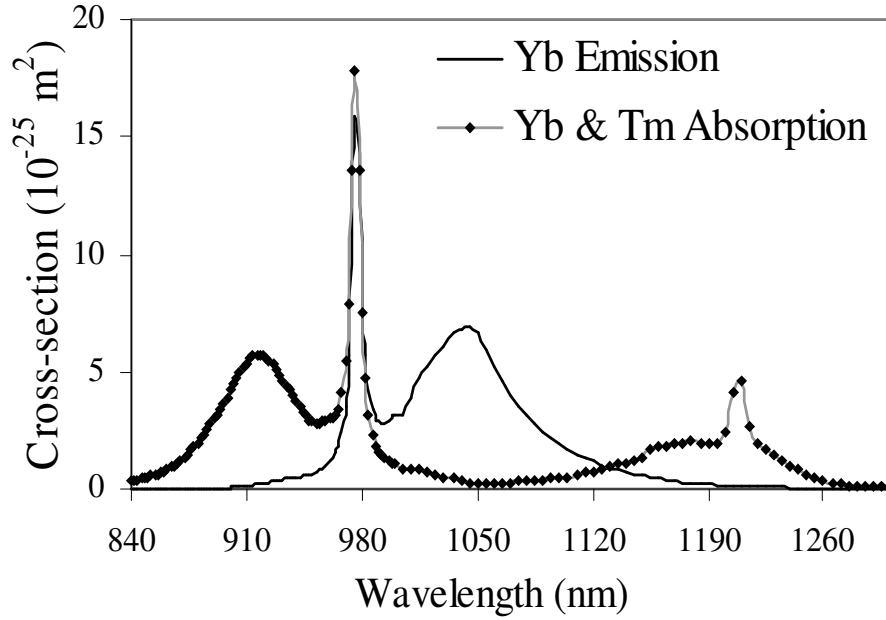


Fig. 4.6  ${}^2F_{7/2} \rightarrow {}^2F_{5/2}$  absorption and emission spectra of  $\text{Yb}^{3+}$  and  ${}^3H_6 \rightarrow {}^3H_5$  absorption spectrum of  $\text{Tm}^{3+}$  used to calculate the first step energy-transfer microparameters

Assuming that the fluorescence decay follows an exponential law, the ET1 probability  $K_1$  can be evaluated using the relations

$$K_1 = \tau_f^{-1} - \tau_{Yb}^{-1} \quad (4.15)$$

$$\text{With } \tau_f^{-1} = \frac{1}{I_0} \int_0^{+\infty} I_{Yb}(t) dt \quad (4.16)$$

$K_1$  corresponds to the mean value of the energy-transfer rate and is time independent. Nevertheless, this parameter is not directly used in the rate equations and, assuming that  $K_1$  is directly proportional to the acceptors concentration, the energy-transfer parameter, noted as  $W_1$ , is preferred:

$$W_1 = \frac{K_1}{N_{Tm}} \quad (4.17)$$

This parameter has the advantage of being directly usable in the population rate equations since it is considered independent of both time and acceptor population.

Parameters related to the first step energy-transfer of the fabricated fibres having different Yb:Tm proportion are listed in Table 4.5.

Table 4.5 Parameters for first step Yb<sup>3+</sup> to Tm<sup>3+</sup> energy-transfer (ET1)

	<b>TYDF-A-3</b>	<b>TYDF-A-4</b>	<b>TYDF-A-5</b>	<b>TYDF-A-6</b>
$C_{Yb-Tm} (\times 10^{-40} \text{ cm}^6 \text{ s}^{-1})$	6.78	6.12	5.02	146.65
$C_{Yb-Yb} (\times 10^{-40} \text{ cm}^6 \text{ s}^{-1})$	99.5	145	220	434
$\tau_f (\mu\text{s})$	818	735	700	666
$K_1 (\text{s}^{-1})$	17.7	155.72	224	297
$W_1 (\times 10^{-24} \text{ m}^3 \text{ s}^{-1})$	1.00	8.65	12.9	17.8

In order to describe the dependence of the energy-transfer probability,  $K_1$ , with the concentration of Tm and Yb ions, Fig. 4.7 presents the value of  $K_1$  versus the product of  $N_{Tm} \times N_{Yb}$  for all fibres. Linear dependence proves the accuracy of the implementation of the migration-assisted energy-transfer model.

The energy-transfer probability can also be calculated experimentally by using equations (4.15)–(4.17) taking into account the experimental Yb (<sup>2</sup>F<sub>5/2</sub> level) fluorescence decay with limited excitation pulse intensity to avoid any undesirable up-conversion effect.

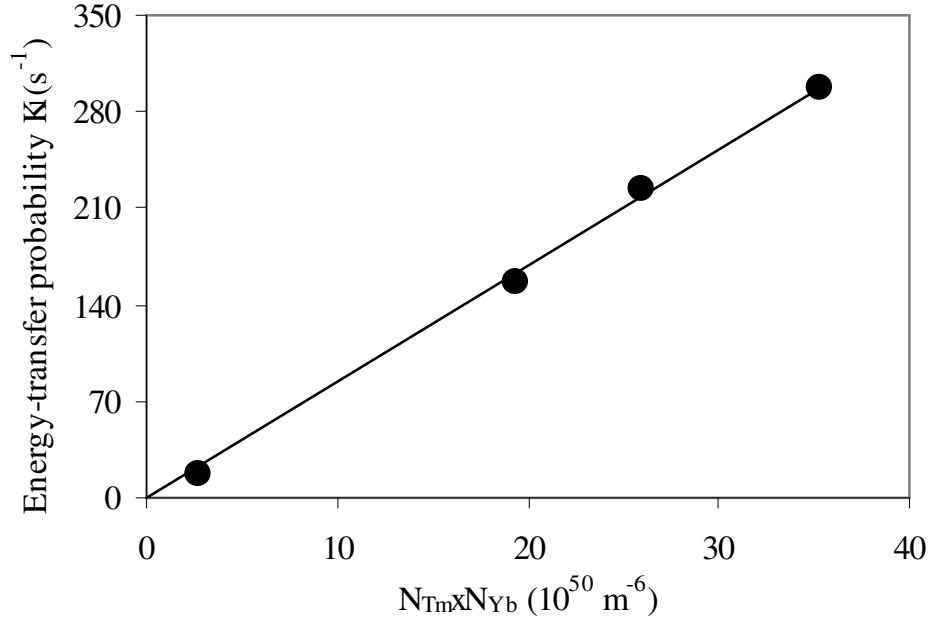
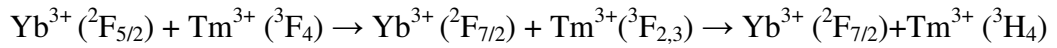


Fig. 4.7 Variation of the energy-transfer probability  $K_1$  for the first step energy-transfer as a function of the product of  $N_{Tm}$  and  $N_{Yb}$

#### 4.4.2 Second step energy-transfer

The second step energy-transfer (ET2, indicated as path  $K_2$  in Fig. 4.8) corresponds to the relaxation/excitation scheme



This step involves interaction of one excited  $Tm^{3+}$  ( $^3F_4$  level) with another excited  $Yb^{3+}$  ( $^2F_{5/2}$ ) to populate the  $^3F_{2,3}$  manifolds of  $Tm^{3+}$ . Multi-phonon decay quickly relaxes any population in the  $^3F_{2,3}$  manifolds to the  $^3H_4$  manifold. Transition from  $^3H_4$  level may occur in two different ways: (i) The  $^3H_4 \rightarrow ^3H_6$  radiative transition causes emission at near 0.8  $\mu\text{m}$  (ii) The small effective energy gap between  $^3H_4$  and  $^3H_5$  levels relaxes any population of  $^3H_4$  levels to  $^3F_4$  level to populate the latter to achieve radiative transition from  $^3F_4 \rightarrow ^3H_6$ . The energy mismatch for ET2 is nearly equal to  $\Delta E_2 \sim 830 \text{ cm}^{-1}$  and necessitates the emission of only one phonon to conserve energy. The reduction in energy mismatch than ET1 indicates better energy-transfer if sufficient number of excited  $Yb^{3+}$  exists.

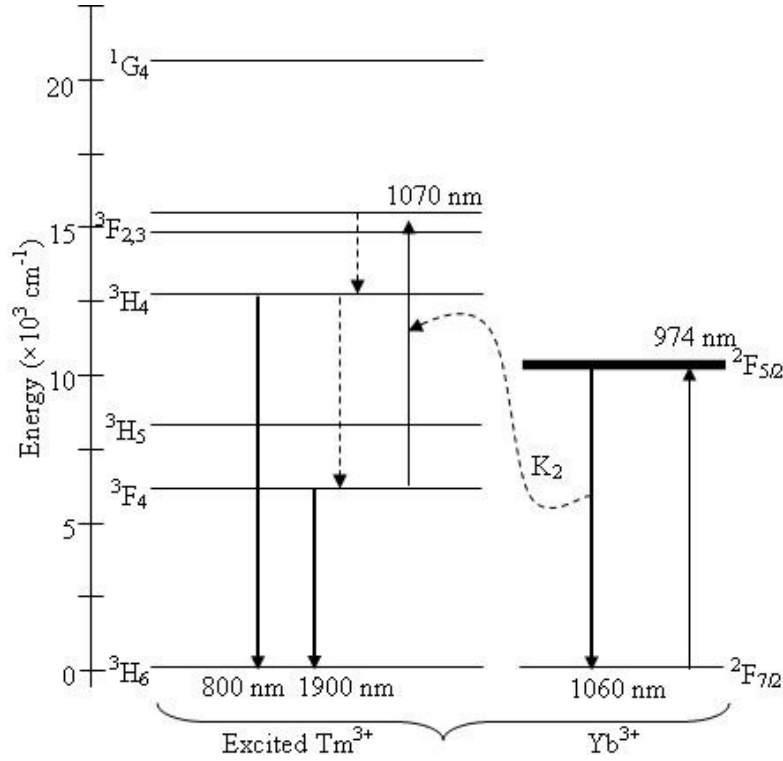


Fig. 4.8 Second energy-transfer (ET2) processes in Tm/Yb-co-doped system

To characterize ET2, the fluorescence decay curves of the  ${}^2F_{5/2}$  level ( $\text{Yb}^{3+}$ ) were recorded after direct excitation with short laser pulses with comparatively high excitation energy to build up population in the  ${}^3F_4$  level. Under the high excitation energy, ET2 contributes significantly to the progressively shortening of fluorescence life-time of the  ${}^2F_{5/2}$  level. The exponential fluorescence decay curve enables the deduction of the energy-transfer probability  $K_2$  for ET2 from the effective life-time of  ${}^2F_{5/2}$  level ( $\tau_f$ ), calculated theoretically for the ET1, and the measured life-time of  ${}^2F_{5/2}$  level at high excitation density using

$$K_2 = \tau_E^{-1} - \tau_f^{-1} \quad (4.18)$$

$\tau_E$  is the measured life-time of  ${}^2F_{5/2}$  level under high excitation. The energy-transfer parameter for this step (noted as  $W_2$ ) is

$$W_2 = \frac{K_2}{N({}^3F_4)_{Tm}} \quad (4.19)$$

assuming that at high excitation, all  $\text{Tm}^{3+}$  are at  $^3\text{F}_4$  excitation level.  $W_2$  can be used in rate equation directly.

Parameters related to the second step energy-transfer of the fabricated fibres are tabulated in Table 4.6.

Table 4.6 Parameters for second step  $\text{Yb}^{3+}$  to  $\text{Tm}^{3+}$  energy-transfer (ET2)

	<b>TYDF-A-3</b>	<b>TYDF-A-4</b>	<b>TYDF-A-5</b>	<b>TYDF-A-6</b>
$\tau_E$ ( $\mu\text{s}$ )	760	580	538	467
$K_2$ ( $\text{s}^{-1}$ )	93.3	364	430	640
$W_2$ ( $\times 10^{-24} \text{ m}^3 \text{ s}^{-1}$ )	5.30	20.2	24.7	38.3

Fig. 4.9 shows the evolution of energy-transfer parameter  $W_2$  versus Yb concentration. The linear dependence of  $W_2$  with Yb is in good agreement with the assumption made for the migration assisted energy-transfer process [18].

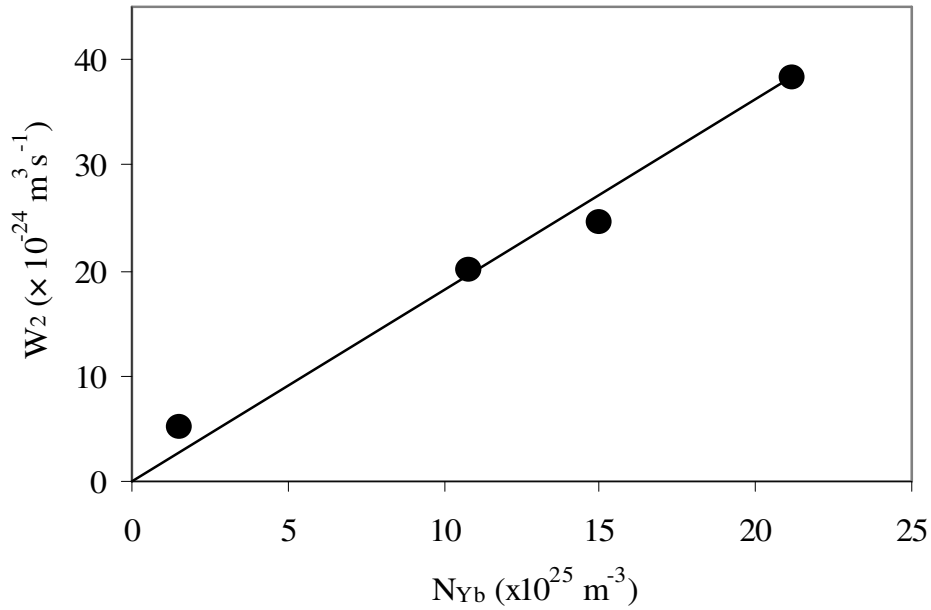


Fig. 4.9 Variation of the second step energy-transfer parameter,  $W_2$ , as a function of the  $\text{Yb}^{3+}$  concentration

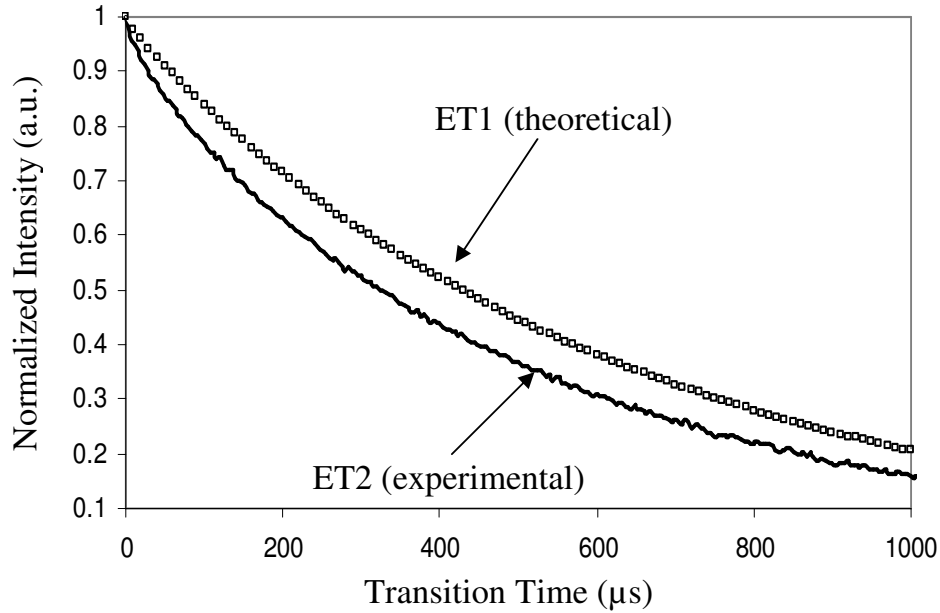
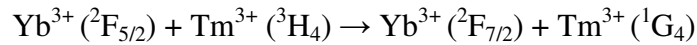


Fig. 4.10 Normalized decay curves for  ${}^2F_{5/2}$  level in TYDF-A-4 considering first step energy-transfer (theoretical) and second step energy-transfer (experimental)

The fluorescence decay curve of  ${}^2F_{5/2}$  level ( $\text{Yb}^{3+}$ ), considering ET1 (calculated using micro-parameters) and ET2 (measured) is shown in Fig. 4.10. The exponential decay mode of the Yb fluorescence in the Tm/Yb system is also a characteristic of migration assisted energy-transfer. The almost exponential measured fluorescence decay implies no clustering effects in the glass for such  $\text{Yb}^{3+}$  concentration.

#### 4.4.3 Third step energy-transfer



As soon as there are enough excited Tm-ions, another energy-transfer (ET3, indicated as path  $K_3$  in Fig. 4.11) may take place to populate  ${}^1G_4$  level from  ${}^3H_4$  resulting in blue emission ( ${}^1G_4 \rightarrow {}^3H_6$ ). The energy mismatch for ET3 is nearly equal to  $\Delta E_3 \sim 660 \text{ cm}^{-1}$  and creates the possibility of most resonant energy-transfer. However, comparatively low radiative life-time of  ${}^3H_4$  level in silica glass negates triggering of the said energy-transfer. Therefore parameters are not determined.

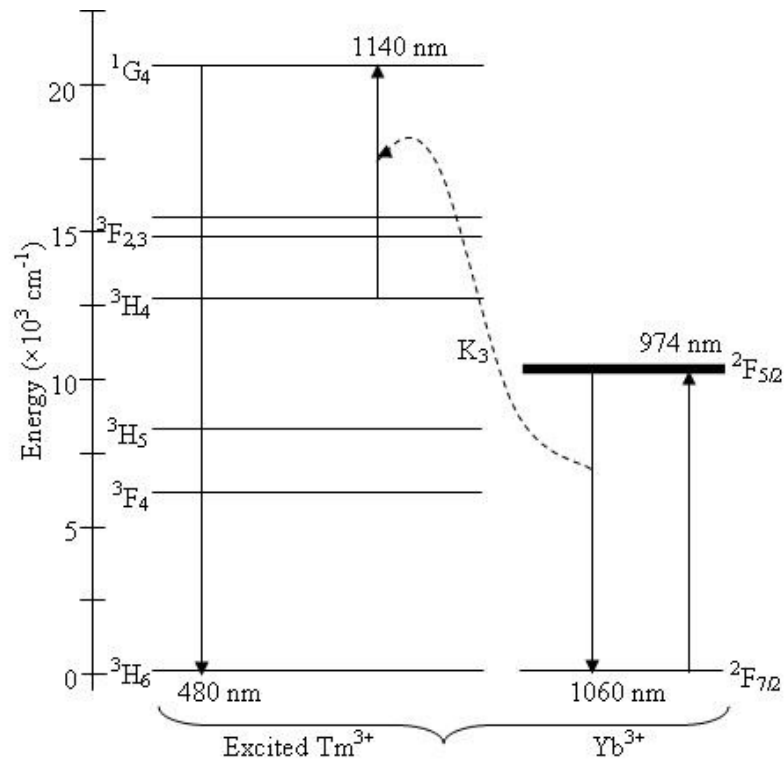


Fig. 4.11 Third energy-transfer (ET3) processes in Tm/Yb-co-doped system

The overall energy-transfer parameters, explained above, reveal that the energy-transfer efficiency increases with the concentration of Yb and shows significant increase compared to fluoride crystal hosts reported in [18]. The efficiency of emissions at wavelength ranges of 2  $\mu\text{m}$ , 0.8  $\mu\text{m}$  and 0.475  $\mu\text{m}$  with pumping at 0.98  $\mu\text{m}$ , are due to single step, double step and triple step energy-transfer respectively and strongly guided by the available donor-ion concentration with respect to the acceptor-ion concentration. Thus the optimization of Yb:Tm proportion is of extreme importance to achieve the desired emission band.

## 4.5 Optimization of Yb:Tm Proportion

The fluorescence intensity of three major emission bands (centred at 0.475, 0.79 and 1.77  $\mu\text{m}$ ) under excitation at 0.976  $\mu\text{m}$  is shown Fig. 4.12 for fibres having different Yb:Tm proportions.

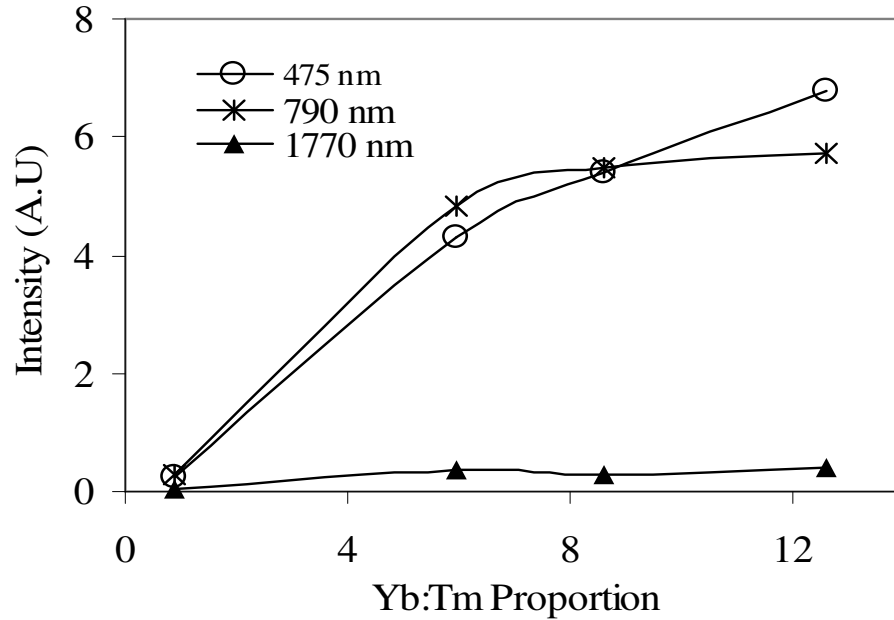


Fig. 4.12 Fluorescence intensity variations with Yb:Tm proportion for fixed pump power at  $0.976 \mu\text{m}$

It has been observed that, for the Yb:Tm concentration ratio approximately equal to unity, up-conversion emission intensity (due to double step and triple step energy-transfer) is 5 times higher than the fluorescence intensity at  $1.77 \mu\text{m}$ . For higher Yb:Tm ratio ( $>5:1$ ), the up-conversion fluorescence intensity is 14 times higher than the  $1.77 \mu\text{m}$  emission. It has also been observed that, the increment of  $1.77 \mu\text{m}$  emission with Yb:Tm proportion is almost insignificant. The lower up-conversion for unity Yb:Tm proportion can be explained by the fact that when concentration of donor-ions is almost equivalent to that of acceptor-ions, the energy-transfer process can occur in a single step in which excited  $\text{Yb}^{3+}$  transfers its energy to a nearby unexcited  $\text{Tm}^{3+}$  for  ${}^3\text{H}_6 \rightarrow {}^3\text{H}_5$  transition (responsible for broad emission from  $1.6 \mu\text{m}$  to  $2 \mu\text{m}$ ). For higher Yb:Tm proportion, one ground state  $\text{Tm}^{3+}$  interacts with more than one excited  $\text{Yb}^{3+}$  and triggers up-conversion energy-transfer. Fig. 4.12 indicates that emission intensity at  $0.79 \mu\text{m}$  saturates for the ratio beyond 5 while that at  $0.475 \mu\text{m}$  continuously increases with the increasing Yb:Tm ratio. The result reveals that to achieve emission in the  $1.77 \mu\text{m}$  range, Yb:Tm ratio

around unity will be effective while to achieve emission in the 0.8  $\mu\text{m}$  wavelength range, Yb:Tm ratio around 5:1 is beneficial. Further increase of Yb:Tm proportion will enhance the blue emission.

The saturated Amplified Spontaneous Emission (ASE) spectrum for 2  $\mu\text{m}$  was measured for the fabricated Tm/Yb-doped fibres using 0.98  $\mu\text{m}$  pumping (shown in Fig. 4.13). For these fibres, emission from  $\text{Yb}^{3+}$  at around 1.06  $\mu\text{m}$  under pumping at 0.98  $\mu\text{m}$  was used to excite the  $\text{Tm}^{3+}$ . To achieve pump saturation of  $\text{Tm}^{3+}$  throughout the length of the fibre, the length of Tm/Yb-doped fibre was optimized for 128 mW pump power at 0.98  $\mu\text{m}$ .

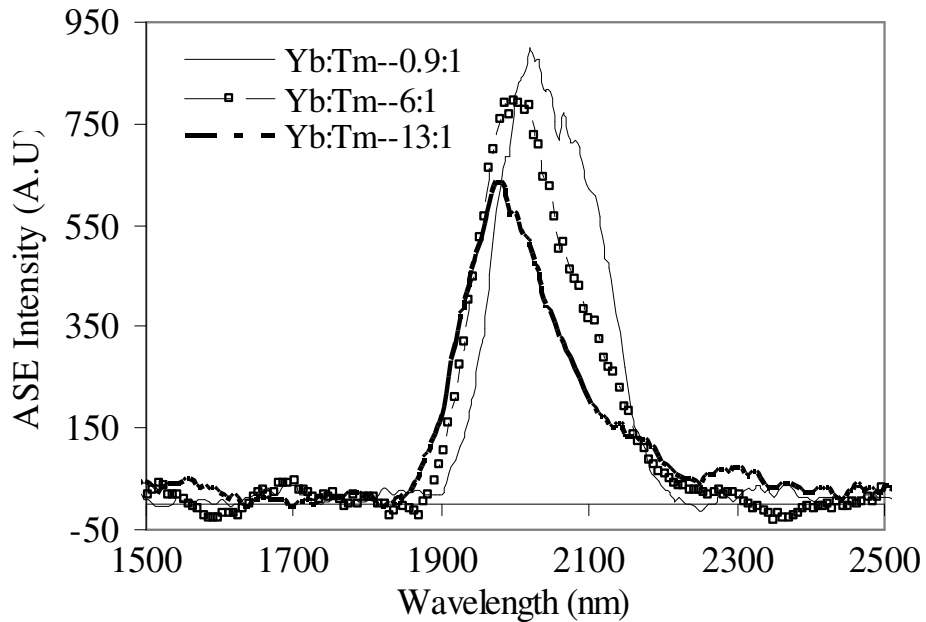


Fig. 4.13 Saturated ASE spectra of Tm/Yb-doped fibre, pumping at 0.98  $\mu\text{m}$

The result was found to be consistent with the optimization of Yb:Tm proportion to achieve efficient lasing or amplification in the 2  $\mu\text{m}$  wavelength range by utilizing the  $\text{Yb}^{3+} \rightarrow \text{Tm}^{3+}$  energy-transfer. With reference to the band structure of  $\text{Tm}^{3+}$  in silica glass, the strong overlap of the absorption and emission of the  $^3\text{F}_4$  level causes the re-absorption of the emission at this level when propagating along the length of the fibre. Longer fibre

allows a lower inversion level and a long interaction length, thereby giving ASE at longer wavelengths up to a wavelength of 2.15  $\mu\text{m}$ , exploiting the tail of  ${}^3\text{F}_4 \rightarrow {}^3\text{H}_6$  transition (the intra-Stark-level multi-phonon transitions which transfer energy from the shorter wavelengths to the longer wavelengths).

## 4.6 Summary

Basic spectroscopic parameters such as absorption/emission cross-section and fluorescence life-time specifically for ( ${}^3\text{F}_4$ ,  ${}^3\text{H}_6$ ) transition of Tm, doped in silica fibre, have been successfully obtained. A detailed spectroscopic characterization of energy-transfer mechanism in Ytterbium-sensitized-Thulium doped single-mode silica fibre has been performed. The energy-transfer parameter for the first  $\text{Yb}^{3+} \rightarrow \text{Tm}^{3+}$  energy-transfer (noted as  $W_1$ ) has been estimated on the basis of migration-assisted energy-transfer model and this has also been done for second  $\text{Yb}^{3+} \rightarrow \text{Tm}^{3+}$  energy-transfer (noted as  $W_2$ ) using the luminescent decay measurement. The linear dependence of energy-transfer parameters on the concentration of Yb under both circumstances indicates strong energy-migration among  $\text{Yb}^{3+}$  and the efficiency of emission at wavelength ranges of 2  $\mu\text{m}$ , 0.8  $\mu\text{m}$  and 0.475  $\mu\text{m}$  with pumping at 0.98  $\mu\text{m}$  are strongly determined by the Yb:Tm proportion due to the possibilities of multistep energy-transfer. It has been found that for 2  $\mu\text{m}$  emission, Yb:Tm proportion ranging from 1:1 to 2:1 is beneficial. However, to achieve up-conversion emission at 0.8  $\mu\text{m}$  the Yb:Tm proportions should be around 5:1. Further increase of Yb:Tm proportion will enhance the blue emission. The results obtained are generic and thus are suitable for analyzing Tm-doped silica fibre amplifiers and lasers providing the opportunity for future device design and optimization. The measured ASE intensity peaked at 2  $\mu\text{m}$  for Yb:Tm proportion of unity confirms the results of the above optimization.

## References

- [1] H Gebavi, D Milanese, G Liao, Q Chen, M Ferraris, M Ivanda, O Gamulin and S Taccheo ‘Spectroscopic investigation and optical characterization of novel highly thulium doped tellurite glasses’, *Journal of Non-Crystalline Solids*, Vol. 355, pp. 548-555 (2009)
- [2] M M Kozak, D Goebel, W Kowalsky and R Caspary ‘Excited state absorption spectroscopy for thulium-doped zirconium fluoride fiber’, *Optics Communications* Vol. 259, pp. 154–157 (2006)
- [3] K S Lim, P Babu, C K Jayasankar, S k Lee, V T Pham and H J Seo ‘Optical spectroscopy of thulium-doped oxyfluoroborate glass’, *Journal of Alloys and Compounds*, Vol. 385, pp. 2–18 (2004)
- [4] S D Agger and J H Povlsen ‘Emission and absorption cross section of thulium doped silica fibers’, *Optics Express*, Vol. 14, pp.50-57 (2006)
- [5] B Faure, W Blanc, B Dussardier and G Monnom ‘Improvement of the  $Tm^{3+}:^3H_4$  level lifetime in silica optical fibers by lowering the local phonon energy’, *Journal of Non-Crystalline Solids*, Vol. 353, pp. 2767–2773 (2007)
- [6] W Blanc, T L Sebastian, B Dussardier, C Michel, B Faure, M Ude and G Monnom ‘Thulium environment in a silica doped optical fiber’, *Journal of Non-Crystalline Solids*, Vol. 354, pp. 435-439 (2008)
- [7] D A Simpson ‘Spectroscopy of thulium doped silica glass’, Ph.D. thesis, Victoria University, Melbourne, Australia (2007)
- [8] C Lester, A Bjarklev, T Rasmussen and P G Dinesen ‘Modeling of  $Yb^{3+}$ -Sensitized  $Er^{3+}$ -Doped Silica Waveguide Amplifiers’ *Journal of Lightwave Technology*, Vol. 13, pp. 740-743 (1995)
- [9] S D Jackson, T A King ‘CW Operation of a 1.064  $\mu m$  Pumped Tm–Ho-Doped Silica Fiber Laser’, *IEEE Journal of Quantum Electronics*, Vol. 34, pp.1578-87 (1998)
- [10] T Yamashita and Y Ohishi ‘Energy transfer analysis between  $Tb^{3+}$  and  $Yb^{3+}$  codoped in silicate glasses under the 0.98  $\mu m$  excitation’, *CMW3, Lasers and Electro-Optics, CLEO* (2007)

- [11] H Suna, L Zhangaa, J Zhanga, L Wena, C Yua, Z Duana, S Daia, L Hua and Z Jianga ‘Intense upconversion luminescence in ytterbium-sensitized thulium-doped oxychloride germanate glass’, *Physica B*, Vol. 358, pp. 50–55 (2005)
- [12] J Pisarska, W Ryba-Romanowski, G Dominiak-Dzik, T Goryczka and W A Pisarski, ‘Energy transfer from Yb to X (X=Tm, Er) in lead borate glasses’ *Optica Applicata*, Vol. XXXV, pp. 837-842 (2005)
- [13] B Richards, S Shen, A Jha, Y Tsang and D Binks ‘Infrared emission and energy transfer in  $\text{Tm}^{3+}$ ,  $\text{Tm}^{3+}\text{-Ho}^{3+}$  and  $\text{Tm}^{3+}\text{-Yb}^{3+}$ -doped tellurite fibre’, *Optics Express*, Vol. 15, pp. 6546-6551 (2007)
- [14] S D Jackson ‘Power scaling method for 2  $\mu\text{m}$  diode-cladding-pumped Tm-doped silica fiber lasers that uses Yb codoping’, *Optics Letters*, Vol. 28, pp. 2192-2194 (2003)
- [15] J Chang, Q P Wang and G D Peng ‘Optical amplification in Yb-codoped thulium doped silica fiber’, *Optical Materials*, Vol. 28, pp. 1088-1094 (2006)
- [16] P R Watekar, S Ju and W T Han ‘800-nm Upconversion Emission in Yb-Sensitized Tm-Doped Optical Fiber’, *IEEE Photonics Technology Letters*, Vol 18, pp. 609-11 (2006)
- [17] P Peterka, W Blanc, B Dussardier, G Monnom, D Simpson and G Baxter ‘Estimation of energy transfer parameters in thulium-and ytterbium-doped silica fiber’, *Proc. of SPIE*, Vol. 7138, pp.71381K-1-6 (2008)
- [18] A Braud, S Girard, J L Doualan, M Thuau, R Moncorge and A M Tkachuk ‘Energy-transfer processes in Yb:Tm-doped  $\text{KY}_3\text{F}_{10}$ ,  $\text{LiYF}_4$ , and  $\text{BaY}_2\text{F}_8$  single crystals for laser operation at 1.5 and 2.3  $\mu\text{m}$ ’, *Physical Review B*, Vol. 61, pp.5280-5292 (2000)
- [19] M J F Digonnet ‘Rare-Earth-Doped Fiber Lasers and Amplifiers’, *Optical Engineering*, Second ed., Marcel Dekker, New York.
- [20] W T Carnall, P R Fields and K Rajnak ‘Electronic energy levels in the trivalent lanthanide aquo ions. I.  $\text{Pr}^{3+}$ ,  $\text{Nd}^{3+}$ ,  $\text{Pm}^{3+}$ ,  $\text{Sm}^{3+}$ ,  $\text{Dy}^{3+}$ ,  $\text{Ho}^{3+}$ ,  $\text{Er}^{3+}$  and  $\text{Tm}^{3+}$ ’, *Journal of Chemical Physics*, Vol. 49, pp. 4424-4442 (1968)

[21] M Louis, S Hubert, E Simoni and J Y Gesland 'Energy transfer between lanthanide and actinide ions in LiYF<sub>4</sub>', *Optical Materials*, Vol. 6, pp.121–127 (1996)

# Chapter 5

## ‘All-fibre’ Tuneable Laser at 2 $\mu\text{m}$ Region

*Abstract: A stable and tuneable Thulium-doped ‘all-fibre’ laser offering a narrow line-width in the 2  $\mu\text{m}$  wavelength region is created with an objective to produce a compact and efficient laser source for absorption spectroscopy based gas sensing. In this chapter, the fabricated Thulium- and Thulium/Ytterbium-doped optical fibres, discussed in detail in Chapter 3, were utilized as a gain medium in a fibre Bragg grating based laser resonator under in-band pumping at 1.6  $\mu\text{m}$  and/or pumping by a laser diode at 0.98  $\mu\text{m}$  utilizing Ytterbium to Thulium energy-transfer. The host composition and the dopant concentration in the single-mode single-clad fibre configuration are optimized for maximum lasing efficiency. The tuning of laser wavelength was achieved using relaxation/compression mechanism of the fibre Bragg grating. A new set of laser resonators was also formed by using a combination of a high reflective fibre Bragg grating with a low reflective broadband mirror, fabricated at the end of the fibre through silver film deposition, to enable only one fibre Bragg grating to be tuned. The stability of the laser output power, line-width and shape were monitored throughout the tuning range and the overall performance of these fibre lasers created is discussed and cross-compared in detail in this chapter.*

### 5.1 Introduction

A focused laser in the range of 2  $\mu\text{m}$  is a key component of an absorption spectroscopy based gas sensor system as the laser wavelength overlaps with strong absorption lines of toxic gases of interest [1]. The ‘in-field’ applications critically need high efficiency, high beam quality, narrow line-width, compact and reliable laser sources. While a known and

Carefully controlled operating wavelength is vital in absorption spectroscopy, semiconductor lasers are usually not readily available at the specific wavelengths that provide a close ‘match’ to the key absorption features of gases of interest. Thus semiconductor lasers have limitations compared to their fibre counterparts in terms of suitability for this type of application, as well-designed fibre lasers offer potentially much wider wavelength ranges, in addition to valuable and distinctive features such as stability, narrow line-width and tuneability at room temperatures. The fibre geometry has an additional advantage over bulk solid-state lasers because it alleviates the need for an additional delivery fibre, thus reducing cost and system complexity.

The enormous bandwidth of Thulium (Tm)  $^3F_4 \rightarrow ^3H_6$  transition in the wavelength range of  $\sim 1.7$  to  $2.1 \mu\text{m}$  in various compositions of glass makes Tm-doped fibre laser a great source of coherent radiation with broad tuneability in the range of  $2 \mu\text{m}$ , unavailable from other rare-earths (REs). Tm-doped fibre laser in low phonon-energy glass composition such as fluoride, tellurite was the research interest over the last few decades due to the high quantum efficiency of Tm in non-oxide glass [2-3]. However, the low phonon-energy non-oxide glasses have shown difficulties in practical implementation and applications, mainly due to their poor chemical durability, complex fabrication process and incompatibility with existing silica fibre-based network infrastructure. Improvement in the quantum efficiency of optical transitions can be achieved in silica glass by modifying the local environment surrounding the RE ion [4]. Tm-doped silica glass with modified host composition has also been studied for achieving lasing in the visible, S-band and NIR region [5-7]. A variety of pumping schemes by using pump sources operating at wavelengths in the region of  $\sim 0.8$  and  $\sim 1.6 \mu\text{m}$  have been explored to achieve Tm-doped fibre laser wavelength near  $2 \mu\text{m}$  [8-10]. As a pump source, diode lasers are always advantageous in terms of compactness and cost. Thus Tm-doped optical fibre sensitized with Ytterbium (Yb) has been studied extensively for up-conversion systems [11-12] and recently for high power lasing in the wavelength region of around  $2 \mu\text{m}$  [13] to take advantage of pumping through commercially available pump laser diode at  $0.98 \mu\text{m}$ . However, most of the early works on Tm- or Tm/Yb-doped fibre laser in the

wavelength range of 2  $\mu\text{m}$  were confined to particular host compositions or specific dopant concentration in ‘free-space’ laser configuration targeting power scaling of laser output power. There was a lack of optimized data on the influence of fibre core composition on the performance of lasing through  $\text{Yb}^{3+} \rightarrow \text{Tm}^{3+}$  energy-transfer process. Instead of considering only the power scaling, development of an economic but stable low power tuneable laser system is much more desirable for absorption spectroscopy based gas sensor system. Furthermore, a number of groups have demonstrated tuneability of the Tm-doped fibre laser emission in the near-IR by using bulk components, such as gratings and birefringent tuning plates [14], [15]. Recently a tuneable Tm-doped fibre ring laser based on Fabry-Perot filter (from Micron Optics) has been reported in the work of Geng et al [16]. For ‘in-the-field’ applications ‘all-fibre’ laser system, over laser system consisting bulk components, has the advantage of being more robust making it more rugged and reliable for installation and maintenance. It has been observed that ideal host composition and suitable pumping scheme in Tm-doped single-mode single-clad silica optical fibre are the major challenges to develop efficient ‘all-fibre’ lasers

With this background, the objective of the work in this chapter is to develop a simple, inexpensive and efficient tuneable ‘all-fibre’ laser in the 2  $\mu\text{m}$  wavelength region targeting applications requiring the use of absorption spectroscopy for gas sensing. A suitable host composition, dopant concentration level and effective pumping scheme have been identified on the basis of lasing efficiency. In order to obtain stable tuneability, two different fibre laser configurations have been set up, tested, evaluated and cross-compared, with an aim of achieving the best compact ‘all-fibre’ laser with a narrow line-width.

## 5.2 Pumping Scheme

A continuous wave (CW) fibre laser consists of three fundamental parts; i) the active fibre doped with RE storing pump energy in a meta-stable state for stimulated emission ii) a pump source with a wavelength matching the absorption band of the active RE ion

iii) a feedback mechanism to support the process of stimulated emission. In Tm-doped fibre laser, lasing at around 2  $\mu\text{m}$  can be achieved by using pump sources operating at wavelengths in the region of  $\sim 0.79 \mu\text{m}$ ,  $\sim 1.2 \mu\text{m}$  and  $\sim 1.6 \mu\text{m}$ . The threshold of Tm-doped fibre laser is typically tens of milliwatts, mostly as a result of the low quantum efficiency of the transition. Thus considering the availability of the pump sources, the advantage of pumping the Tm-doped fibre at 1.6  $\mu\text{m}$  rather than 0.79  $\mu\text{m}$  is twofold. First, the unavailability of a single-mode pump source operating at 0.79  $\mu\text{m}$  beyond output power of 100 mW restricts the use of a single-mode and single-clad Tm-doped fibre. But a single-mode pump source at 1.6  $\mu\text{m}$  can be readily built up by utilizing Erbium (Er)-doped fibre, pumped by a commercially available laser diode at 0.98  $\mu\text{m}$ , allowing the creation of ‘all-fibre’ laser system in standard single-clad configuration. Second, the lasing efficiency for in-band pumping at 1.6  $\mu\text{m}$  is higher than that for pumping at 0.79  $\mu\text{m}$  unless cross-relaxation phenomena is triggered by means of very high concentrations of  $\text{Tm}^{3+}$ . An alternative approach to this is co-doping the fibre core with Yb and pumping over the wavelength region from 0.91 to 0.98  $\mu\text{m}$ . The quasi-resonant energy levels of  $\text{Tm}^{3+}$  with the excited  $\text{Yb}^{3+}$  level ( ${}^2\text{F}_{5/2}$ ) allows possible  $\text{Yb}^{3+} \rightarrow \text{Tm}^{3+}$  energy-transfer; the phenomenon is similar to that in  $\text{Yb}^{3+}$  sensitized  $\text{Er}^{3+}$  doped fibres [17].

The energy level diagram of the Tm and Yb doped in a silica host is shown in Fig. 5.1. The three possible Yb to Tm energy-transfer paths are indicated as  $\text{K}_1$ ,  $\text{K}_2$  and  $\text{K}_3$ . The detailed mechanism has been described in Chapter 4, Section 4.4. During in-band pumping at 1.6  $\mu\text{m}$ , the pump photon generates population inversion between ground state and metastable state for radiative transition  ${}^3\text{F}_4 \rightarrow {}^3\text{H}_6$ . Fig. 5.1 also illustrates the strong resonance between the  $\text{Yb}^{3+}$  emission transition ( ${}^2\text{F}_{5/2} \rightarrow {}^2\text{F}_{7/2}$ ) and the excited  $\text{Tm}^{3+}$  absorption ( ${}^3\text{F}_4 \rightarrow {}^3\text{F}_2$ ) that indicates a very efficient energy-transfer. The lifetime of the  ${}^3\text{F}_2$  level can be expected to be extremely short because of narrow energy gap between the  ${}^3\text{F}_2$  and  ${}^3\text{F}_3$  energy levels of  $\text{Tm}^{3+}$ . This signifies that energy-transfer will not occur in the ‘backward’ direction. Similarly, the lifetime of the  ${}^3\text{H}_4$  and  ${}^3\text{H}_5$  levels are sufficiently short and multi-phonon decay allows the relaxation of population in the  ${}^3\text{F}_2$

and  ${}^3F_3$  levels to the  ${}^3F_4$  level via the  ${}^3H_4$  and  ${}^3H_5$  levels. This population mechanism of  ${}^3F_4$  level activates the radiative transition from  ${}^3F_4 \rightarrow {}^3H_6$  i.e. producing broadband emission in the wavelength range of 2  $\mu\text{m}$ . However, the presence of some initially excited  $\text{Tm}^{3+}$  brings down the threshold of the above-mentioned energy-transfer. Additionally the quasi-resonant energy-transfers from  ${}^3H_6 \rightarrow {}^3H_5$  /  ${}^3H_4 \rightarrow {}^1G_4$  also take place as soon as there is sufficient excited population of  $\text{Tm}^{3+}$  and blue ( ${}^1G_4 \rightarrow {}^3H_6$ ) and dark red ( ${}^3H_4 \rightarrow {}^3H_6$ ) emissions occur simultaneously with the NIR.

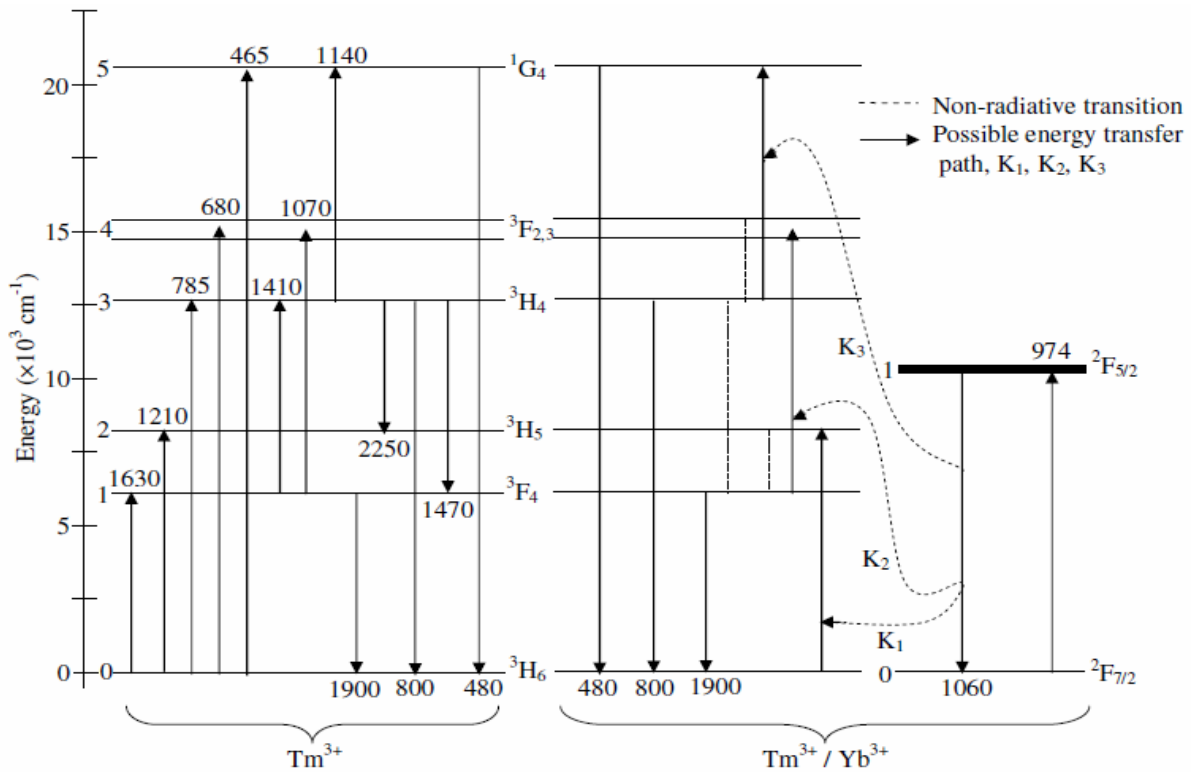


Fig. 5.1 Energy level of Tm/Yb doped in silica using Russell-Saunders Coupling. All transition wavelengths are in ‘nm’

Consequently, the use of auxiliary pumping of  $\text{Tm}^{3+}$  at  $\sim 1.6 \mu\text{m}$  has been explored to achieve the initial  ${}^3H_6 \rightarrow {}^3F_4$  excitation to trigger the efficient  $\text{Yb}^{3+} \rightarrow \text{Tm}^{3+}$  energy-transfer [ $\text{Yb}^{3+} ({}^2F_{5/2}), \text{Tm}^{3+} ({}^3F_4) \rightarrow \text{Yb}^{3+} ({}^2F_{7/2}), \text{Tm}^{3+} ({}^3F_2)$ ], when pumped with 0.98  $\mu\text{m}$  primary pump. The proposed pumping scheme is highly effective for achieving lasing near 2  $\mu\text{m}$  in single-mode single-clad silica fibre configuration.

## 5.3 Experimental Work

### 5.3.1 Design of a laser resonator

#### 5.3.1.1 Pump laser at 1.6 $\mu\text{m}$

Prior to setting up the Tm-doped ‘all-fibre’ laser system, an Er-doped fibre laser operating at 1.6  $\mu\text{m}$  was configured to utilize as a pump source. Er-doped fibres have been fabricated in-house by using Modified Chemical Vapour Deposition (MCVD) system coupled with solution doping technique as discussed in detail in Chapter 3. The main laser transition in Er-doped silica fibre ( ${}^4I_{13/2} \rightarrow {}^4I_{15/2}$ ) for the wavelength range of  $\sim 1.5 \mu\text{m}$  to  $1.62 \mu\text{m}$ , centred at  $1.55 \mu\text{m}$  under pumping at  $0.98 \mu\text{m}$  has been utilized. Pumping of Er-doped fibre lasers at near  $0.98 \mu\text{m}$  wavelength exhibits highest gain efficiency as there is no possibility of Excited State Absorption (ESA). In such a three-level laser system, the fibre length is an important design parameter that affects the threshold, slope-efficiency and operating wavelength. As the fibre length is increased, the laser shifts toward longer wavelength [1]. The schematic diagram of the laser resonator is shown in Fig. 5.2.

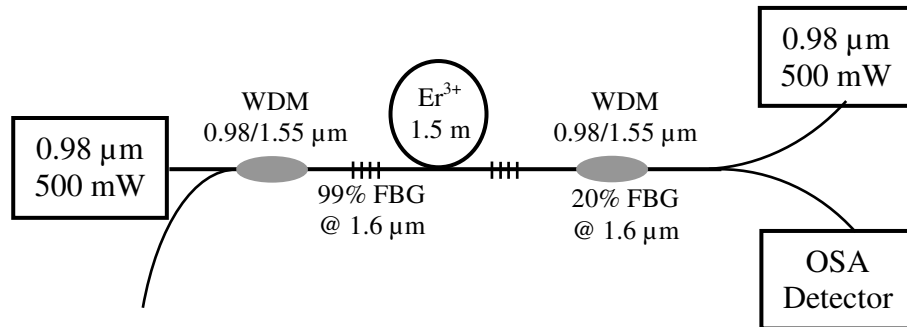


Fig. 5.2 Schematic of a 1.6  $\mu\text{m}$  Er-doped fibre laser set-up to be used as a pump source for a Tm-doped fibre laser

The laser resonator was designed using 1.5 m long Er-doped fibre (Er<sup>3+</sup> concentration:  $\sim 0.5 \text{ mol}\%$ ), a matched pair of fibre Bragg gratings (FBGs) having Bragg wavelengths

centred at 1.6  $\mu\text{m}$  with reflectivity of  $\sim 99.9\%$  (HR: High Reflective) and  $\sim 20\%$  (LR: Low Reflective) and bidirectional pump at 0.98  $\mu\text{m}$ . FBGs were fabricated ‘in-house’ by using commercial photosensitive fibres through ‘Phase-mask Technique’ [18]. Both the length of the active fibre and the reflectivity of the LR FBG were optimized in order to achieve the maximum laser output power. As shown in Fig. 5.3, a stable laser output power of 130 mW at 1.6  $\mu\text{m}$  has been achieved when the pump power is 850 mW at 0.98  $\mu\text{m}$  and used for pumping Tm-doped fibre laser. Inset shows the spectrum of the laser.

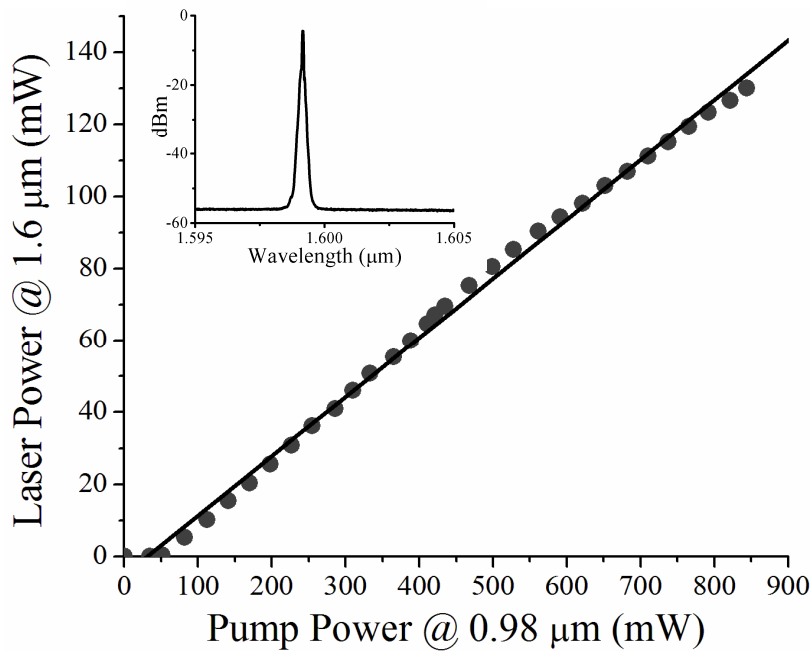


Fig. 5.3 Variation of laser output power with pump power; Inset: Spectrum of the laser

### 5.3.1.2 Laser resonator at $\sim 2 \mu\text{m}$

Two different fibre laser configurations were set up: one using a matched pair of narrow line-width FBGs and the other with a combination of a high reflective FBG and a low reflective broadband mirror fabricated on the end surface of the fibre. The active Tm- and Tm/Yb-doped silica fibres were fabricated using the MCVD-solution doping technique, discussed in detail in Chapters 3.

### FBG-pair based laser resonator

In a FBG-pair based laser resonator, fibre laser at 1.6  $\mu\text{m}$  was used as a pump source for Tm-doped active fibre while a combination of auxiliary pump at 1.6  $\mu\text{m}$ , unidirectional with the standard 0.98  $\mu\text{m}$  pump laser diode was utilized for Tm/Yb-doped active fibre. The schematic diagrams of the laser resonator operating wavelength at around 2  $\mu\text{m}$  under above mentioned pumping schemes are shown in Fig. 5.4(a) and Fig. 5.4(b) respectively.

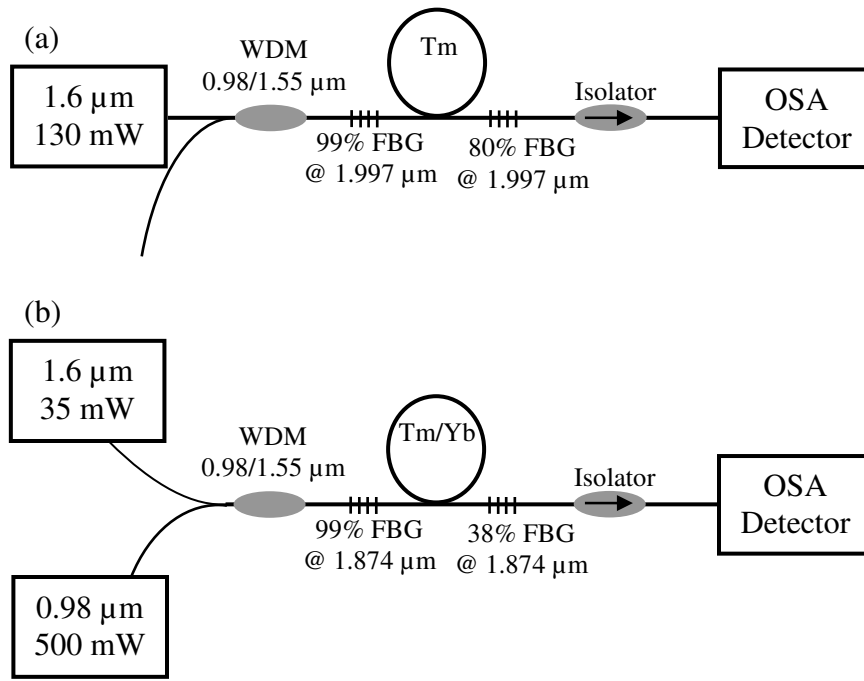


Fig. 5.4 Schematic of the laser resonator (a) at 1.997  $\mu\text{m}$  under pumping at 1.6  $\mu\text{m}$  (b) at 1.874  $\mu\text{m}$  under dual pump combination of 1.6  $\mu\text{m}$  and 0.98  $\mu\text{m}$

Under condition of pumping at 1.6  $\mu\text{m}$ , for the Tm-doped fibre laser operating at 1.997  $\mu\text{m}$ , selected reflectivity of the HR FBG and the LR FBG were 99.9% and 80% respectively while for laser resonator operating at 1.874  $\mu\text{m}$ , the reflectivity of the HR FBG and the LR FBG were 99.9% and 38% respectively. This specific difference was aimed to achieve a lower threshold as the emission cross-section of Tm in silica glass is lower at 1.997  $\mu\text{m}$  than that of at 1.874  $\mu\text{m}$  [19]. The obtained line-width of both lasers

was 0.14 nm, measured in the OSA–AQ6375 (with a resolution of 0.05 nm). The length of the active fibre was optimized for each fibre having different level of Tm and different host composition on the basis of maximum obtained laser output power. The variation of the laser output power at 1.997 and 1.874  $\mu\text{m}$  with pump power at 1.6  $\mu\text{m}$  is shown in Fig. 5.5.

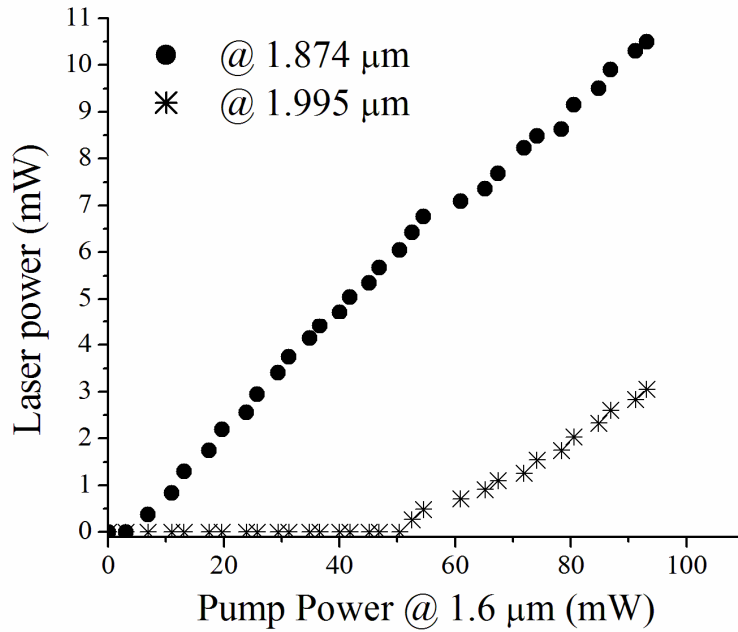


Fig. 5.5 Variation of the Tm-doped fibre laser output power with pump power at 1.6  $\mu\text{m}$

Under condition of dual pumping, for the Tm/Yb-doped fibre laser, a FBG-pair centred at wavelength at 1.874  $\mu\text{m}$  with reflectivity of 98% and 38% were used. The power of the auxiliary pump at 1.6  $\mu\text{m}$  was fixed at a minimum level ( $\sim 35$  mW power for this work) to prevent starting of lasing at 1.874  $\mu\text{m}$ . Thus the 1.6  $\mu\text{m}$  pump was used only for initial excitation of  $\text{Tm}^{3+}$  to  $^3\text{F}_4$  energy level; not for power scaling. The active fibre length was optimized for each fibre having different host compositions, Tm-ion concentrations and Yb to Tm proportions on the basis of the obtained maximum laser output power. The variation of laser power with pump power at 0.98  $\mu\text{m}$  is shown in Fig. 5.6.

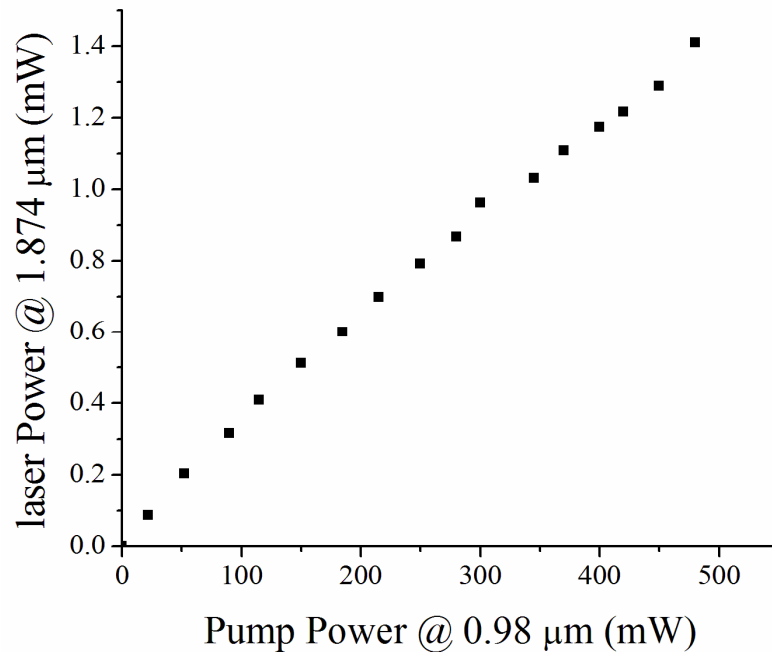


Fig. 5.6 Variation of Tm/Yb-doped fibre laser output power with pump power at 0.98 μm

#### *FBG-Mirror based resonator*

A new set of laser resonator was designed where LR FBG in Fig. 5.4 was replaced by a low reflective broadband mirror to enable only one FBG to be tuned to obtain tuneability of laser wavelength. In order to fabricate such broadband mirror, the cleaved fibre end was carefully prepared to achieve high quality outcome: it was cleaned with a stannous chloride solution (0.2%) to sensitize the coating area and then rinsed with de-ionized water. A dextrose solution (0.4 ml, 0.25 M) was poured into a tube containing Tollen's reagent and the fibre end was then dipped into the solution. The silver film was thus formed very rapidly. Finally, the fibre was thoroughly cleaned with de-ionized water [20]. The rate of deposition as well as the reflectivity of the fabricated mirror was controlled through the modification of the strength of the Tollen's reagent and as a result the fabrication process was very repeatable. The reflection spectrum of the fabricated mirror was monitored on-line through a white light source (WLS), 3dB coupler and OSA over the wavelength range from 1.5 μm to 1.6 μm and is shown in Fig. 5.7.

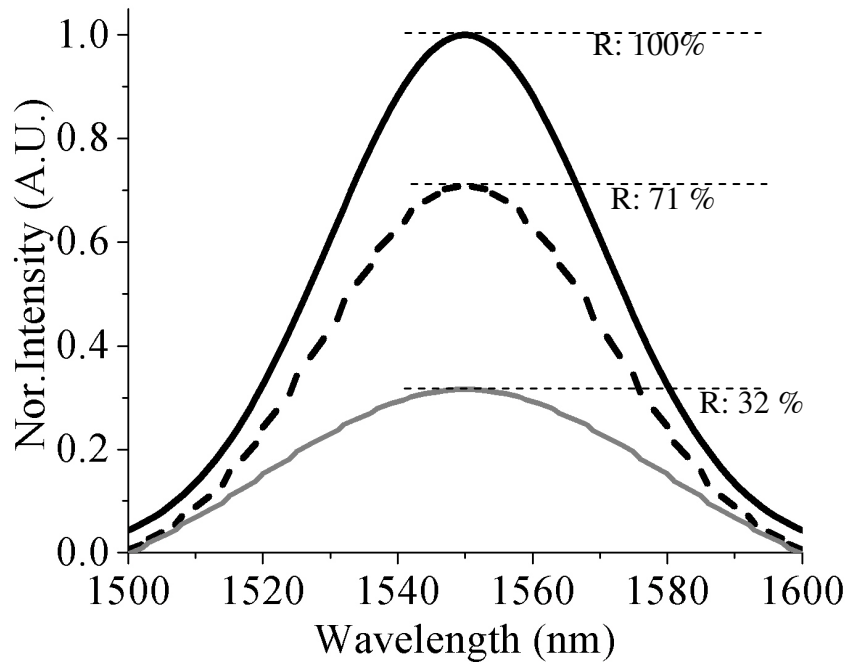


Fig. 5.7. Reflection spectrum of a mirror fabricated at the fibre end face

A reference mirror was fabricated and calibrated against a standard mirror having 100% reflectivity. Then a set of mirrors was fabricated with reflectivity ranging from 10% to 85% through the control of the silver film deposition rate and deposition time. These mirrors were utilized together with a HR FBG with centred wavelength at 1.997  $\mu\text{m}$ , to form a laser resonator, as shown schematically in Fig. 5.8. It was observed that when the mirror has the reflectivity of 80%, a maximum output power of the fibre laser was achieved. The variation of laser output power with pump power at 1.6  $\mu\text{m}$  is shown in Fig. 5.9.

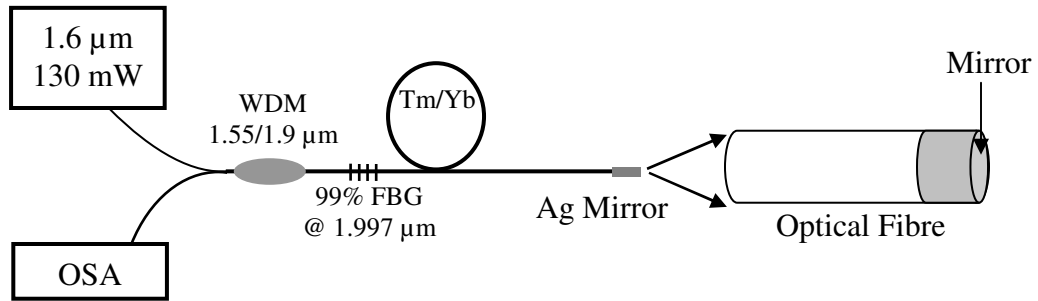


Fig.5.8 Schematic of the laser resonator by using a HR FBG and a broadband mirror (LR) fabricated at fibre end face

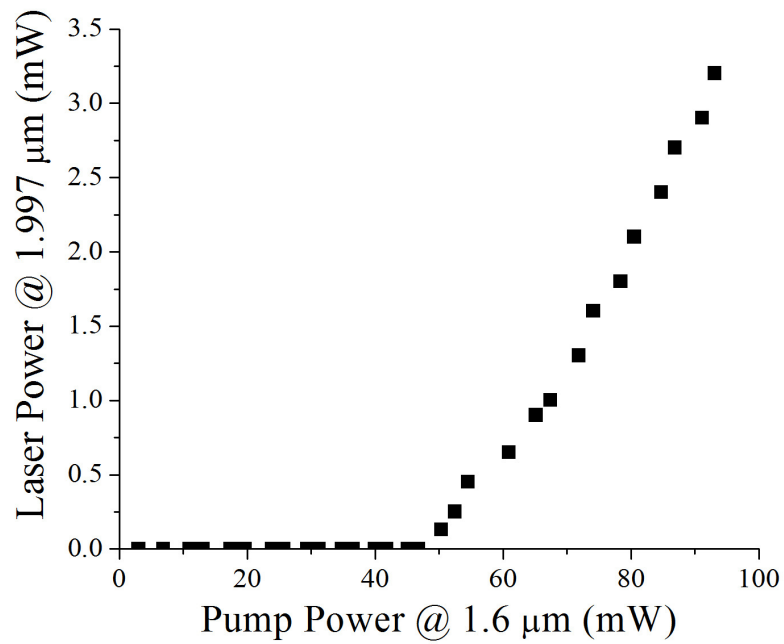


Fig. 5.9 Variation of the Tm-doped fibre laser (FBG-Mirror) output power with pump power at 1.6 μm

## 5.3.2 Performance of Laser at ~ 2 $\mu\text{m}$

### 5.3.2.1 Effect of host composition

The emission and lasing property of rare-earth-doped glass are strongly influenced by the local environment of doped rare-earth ions. For example the host composition has a significant influence on the radiative transition of  $\text{Tm}^{3+}$  as well as on the  $\text{Yb}^{3+} \rightarrow \text{Tm}^{3+}$  energy transfer. For  $\text{Tm}^{3+}$  in oxide glass, the energy gap between  $^3\text{F}_4$  and  $^3\text{H}_6$  levels ( $5800 \text{ cm}^{-1}$ ) is not broad enough for efficient radiative transition ( $^3\text{F}_4 \rightarrow ^3\text{H}_6$ ) and thus the NIR emission is very much host composition sensitive. In an effort to identify suitable host composition for only Tm-doped fibre (TDF), a set of fibres has been selected from Table 3.3 in Chapter 3 where the doping level of Tm-ions is almost identical but in a variety of host glass composition. Similarly for Tm/Yb-doped fibre (TYDF), the selected fibres have almost identical Tm-ion and Yb-ion concentrations with unit Yb:Tm proportion but in different host composition. The laser characteristics at operating wavelength of  $1.874 \mu\text{m}$  for each set of fibres were carried out under direct pumping at  $1.6 \mu\text{m}$  as well as under dual pumping at  $0.98 \mu\text{m}$  and  $1.6 \mu\text{m}$ . The parameters of the TDF as well as TYDF fibres and their corresponding laser output power are presented in Table 5.1.

Table 5.1: Fibre parameters for TDF and TYDF having different host composition

Fibre ID	Host Composition	$\text{Tm}^{3+}$ (mol%)	$\text{Yb}^{3+}$ (mol%)	$^3\text{F}_4 \tau_{\text{rad}}$ (ms) calculated	Laser Output Power (mW)
Direct pumping at $1.6 \mu\text{m}$					
TDF-A-2	$\text{Al}_2\text{O}_3 + \text{SiO}_2$ (Al: 4 mol%)	0.03	---	7.0	10.9
TDF-A-1	$\text{Al}_2\text{O}_3 + \text{GeO}_2 + \text{SiO}_2$ (Al: 0.9 mol%; Ge: 7 mol%)	0.024	---	7.1	10.3
TDF-A-3	$\text{Al}_2\text{O}_3 + \text{P}_2\text{O}_5 + \text{SiO}_2$ (Al: 9 mol%; P: 6.3 mol%)	0.031	---	3.8	3.6

Dual pumping at 0.98 $\mu\text{m}$ and 1.6 $\mu\text{m}$					
TYDF-A-1	$\text{Al}_2\text{O}_3+\text{SiO}_2$ (Al: 4 mol%)	0.03	0.028	6.4	0.5
TYDF-AG-2	$\text{Al}_2\text{O}_3+\text{GeO}_2+\text{SiO}_2$ (Al: 0.9 mol%; Ge: 7.94 mol%)	0.024	0.023	7.2	0.6
TYDF-AP-2	$\text{Al}_2\text{O}_3+\text{P}_2\text{O}_5+\text{SiO}_2$ (Al: 9.86 mol%; P: 6.3 mol%)	0.031	0.041	3.0	----

The data given in the table indicate that the calculated radiative life-time ( $\tau_{\text{rad}}$ ) of  $^3\text{F}_4$  level of Tm is lowest for alumino-phospho-silicate host and highest for alumino-germano-silicate host. Fig. 5.10 and Fig. 5.11 show the variation of Tm laser output power at 1.874  $\mu\text{m}$  with pump power at 1.6  $\mu\text{m}$  and 0.98  $\mu\text{m}$  respectively for the fibres having alumino-silicate, alumino-germano-silicate and alumino-phospho-silicate hosts. The length of Tm-doped fibre in resonator was optimized on the basis of obtained maximum laser output power. The laser output power can be scaled up by increasing the pump power.

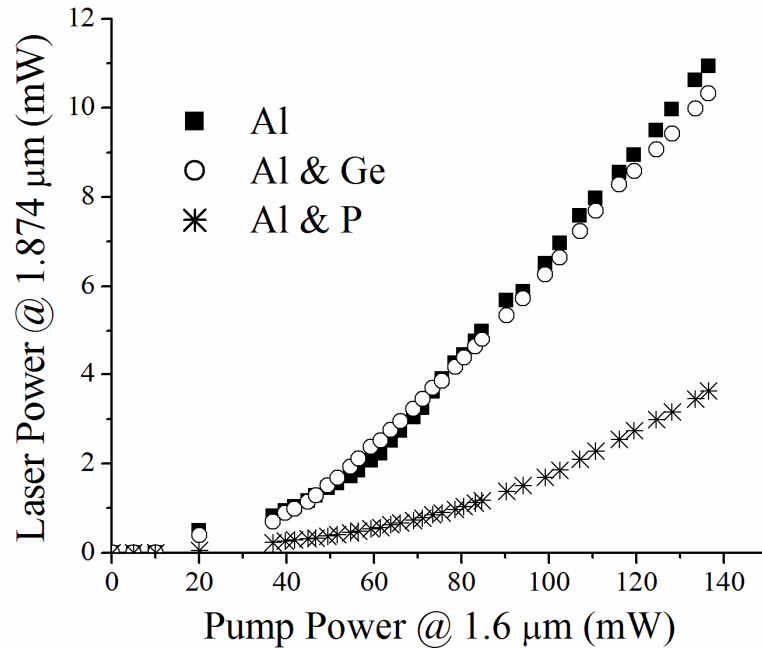


Fig. 5.10 Tm-doped fibre laser output power at 1.874  $\mu\text{m}$  against 1.6  $\mu\text{m}$  pump

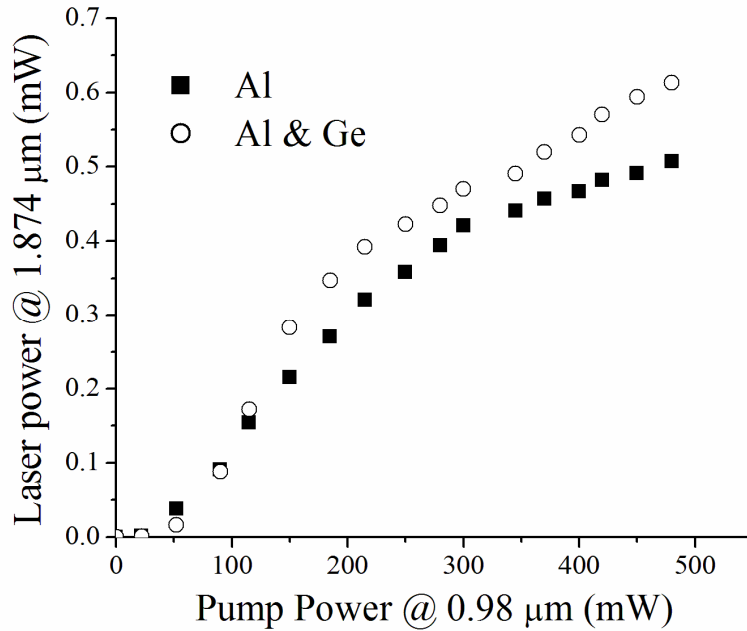


Fig. 5.11 Tm-doped fibre laser output power at 1.874  $\mu\text{m}$  against 0.98  $\mu\text{m}$  pump

The curves indicate that, the fibres having alumino-silicate and alumino-germano-silicate host show very good laser output under both pumping schemes. Phosphorus (P) co-doped fibre provides poor lasing performance under 1.6  $\mu\text{m}$  pumping while there was no detectable laser output power for 0.98  $\mu\text{m}$  pumping. It produces only 15  $\mu\text{W}$  laser power under pump power of 480 mW at 0.98  $\mu\text{m}$ , which indicates the population of  $\text{Tm}^{3+}$  ions in the  $^3\text{F}_4$  level is not sufficient for lasing. The reason behind this appears to be the increase in phonon energy and reduction of lifetime due to the addition of P into the fibre core [21]. On the other hand, co-doping of Al reduces the local phonon energy of silica glass and consequently increases the lifetime of the  $\text{Tm}^{3+}$  energy levels. Ge is a four-coordinated network former, hence does not significantly alter the tetrahedral structure of the silica network. So it is expected that the effect of Ge is not very prominent in altering the lifetime [20]. Of the two TYDFs studied, the alumino-germano-silicate (TYDF-AG-2) host provides slightly better lasing performance as well as energy-transfer compared to the alumino-silicate host fibre (TYDF-A-1). It is noted that TYDF-AG-2 contains lower Al concentration than TYDF-A-1. The influence of Al is, in general, beneficial to increase

the lifetime (up to 3 times for  $^3F_4$  and  $^3H_4$  levels of  $Tm^{3+}$ ) and thus the radiative transition of  $Tm^{3+}$ . It should be noted that with the enhancement of the  $^3F_4$  lifetime, there is also significant increase in the  $^3H_4$  lifetime. For the energy-transfer mechanism proposed in this work, longer  $^3H_4$  lifetime will trigger the third step energy-transfer ( $^3H_4 \rightarrow ^1G_4$ ), leading to more enhanced blue emission ( $^1G_4 \rightarrow ^3H_6$ ) and radiative transition  $^3H_4 \rightarrow ^3H_6$  causing red emission. That will deteriorate the mechanism for population of the  $^3F_4$  level from the  $^3F_2$  level via non-radiative transition of the  $^3H_4$  level. As the laser output in the NIR depends strongly on the population of the  $^3F_4$  level, fibre TYDF-AG-2 provides a better laser output than does TYDF-A-1. The radiative lifetime of  $^3F_4$  level, calculated from the measured absorption spectra (provided in Table 5.1), also shows that the lifetime of TYDF-AG-2 is slightly longer than that of TYDF-A-1 whereas TYDF-AP-2 shows a very low value with respect to the other two fibres. These calculated values are in good agreement with the results shown in Fig. 5.10 and Fig. 5.11. Thus observing the lasing performance, alumino-silicate host fibre is found to be the most suitable in terms of fabrication process and waveguide properties.

### 5.3.2.2 Effect of Yb:Tm proportion

For radiative energy-transfer, i.e. one ion emitting a photon and being absorbed by another ion, the proportion of donor to acceptor ions plays an important role. In the Tm/Yb system, there are three possible energy-transfer paths as discussed in section 5.2 and it is reasonable to expect that an optimized Yb:Tm proportion exists which will allow one particular energy-transfer path to be dominant. To study the effect of Yb:Tm proportion on the lasing performance in the NIR, the following alumino-silicate fibres (TYDF-A) were selected where concentration level of Tm-ion and Al are almost similar with variation of Yb:Tm proportion. The parameters of the fibres and their corresponding laser output power at  $1.874 \mu m$  (for 480 mW pump power at  $0.98 \mu m$ ) are presented in Table 5.2.

Table 5.2 Fibre parameters for TYDF having different Yb:Tm proportion

<b>Fibre ID</b>	<b>Tm<sup>3+</sup> (mol%)</b>	<b>Yb:Tm</b>	<b>Laser Output Power (mW)</b>
TYDF-A-2	0.090	1.05	1.156
TYDF-A-7	0.081	1.85	1.002
TYDF-A-8	0.07	3.0	0.231
TYDF-A-4	0.082	5.98	0.219
TYDF-A-11	0.08	12.1	0.2

The variation of maximum laser output power with the Yb:Tm ratio is presented in Fig. 5.12. The results indicate that the laser output power of 1.15 mW was achieved when the Yb:Tm ratio is approximately equal to unity. It was also observed that laser output for the fibres varies with the Yb:Tm ratio. When the ratio is greater than two, there is a significant drop in the output power, suggesting photodarkening effect is prominent in fibres doped with higher level of Yb. On the other hand the blue and red emissions were very prominent. This indicates that when Yb:Tm ratio is more than two, each unexcited Tm interacts with more than one excited Yb thus supporting up-conversion through  $\text{Yb}^{3+} \rightarrow \text{Tm}^{3+}$  energy-transfer by reducing the laser power at 1.874  $\mu\text{m}$ . The result leads to the conclusion that a ratio close to unity is most suitable to populate the  $^3\text{F}_4$  level of  $\text{Tm}^{3+}$  through energy-transfer and consequently for the efficient lasing in the NIR range with minimum up-conversion loss.

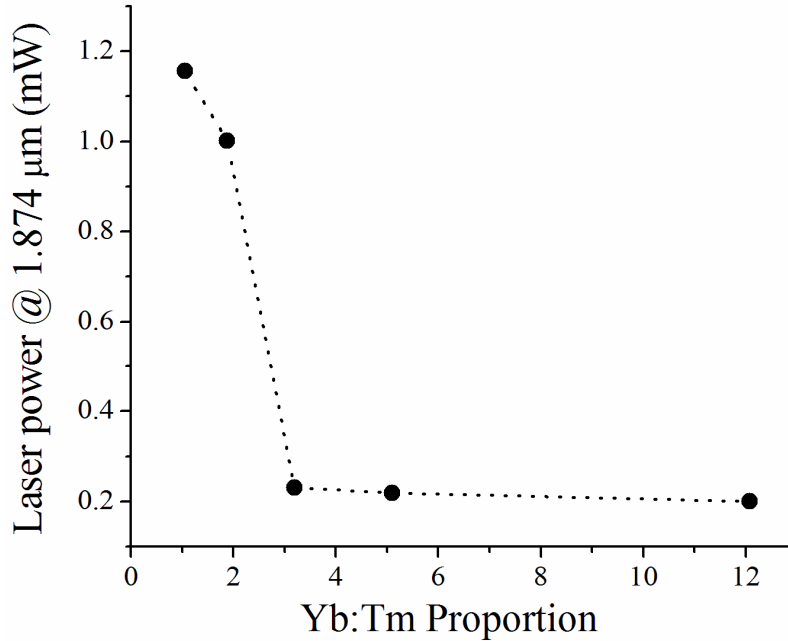


Fig. 5.12 Laser output power at 1.874  $\mu\text{m}$  against 0.98  $\mu\text{m}$  pump (480 mW) for fibres with different  $\text{Yb}^{3+}:\text{Tm}^{3+}$  ratio

### 5.3.2.3 Effect of Tm-ion concentration

Since the spatial electronic distribution is different for each energy level, the overlap integral as well as the energy-transfer probability of each path depends on the concentration in a different way. To investigate this, for a set of alumino-silicate host fibres with increasing Tm-ion concentration but having the Yb:Tm ratio approximately unity, the laser output powers were measured at 1.874  $\mu\text{m}$  with variation of 0.98  $\mu\text{m}$  pump power. It was noted that, with the increase of Tm-ion concentration, a shorter fibre length is required to obtain higher laser output power. Details of the fibre parameters and laser output power are given in Table 5.3. The power level of auxiliary  $\sim 1.6 \mu\text{m}$  pump was fixed in a range of 40 to 60 mW depending on the ground state  $\text{Tm}^{3+}$  concentration. For each fibre, the laser output power increases with the increase of pump power. Maximum laser output power (with 480 mW pump power at 0.98  $\mu\text{m}$ ) increases with the increase of the  $\text{Tm}^{3+}$  concentration up to a certain level and beyond that, the laser power starts to drop, as shown in Fig. 5.13. This indicates that, the Tm-doped active fibre in

single mode and single clad configuration can contain Tm-ion concentration of around 0.1061 mol% with minimum clustering effect.

Table 5.3 Fibre parameters for TYDF having different Tm concentration

Fibre ID	Tm <sup>3+</sup> (mol%)	Laser Output Power (mW)
YTDF-A-1	0.03	0.507
YTDF-A-9	0.056	0.766
YTDF-A-4	0.082	1.156
YTDF-A-10	0.1061	1.325
YTDF-A-11	0.1806	0.873

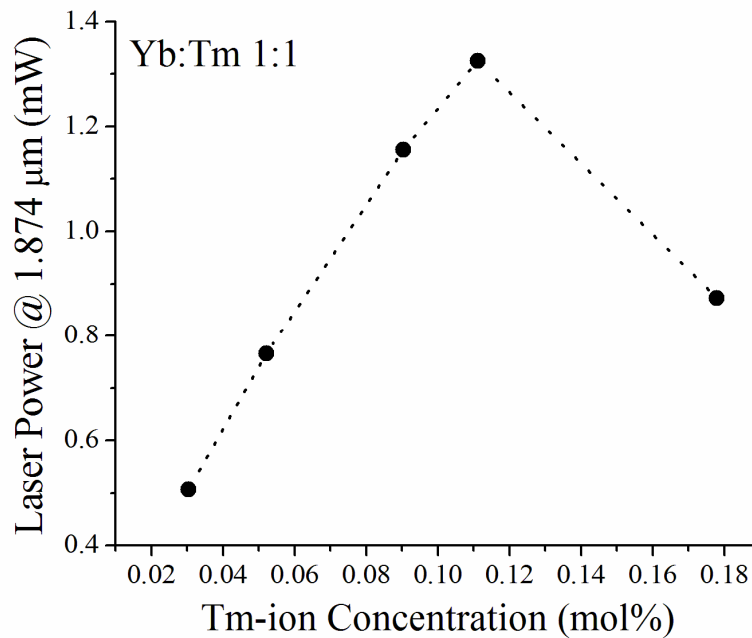


Fig. 5.13 The variation of the maximum laser output power with Tm<sup>3+</sup> concentration variation

These results indicate that the energy-transfer rate of this process is proportional to the ground state Tm<sup>3+</sup> concentration; however with the increase of Tm<sup>3+</sup> concentration

beyond 0.1 mol% in a single-mode single-clad fibre configuration, the laser performance deteriorates indicating the clustering of rare-earth-ions even for alumino-silicate glass host.

### 5.3.3 Tuning of laser resonator

Once a laser resonator has been designed with optimum length of active fibre having suitable host composition and dopant concentration, the laser wavelength can be tuned by imposing strain to the FBGs forming the laser resonator. Thus the wavelength shift  $\Delta\lambda_B$  of the FBG centre wavelength for a given longitudinal strain  $\varepsilon_z$  is given by

$$\frac{\Delta\lambda_B}{\lambda_B} = (1 - p_e)\varepsilon_z \quad (5.1)$$

The term  $p_e$  is an effective photoelastic constant of the fibre. In particular, the wavelength shift is negative for compressive strains and positive for tensile strains. Bragg wavelength tuning by tensile stress is limited by fibre strength and the limitations are relieved when compressive stress is implemented, because silica is 23 times stronger under compression than under tension [22].

Thus an axial compression technique was considered that uniformly compresses FBGs embedded into a beam made of flexible material (Makroform vivak clear 099) having a Young's modulus of 2050 N/mm<sup>2</sup>, by using cyanoacrylic adhesive (Loctite 435). This material firmly adheres to the fibre to prevent any drift during the tuning process. The beam was then fixed tightly on a system of fixed mount and a movable mount. The inward translation of the movable mount, driven by a micro-screw, transfers axial compression to the beam as well as to the FBGs embedded on the beam. Thus in the compression mount, a horizontal displacement ( $\Delta z$ ) was achieved resulting mechanical compression ( $\varepsilon_z = \Delta z/L$ ) imposed on the FBG. The applied compression modified the period and effective refractive index resulting in a Bragg wavelength shift. The stressed fibre length, L, was 44 mm.

In order to tune the laser wavelength for the FBG-pair based laser resonator, both the FBGs were embedded in the beam while for the FBG-mirror based resonator, only the HR FBG was embedded. Together with the FBGs, a reference FBG, with a centred wavelength at 1.548  $\mu\text{m}$  was also embedded in the same material to monitor the laser wavelength shift through an interrogator instead of expensive long wavelength OSA.

Fig. 5.14 illustrates the normalized laser spectrum, as a function of the compression (negative strain) over the tuning wavelength range for the FBG-pair based laser resonator, achieved by tuning the FBG-pair simultaneously.

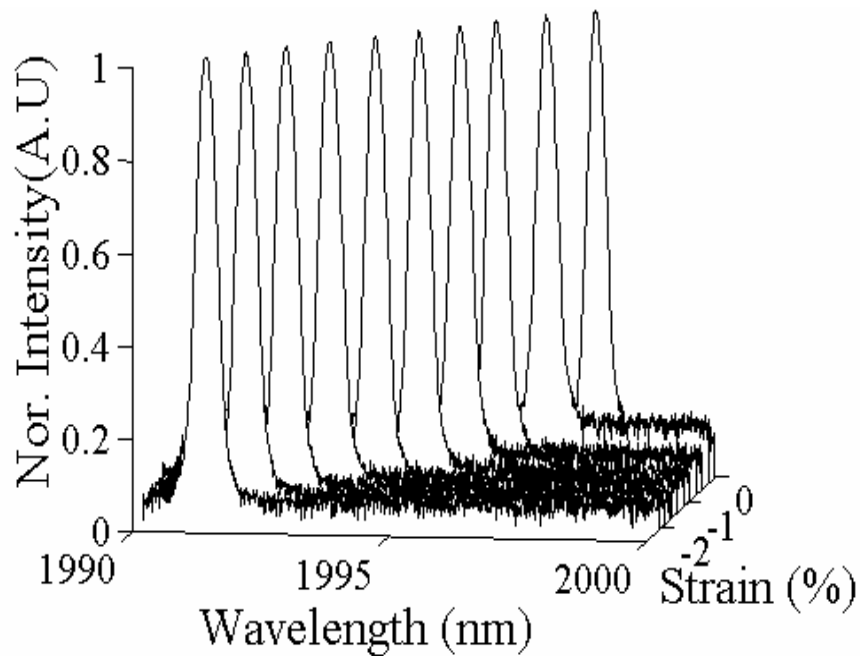


Fig. 5.14 3-D trace of normalized laser spectrum (at  $\sim 1.997 \mu\text{m}$ ) as a function of negative strain or compression

Fig. 5.15 shows the linearity and repeatability of the tuning wavelength for both the FBG pair-based laser and the laser created by using a combination of HR FBG and LR broadband mirror (for laser at 1.997  $\mu\text{m}$ ). It was observed that a repeatable tuning over a range of 7 nm was obtained for the laser resonator formed by using the HR FBG and the LR broadband mirror while the tuning range is less, at only 3.8 nm for the laser resonator

with a FBG-pair. Beyond this tuning range, the laser power, the line-width and the line-shape were found to be difficult to maintain.

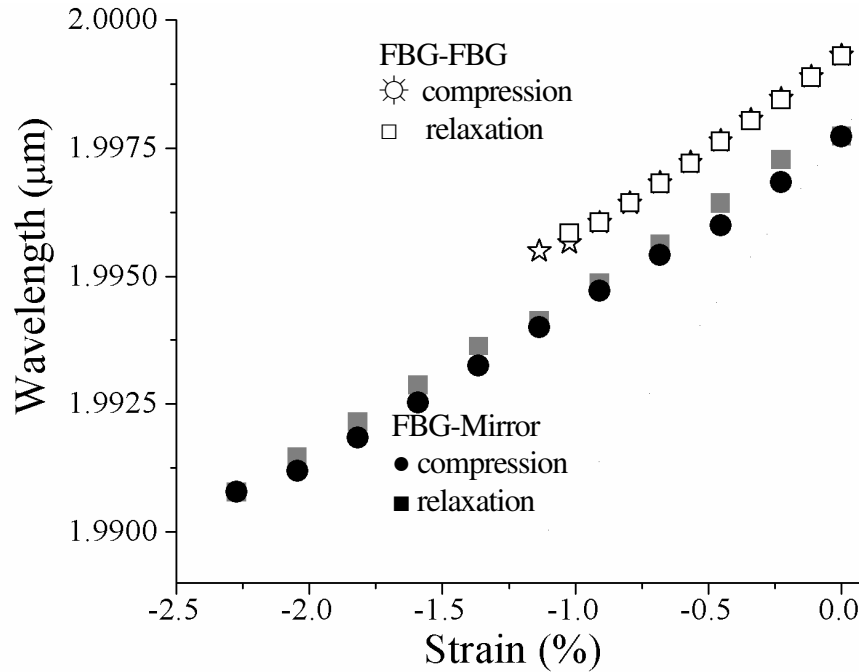


Fig. 5.15 Variation of the laser wavelength (at  $\sim 1.997 \mu\text{m}$ ) with compression of FBG(s)

Fig. 5.16 shows the constant power seen over the lasing wavelength range of  $1.997 \mu\text{m}$ . As the constant power and the stable line-width are the key requirements for the spectroscopic-based sensor systems, the laser line-shape, the full width half maxima (FWHM) and the  $1/e^2$  line-width were characterized over the tuning range and are shown in Fig. 5.16. It was observed that the tuneable range is restricted not only by the capability of compressing the FBGs used but also by the loss of the fibre in the wavelength range around  $2 \mu\text{m}$ . Further tuning was restricted here by the bending loss in the  $2 \mu\text{m}$  range as the photosensitive fibre for FBG used in the system has a cut-off wavelength of  $1.3 \mu\text{m}$ . The tuning range for the laser resonator using a FBG pair is thus lower due to the difficulty in ensuring that the same amount of compression is transferred to both FBGs, thus meeting the 'matching' condition. This limitation, however, has shown to be eliminated by using the laser resonator with HR FBG and LR mirror.

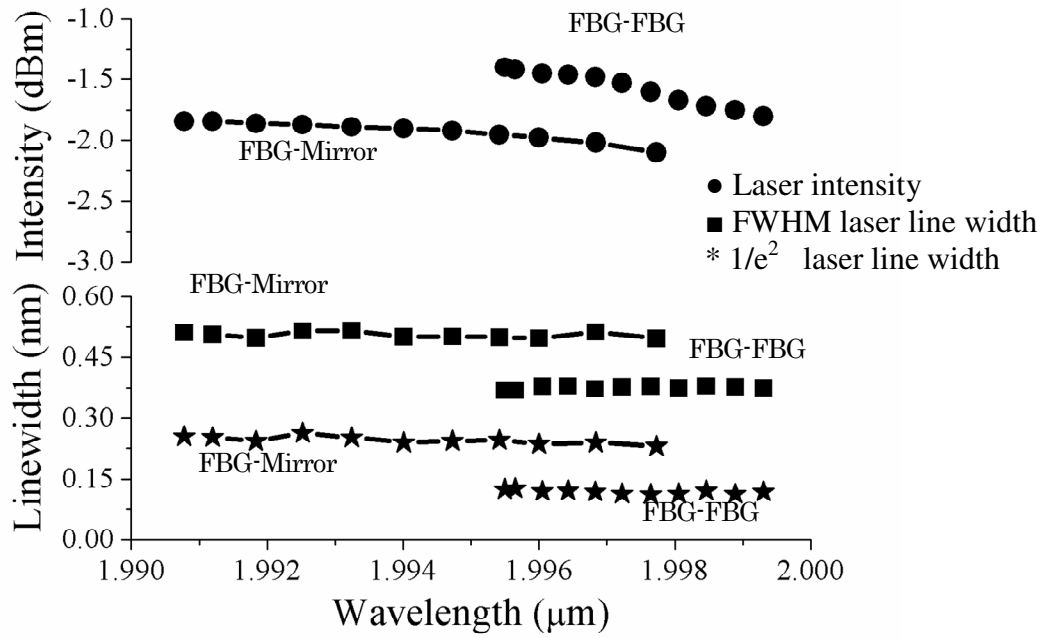


Fig. 5.16 Laser power, FWHM and  $1/e^2$  line width as a function of tuned lasing wavelength range of 1.997  $\mu\text{m}$  for both resonator configurations.

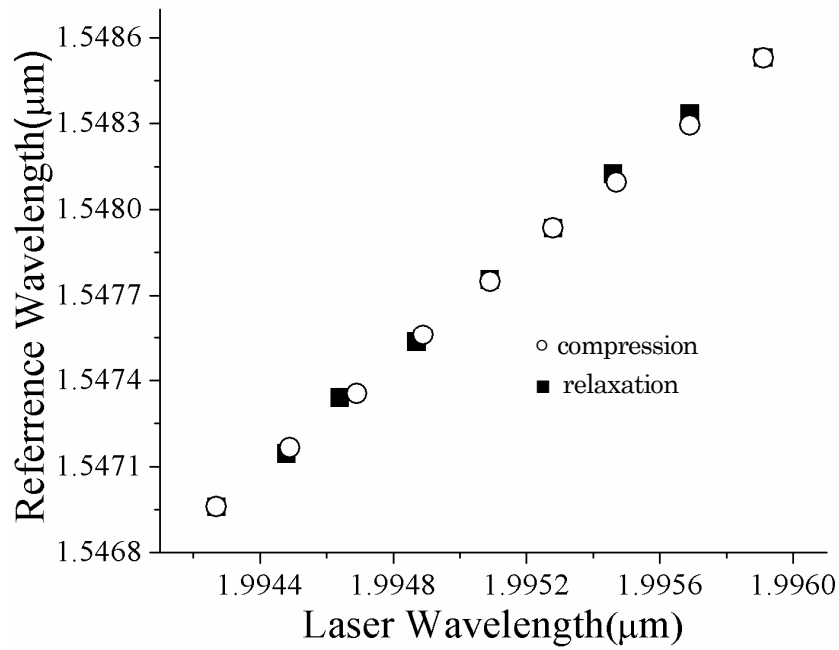


Fig. 5.17 Wavelength variation of the reference FBG as a function of laser wavelength

The linear variation of the reference FBG wavelength with the laser tuning wavelength is shown in Fig. 5.17. Thus by means of a reference FBG, determination of the laser wavelength in the 2  $\mu\text{m}$  range is possible by using a simple interrogator in the range of 1.55  $\mu\text{m}$  and previously calibrated data rather than an expensive OSA with extended wavelengths.

## 5.4 Summary

The Chapter has successfully demonstrated the creation of a set of compact, stable, and tuneable ‘all-fibre’ lasers in the 2  $\mu\text{m}$  wavelength range with output power of 11 mW and line-width of 0.14 nm, required for the establishment of spectroscopic-based sensor systems. The significant advantages of such tuneable laser-based sensors compared to their semiconductor counterparts lie in their simplicity, robustness, low cost and convenience for use ‘in-the-field’. In order to design an optimum Tm-doped fibre based laser system, both Tm-doped fibre under pumping at 1.6  $\mu\text{m}$  and Tm/Yb-doped fibre under dual pumping comprising a 1.6  $\mu\text{m}$  auxiliary pumping to support 0.98  $\mu\text{m}$  primary pumping are explored extensively. The latter facilitates effective population inversion between the relevant energy levels  $^3F_4$  and  $^3H_6$  of  $\text{Tm}^{3+}$  through promoting a strong energy-transfer of  $\text{Yb}^{3+} \rightarrow \text{Tm}^{3+}$ . The experimental results demonstrate that aluminosilicate and aluminogermanosilicate with suitable amount of Al are good host materials for  $\text{Tm}^{3+}$ . An efficient energy-transfer occurs when Yb:Tm proportion is approximately equal to unity and the increment of ground state Tm-ion is found to be beneficial for better laser output. The laser resonator created with the combination of a HR FBG and a broadband mirror coated at the end of the fibre produced a wider tuning range of 7 nm, compared to that created with a FBG-pair, which is limited by the non-uniform strain transfer to both FBGs. The optimized tuneable laser resonator in the 2  $\mu\text{m}$  wavelength range offers the potential for multiple gas detection through the tuning of the fibre laser created.

## References

- [1] M J F Digonnet, Editor, 'Rare-Earth-Doped Fiber lasers and Amplifiers' Second Edition, Marcel Dekker, Inc (2001)
- [2] J Y Allain, M Monerie and H Poignant 'Tunable CW lasing around 0.82, 1.48, 1.88 and 2.35  $\mu\text{m}$  in thulium-doped fluorozirconate fibre', Electronics Letters, Vol. 25, pp. 1660 – 1662 (1989)
- [3] R M Percival, D Szebesta, C P Seltzer, S D Perrin, S T Davey and M Louka 'A 1.6- $\mu\text{m}$  pumped 1.9- $\mu\text{m}$  thulium-doped fluoride fiber laser and amplifier of very high efficiency', IEEE Journal of Quantum Electron. Vol. 31, pp. 489-493 (1995)
- [4] S Tanabe and T Hanada 'Local structure and 1.5  $\mu\text{m}$  quantum efficiency of erbium-doped glasses for optical amplifiers', Journal of Non-Crystalline Solids, Vol. 196, pp. 101-105 (1996)
- [5] G Frith, D G Lancaster and S D Jackson, '85 W  $\text{Tm}^{3+}$  -doped silica fibre laser', Electronics Letter, Vol. 41, pp. 687-688 (2005)
- [6] S D Jackson and T A King 'Theoretical Modelling of Tm-Doped Silica Fiber Lasers' Journal of Lightwave Technologies, Vol. 17, pp.948-956 (1999)
- [7] P R Watekar, S Ju and W T Hu 'A Nd-YAG laser-pumped Tm-doped silica glass optical fiber amplifier at 840 nm', IEEE Photonics Technology Letter, Vol. 18, pp.1651–1653 (2006)
- [8] S D Jackson and T A King 'High-power diode-cladding-pumped Tm doped silica fiber laser', Optics Letters, Vol. 23, pp.1462–1464 (1998)
- [9] R A Hayward, W A Clarkson, P W Turner, J Nilsson, A B Grudinin and D C Hanna 'Efficient cladding-pumped Tm-doped silica fiber laser with high power single mode output at 2  $\mu\text{m}$ ', Electronics Letters, Vol. 36, pp.711–712 (2002)
- [10] S D Jackson and S Mossman 'Efficiency dependence on the  $\text{Tm}^{3+}$  and  $\text{Al}^{3+}$  concentrations for  $\text{Tm}^{3+}$  doped silica double-clad fiber lasers', Applied Optics, Vol. 42, pp. 2702–2707 (2003)

- [11] P R Watekar, S Ju and W T Han ‘800-nm Upconversion Emission in Yb-Sensitized Tm-Doped Optical Fiber’, *IEEE Photonics Technology Letters*, Vol. 18, pp.1609-1611 (2006)
- [12] J Chang, Q P Wang, X Zhang and Z Liu ‘S-band optical amplification by an internally generated pump in thulium ytterbium codoped fiber’, *Optics Express*, Vol. 13, pp.3902-3912 (2005)
- [13] S D Jackson ‘Power scaling method for 2  $\mu\text{m}$  diode-cladding-pumped  $\text{Tm}^{3+}$  doped silica fiber lasers that uses  $\text{Yb}^{3+}$  codoping’, *Optics Letters*, Vol. 28, pp.2192-2194 (2003)
- [14] F J McAleavey, J O’Gorman, J F Donegan, B D MacCraith, J Hegarty and G Mazé ‘Narrow Linewidth, Tunable Tm Doped Fluoride Fiber Laser for Optical-Based Hydrocarbon Gas Sensing’, *IEEE Journal of Selected Topics in Quantum Electronics*, Vol. 3, pp.1103-1111 (1997)
- [15] L E Nelson, E P Ippen and H A Haus ‘Broadly tunable sub-500 fs pulses from an additive-pulse mode-locked thulium doped fiber ring laser’, *Applied Physics Letter.*, Vol. 67, pp.19–21 (1995)
- [16] J Geng, Q Wang, J Wang, S Jiang and K Hsu ‘All-fiber wavelength-swept laser near 2  $\mu\text{m}$ ’, *Optics Letters*, Vol. 36, pp. 3771-3773 (2011)
- [17] S Taccheo, P Laporta, S Longhi, O Svelto and C Svelto ‘Diode-pumped bulk erbium-ytterbium lasers’, *Applied Physics B*, Vol. 63, pp. 425–436 (1996)
- [18] R Kashyap ‘Fiber Bragg Gratings’, 2<sup>nd</sup> Edition Academic Press (2009)
- [19] A Pal, A Dhar, S Das, S Y Chen, T Sun, R Sen and K T V Grattan ‘Ytterbium-sensitized Thulium-doped fiber laser in the near-IR with 980 nm pumping’, *Optics Express* Vol. 18, pp. 5068-5074 (2010)
- [20] D W Kim, Y Zhang, K L Cooper and A Wang ‘In-fiber reflection mode interferometer based on a long-period grating for external refractive-index measurement’, *Applied Optics*, Vol. 44, pp. 5368-5373 (2005)
- [21] B Faure, W Blanc, B Dussardier and G. Monnom ‘Improvement of the  $\text{Tm}^{3+}$ -  $^3\text{H}_4$  level lifetime in silica optical fibers by lowering the local phonon energy’, *Journal of Non-Crystalline Solids*, Vol. 353, pp. 2767–2773 (2007)

[22] G A Ball and W W Morey 'Compression-tuned single-frequency Bragg grating fiber laser' Optics Letters, Vol. 19, pp. 1979–1981 (1994)

# Chapter 6

## Thulium-doped Microsphere Laser

*Abstract: A high-Q, narrow line-width and low threshold laser resonator, operating in the 2  $\mu\text{m}$  wavelength region, has been designed by coupling a Thulium-doped silica microsphere to a tapered fibre. Microspheres with diameters ranging from fifty to a few hundred micrometers were carefully fabricated by melting an etched-clad Thulium-doped silica fibre tip using a focused beam from a  $\text{CO}_2$  laser, while the tapered fibre with a waist diameter in the desired range of 2  $\mu\text{m}$  was fabricated by heating and stretching of a standard single mode telecommunication fibre. The tapered fibre serves the dual purpose of transporting pump power into the sphere and allowing the extraction of the resulting laser emission. When the micro-cavity was excited at a wavelength of around 1.6  $\mu\text{m}$ , lasing occurred at wavelengths over the range from 1.9 to 2.0  $\mu\text{m}$ . Single-mode laser operation was obtained through the excitation of the fundamental whispering gallery mode resonance of the microsphere while multi-mode lasing occurred for non-fundamental mode excitation. The threshold power of the laser was measured to be about 50  $\mu\text{W}$  (delivered pump power) and a maximum laser power of 0.8 mW at around 1.94  $\mu\text{m}$  was observed for a 6 mW pump power, operating at wavelengths around 1.6  $\mu\text{m}$ .*

### 6.1 Introduction

In the areas of bio-medical measurements and selective, yet potentially very sensitive gas sensing, it is essential for a laser not only to be compact and low power but to demonstrate a narrow line-width (in order to avoid overlapping with the absorption features of other materials) and good spectral purity to be a suitable light source for applications of this type. To date, the micro-resonator design is an important and realistic

solution [1] that meets these criteria and is very well suited to the critical requirements indicated. In multilayer semiconductor microlasers and in microdisks, the coupling of the gain medium can be limited to only a few modes of radiation so that strongly enhanced stimulated emission is achieved and ‘thresholdless’ laser action is observed. However, these devices typically operate in the low-quality factor ( $Q$ ) regime [2]. Small Fabry-Perot cavities with very high finesse can provide very high  $Q$ , but this involves special supermirrors as well as atomic beams and the concept is yet to be translated to effective and convenient implementation [3].

The circulation of light within dielectric volumes enables the storage of optical power at specific resonant frequencies where the beam path of the light in the material occurs near the interface of the volume with its surroundings. With a nearly atomic-scale surface finish, surface-tension-induced micro-cavities such as liquid droplets or spheres [4-5] are known to be superior to all other dielectric micro-resonant structures in respect of photon lifetime or, equivalently, the cavity  $Q$  factor. In a microsphere, light is confined at the surface by repeated total internal reflection, leading to the whispering gallery mode (WGM) resonance with a high  $Q$  factor. Since it was first demonstrated in 1987, the achievable  $Q$  from a microsphere laser has improved, from the order of  $10^6$  to  $10^9$ , in the important red and near-IR areas of the spectrum [6]. Although its laser oscillation has already been demonstrated using microdroplets and polymer spheres, the glass microsphere is one of the most widely investigated structures, because of its high  $Q$  value and ease of manufacture and handling [6]. Doped with different rare-earth dopants such as Neodymium (Nd) and Erbium (Er) [7-8], microsphere lasers at various wavelengths have been demonstrated in phosphate and tellurite glasses. Thulium (Tm)-doped tellurite glass microsphere lasers in the S-band and 2  $\mu\text{m}$  region have also been studied previously [9-10].

In order to form such micro-resonator, light must be coupled into the sphere without disturbing the high- $Q$  characteristics. Evanescent coupling, through which an exterior field tunnels into the sphere, is the most promising approach for the micro-resonator formation [11]. There are numerous methods for coupling energy evanescently into the

modes of a sphere. Among the most widely used are the prism coupler [12], tapered fibre [13] and polished half-block coupler [14]. For device applications the tapered fibre and half-block are expected to be more robust. The coupling strength and resulting performance vary considerably depending on the refractive index and the dimension of the sphere, the dimension of the coupler fibre, the relative positions of the sphere with respect to the coupler, the difference in propagation constants between the fibre and sphere and on the spherical mode orders. In initial work, Knight et al. [13] showed the feasibility of forming micrometer-diameter fibre tapers by heating and stretching silica fibre for excitation of microsphere resonators. It was reported that the use of a fibre taper not only provides an efficient input and output coupling port but also plays an important role in producing single-mode lasing. It has been demonstrated that the fibre taper forms a natural backbone for connecting a series of different active and passive microsphere devices, with each device addressing a different wavelength signal.

The objective of this chapter is to develop a compact, miniaturized and narrow line-width Tm-doped silica microsphere laser in the 2  $\mu\text{m}$  wavelength region, coupled by a tapered fibre and suitable for a range of sensing applications, including the detection of important and hazardous environmental gases. The broad fluorescence spectrum of the Tm-ion in the silica glass allows the fabrication of a laser widely tuneable over a range from 1.7 to 2.1  $\mu\text{m}$ . Silica glass-based microspheres possess advantages over other non-oxide glasses, reported previously in the literature [8-9], in terms of their chemical durability, stability, potential for bubble-free microsphere formation in the laboratory environment and importantly, good structural compatibility with readily available telecommunication optical fibres. In order to design the laser system, a single tapered fibre is used to an efficient coupler, both guiding the pump laser beam to the microsphere and collecting the resulting laser emission. Compared to the other couplers discussed above, the fibre-taper coupling has several distinct advantages including built-in alignment, a relatively simple fabrication approach and ideal matching to the WGMs of the sphere. In this research, these lasers have been developed and fabricated with their

performance under a range of different coupling conditions and over several different excitation wavelengths being evaluated and cross-compared.

## 6.2 Basic Principle of Operation

Dielectric spheres can sustain high  $Q$  electromagnetic modes, termed morphological resonances, which can be interpreted as strongly confined circulating waves within the sphere and being totally internally reflected and focused by the surface. The resonances occur when an integral number of wavelengths ‘fit’ to the length of the circumference. Such morphological resonances are sensitive to key parameters: the index of refraction,  $N_s$ , and the radius,  $a_s$ , of the sphere. The modes of the dielectric microspheres are well known and their detailed structure and spectroscopic properties are known [15] and referenced therein. A brief description of the principal features of the laser designed, as implemented in this work, is presented below.

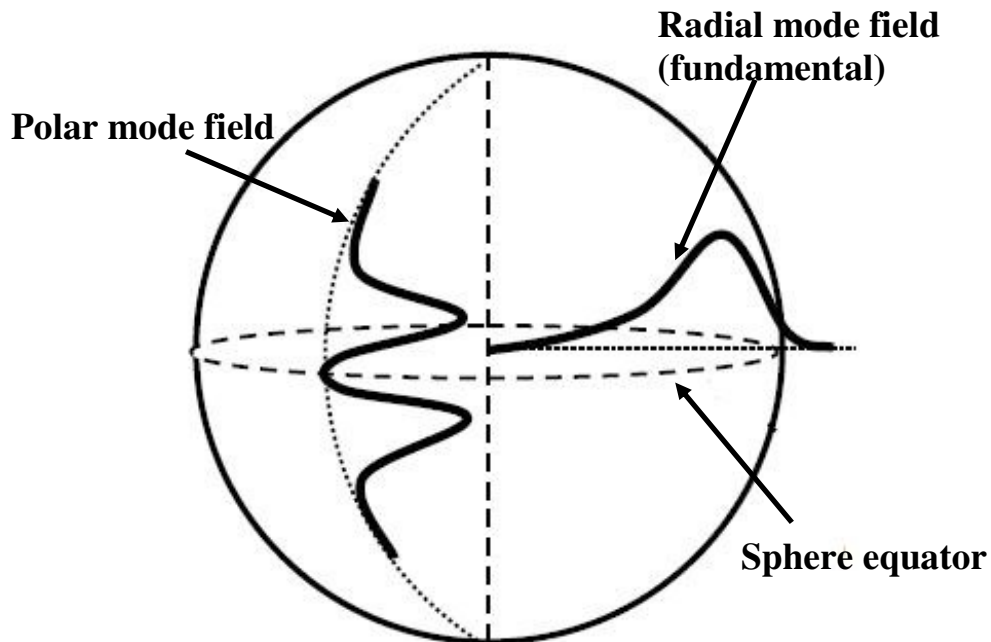


Fig. 6.1 Schematic of WGM field components in a microsphere resonator (not to scale)

Morphological resonance can be identified in terms of three mode numbers ( $n, m, l$ ) which together represent the radial, equatorial and polar electromagnetic field components, in addition to their TE or TM polarization. The mode number,  $l$ , is approximately the number of wavelengths in the circumference of the sphere. The mode order,  $n$ , is the number of radial intensity maxima of the internal electric field between the centre and the surface of the sphere, and  $l - |m| + 1$  (where  $|m| \leq l$ ) gives the number of maxima in the ‘latitude’. Resonances with small radial mode number and large angular mode number are so-called Whispering Gallery (WG) type modes. The ‘fundamental’ WGM has  $n = 1$  and  $|m| = l$  and thus a single transverse maximum. The radial part of a sphere WGM can be described by spherical Bessel function with an external evanescent tail, while the polar-longitudinal-field dependence follows spherical harmonics and the equatorial-latitude-field variation is sinusoidal as shown in Fig. 6.1 [16]. The WGM resonant frequencies are given approximately by [17]

$$\nu_{nlm}^i = \delta \left[ l + 1/2 + A_n \left( \frac{l + 1/2}{2} \right)^{1/3} - \Delta^i + (l - |m|) \frac{a_e - a_a}{a_s} \right] \quad (6.1)$$

In Equation (6.1),  $i$  denotes the TE or TM mode,  $\delta = c/2\pi a_s N_s$  is the nominal free spectral range (FSR),  $N_s$  is the refractive index of the sphere,  $a_s$  is the sphere radius ( $a_e$ , equatorial;  $a_a$ , axial), the  $\Delta^i$  are polarization-dependent shifts,  $A_n$  is the  $n^{\text{th}}$  zero of the Airy function:  $\text{Ai}(-A_n) = 0$ . During the formation of a microsphere, a small amount of eccentricity appears, so that  $a_e$  and  $a_a$  typically differ by about 1%. Due to the small ellipticity, the WGMs differing only in  $|m|$  exhibit different resonant frequencies. For a given FSR, frequency scanning combined with appropriate beam settings allows the excitation of modes of various values of  $n$  or  $l - |m|$ , which can be identified by spectroscopic methods.

For modes with low  $n$  and with  $m \cong l$ , the propagation constant,  $\beta$  can be approximated as

$$\beta = \kappa l / x_{n,l,m} \quad (6.2)$$

where  $x_{n,l,m}$  is the size parameter that corresponds to the  $n$ ,  $l$  and  $m$  resonances and  $k$  is the free space propagation constant. The resonance size parameters,  $x_{n,l,m}$ , are related to the angular resonance frequencies ( $\omega_{n,l,m}$ ) by [18]

$$\omega_{n,l,m} = x_{n,l,m} c / n_e a_s \quad (6.3)$$

where  $n_e$  is the refractive index of the environment surrounding the sphere.

In order to form the laser resonator, a tapered fibre can be used to couple light into the sphere to excite the WGM resonance in the microsphere and then to collect the laser signal from the microsphere. In the waist region of the tapered fibre, the fibre core is no longer significant and the light travels in the fundamental mode along the waveguide formed by the silica waist surrounded by air. The tapered waist can be as small as one micrometer in diameter. On reaching the other end of the waist, the light remaining in the waist is returned to the guided mode in the fibre core. If the waist is small, the fundamental mode will have an evanescent tail extending significantly out into the free space surrounding the taper and the propagation constant of the mode will be a function of the waist radius. Hence the propagation constant can be readily calculated as [19]

$$\beta^2 = k^2 N_f^2 - \frac{2.405^2}{\rho^2} \quad (6.4)$$

where  $k$  is the free space propagation constant of the light,  $N_f$  is refractive index of the fibre and  $\rho$  is the radius of the tapered fibre.

To pump the microsphere efficiently, it is crucial to obtain a good match between the fundamental taper mode and the WGMs of the sphere and also to match the input coupling strength to the round-trip resonator loss (achieving critical coupling). By tailoring the taper waist diameter, the fundamental taper mode can be phase-matched to a given WGM of a sphere, thus improving the coupling efficiency of the coupler.

## 6.3 Experimental Work

### 6.3.1 Fabrication of tapered-optical fibre

Adiabatic tapered fibres were fabricated by heating and stretching a standard single mode optical fibre (SMF-28) using an in-house CO<sub>2</sub> laser-based optical fibre taper fabrication system as illustrated in Fig. 6.2. This system was designed specifically for the fabrication of low loss tapers with a waist diameter of around 2 μm with transmission loss within 2-10%. The CO<sub>2</sub> laser (SYNDAS) system, with a maximum output power of 20W, comprises of a shutter unit, a reflecting corner mirror, a beam expander and a positioning beam (in the visible range at a wavelength of 0.63 μm for ease of alignment) and it was used for heating the fibre while a translational stage was employed to stretch the fibre simultaneously. The pulling speed of the fibre, the rotation speed and angle of the galvanometer mirror and the power of the laser were carefully controlled by software designed using LABVIEW.

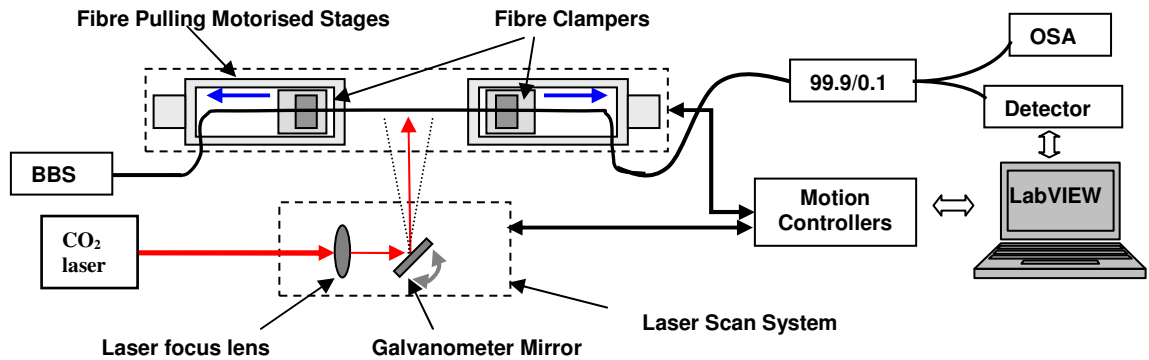


Fig. 6.2 Schematic of CO<sub>2</sub> laser based setup for tapered fibre fabrication; BBS: broadband source; OSA: optical spectrum analyzer

The detailed process for the fabrication of a fibre taper is as follows. First the fibre followed by a careful cleaning to avoid loss and breakage of the tapered fibre during fabrication. Subsequently, each end of the fibre was clamped (on the post mountable fibre

clamps (Thorlabs)) on to two separate computer controlled motorized stages, allowing the fibre to be pulled into a taper when the laser beam from the CO<sub>2</sub> laser was focused onto the fibre, thus heating the fibre beyond the glass melting point. A rotatable galvanometer mirror was used to change the laser direction and scan the laser beam along the length of the fibre. In order to heat the fibre properly during the tapering process, the fibre was pre-heated with the laser power, increased from 0.5W to 3.5W before the stretching. During the stretching process, the laser power was increased accordingly to keep the fibre above the melting point. The transmission property of the fibre during the tapering process was monitored through using a broadband source (BBS), coupled through the tapered fibre to an Optical Spectrum Analyzer (OSA) and the transmitted power was measured by using a standard detector. The formation of taper was imaged by a camera from the top (using a ×20 objective). Fig. 6.3 shows the software interface designed for monitoring and control of the taper manufacturing process. Fig. 6.4 shows spectra loss during the tapering.

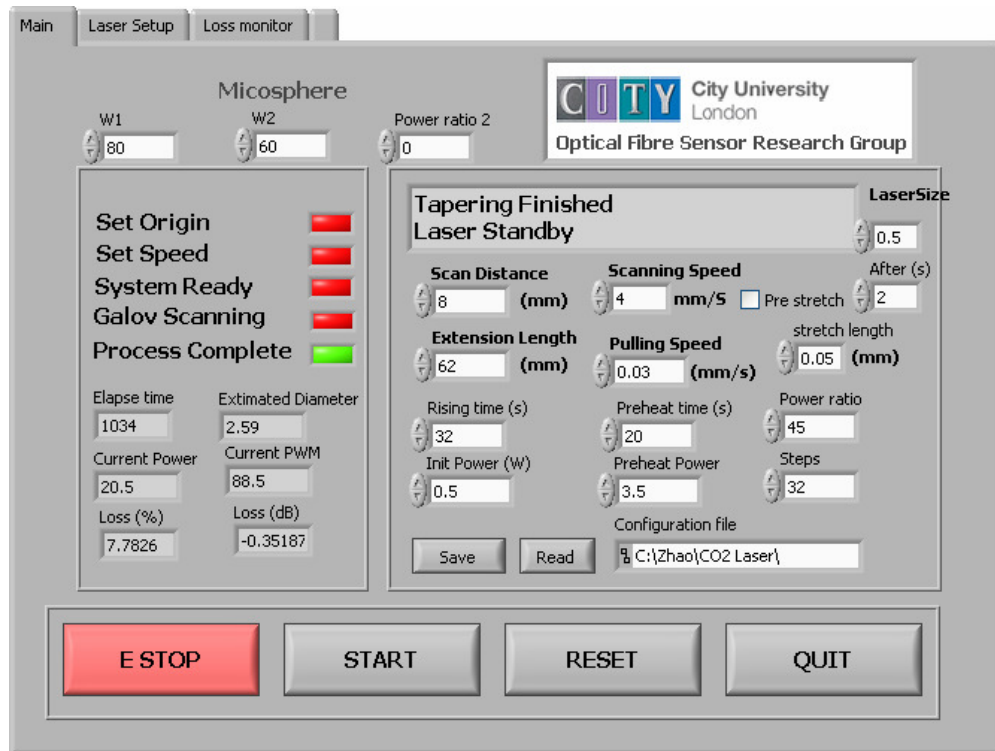


Fig. 6.3 GUI with set parameter for tapered fibre fabrication process

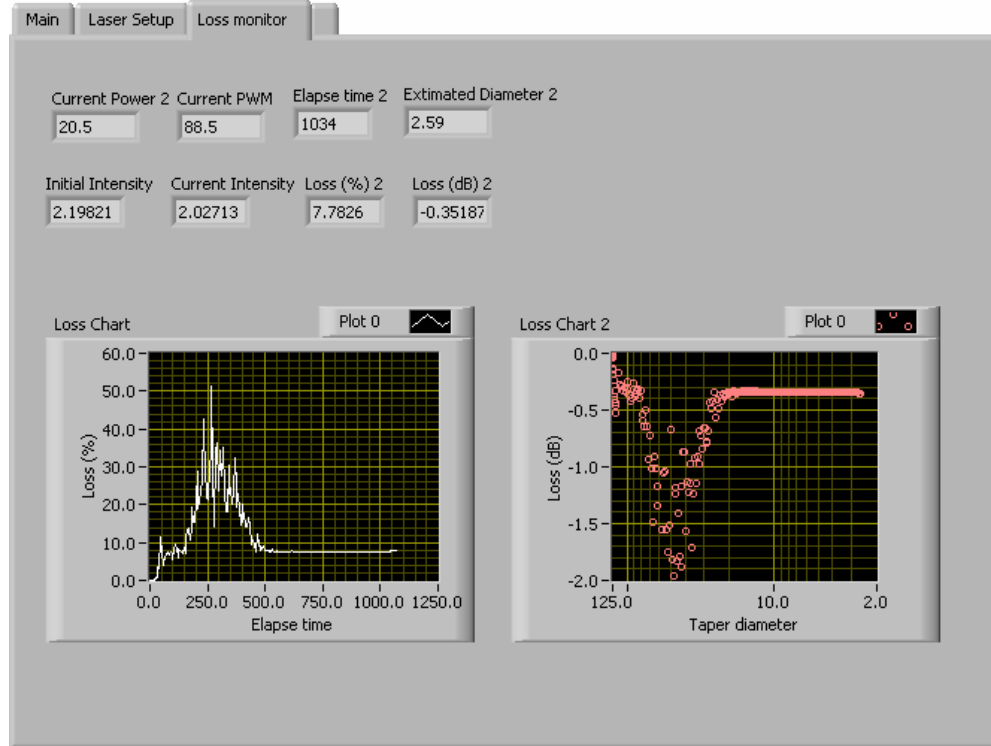


Fig. 6.4 GUI with set parameter for the spectral loss property during fabrication; elapsed time in second and taper diameter in  $\mu\text{m}$

The key manufacturing parameters as indicated in Figures 6.3 and 6.4 include constant heating length and extension length of the taper, tapering speed, stretch length, power control of the laser during the tapering, and the power of the laser. A CCD image of the fabricated tapered fibre is shown in Fig. 6.5. The measured waist diameter of the tapered fibre is in the range of 2-3  $\mu\text{m}$ . After the tapering process was finished, the taper was mounted on a glass platform and subsequently used for coupling light from a light source to a microsphere cavity fabricated using the approach discussed in Section 6.3.2.

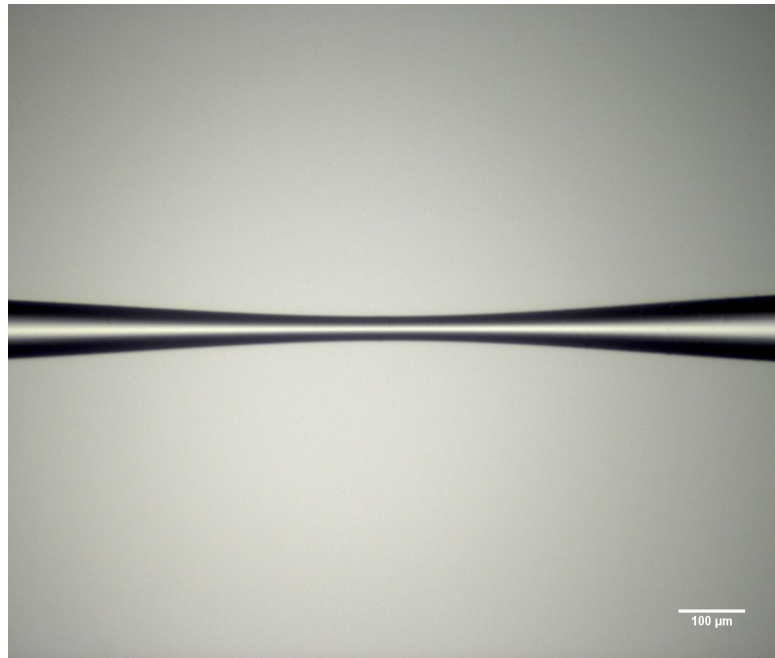


Fig. 6.5 Image of fabricated tapered fibre showing the smooth, symmetric taper

### **6.3.2 Fabrication of Tm-doped silica microspheres**

The Tm-doped silica microspheres used in this work were fabricated by melting the tip of an unclad Tm-doped silica optical fibre using the focused beam of a CO<sub>2</sub> laser. The cladding of the doped fibre was etched away as only the fibre core of 10 μm diameter is doped with Tm and after the melting process, the dopant could be uniformly distributed on the surface of the microsphere created. The Tm-ion concentration in the core was in the range of 0.1 to 0.3 mol%. In order to etch the silica cladding, the stripped end of a small piece of fibre, no longer than 20 cm, was dipped in a hydrofluoric acid (HF) solution (24%). The etching process was carried out till the diameter of the fibre tip reached around 10 μm. The length of the etched region was maintained in the range of 2-5 cm and a smooth tapered zone was formed at the transition point between the primary fibre and the etched fibre. After the inspection of the surface of the etched region of the fibres using a microscope, the coated region of the processed fibre was mounted on to a three dimensional translation stage with the etched end being positioned at the focal zone

of the CO<sub>2</sub> laser beam. Fig. 6.6 shows a schematic of the CO<sub>2</sub> laser microsphere fabrication system used, where the major differences between the fibre taper fabrication system and the microsphere fabrication system (both of which use the heat from the CO<sub>2</sub> laser beam) lie in the fibre clamping system and the movement of the translation stage. The microsphere fabrication process is as follows. Light from a CO<sub>2</sub> laser was focused to the tip of the unclad doped fibre to melt the glass with the surface tension being able to shape the microdrop into a spherical form. After turning off the laser, a solid sphere was produced. The entire procedure lasts less than 1s and the shaping process of the microspheres was monitored by using a CCD camera. The fibre wire attached to the sphere was found not to affect the WGMs of the microsphere, therefore was kept to provide a useful stem for mounting the sphere on the x-y-z stage for further manipulation. By changing the initial fibre size (the diameter) and position (the length beyond the focused point of laser beam) and the power of the laser beam, the size and ellipticity of the microsphere can be controlled. Using this procedure, a set of microspheres having diameters in the range of 50-200 μm was fabricated for further experimentation to create microsphere-based laser systems.

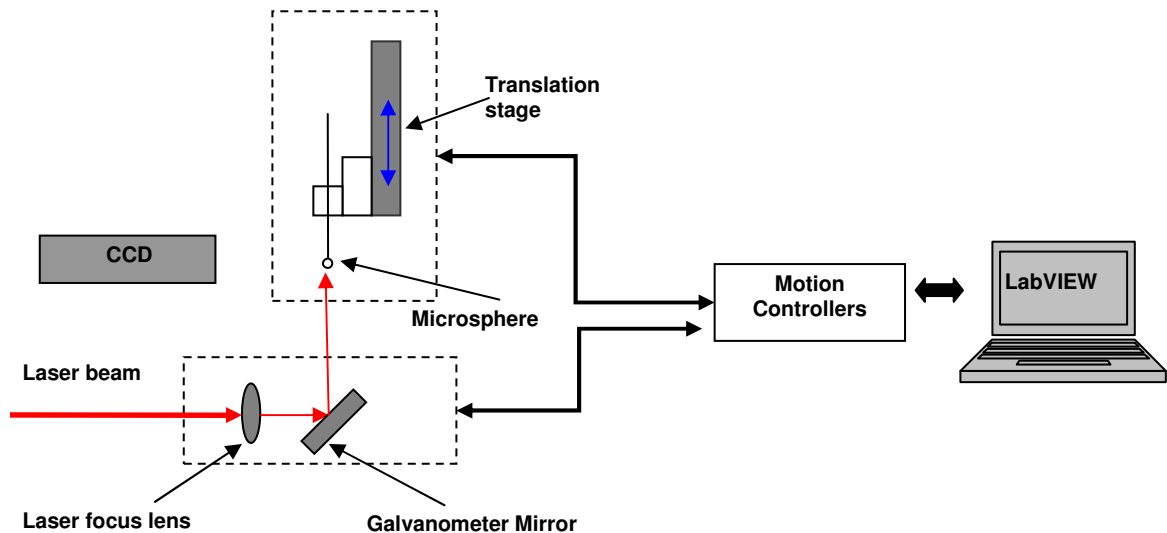


Fig. 6.6 Schematic of CO<sub>2</sub> laser based setup for microsphere fabrication

The images of the etched fibre end and formed microsphere at the fibre tip are shown in Fig. 6.7 (a) and (b) respectively. Fig. 6.8 shows a scanning electron microscope (SEM) image of the fabricated microsphere, which reveals a smooth surface without observable defects.



Fig. 6.7 Images of the (a) etched fibre end and (b) formed microsphere at the fibre tip

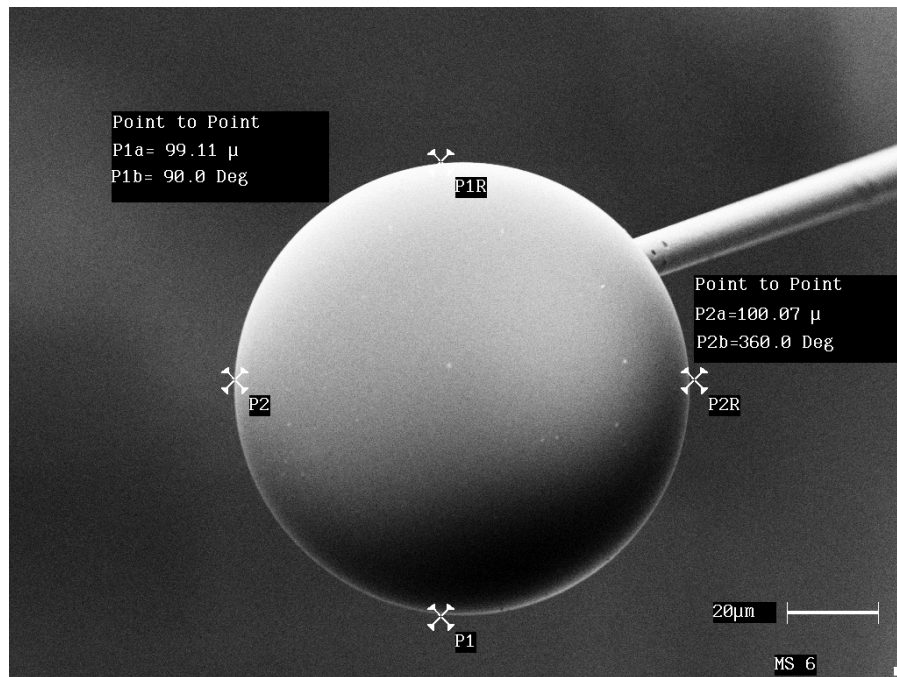


Fig. 6.8 SEM image of the fabricated Tm-doped silica microsphere with a diameter 99  $\mu\text{m}$

### 6.3.3 Formation of a laser resonator

In order to design a laser resonator utilizing the above discussed efficient coupling between a microsphere and a tapered fibre, a separate alignment system was created involving precision control and monitoring. First of all, the tapered fibre was fixed onto the mounts of a precision controller, allowing three-dimensional movement and the microsphere was clamped separately onto a three-dimensional translation stage, which allows a wide range movement as well as fine tuning within a shorter range. A CCD camera was positioned to capture the image of the tapered fibre and the microsphere to facilitate fine tuning for efficient coupling. A calibrated microscope image of the microsphere coupled to the tapered fibre is shown in Fig. 6.9.

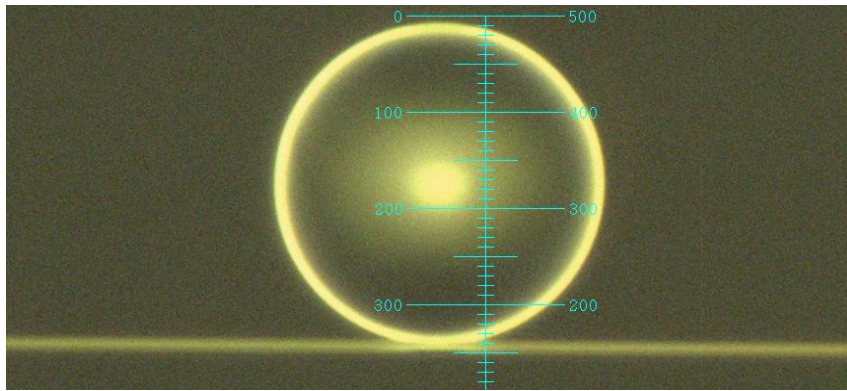


Fig. 6.9 Magnified image of Tm-doped microsphere with the tapered fibre. The divisions on the graticule are equivalent to a distance of  $0.214 \mu\text{m}$

Fig. 6.10 shows a schematic diagram of the essentials of the microsphere laser system thus created. The resonances arising from the WGMs in the microsphere coupled to the tapered fibre were observed using an OSA and achieved by launching light from a broadband source (an LED source centred at  $1.53 \mu\text{m}$  was used) at the input end of the taper. In order to excite the Tm-doped microsphere at a wavelength of around  $1.6 \mu\text{m}$ , a tuneable laser source (TLS) in the range of  $1.53$  to  $1.62 \mu\text{m}$ , with maximum output power of  $8 \text{ mW}$ , was used as a pumping source, and the excitation wavelengths were selected

from data measured from the WGM. The laser emission was captured by a monochromator which was connected to the other end of the tapered fibre.

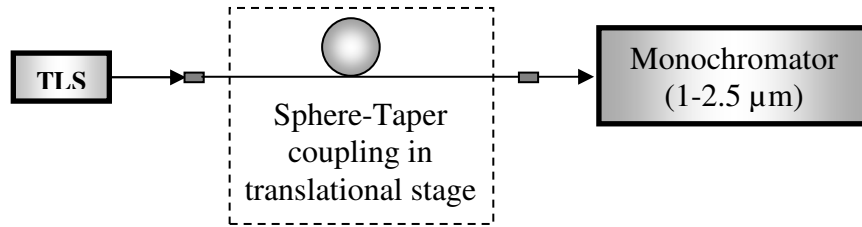


Fig. 6.10 Schematic of Tm-doped microsphere laser system (TLS: Tuneable Laser Source)

## 6.4 Laser Performance

The resonance peaks arising from the WGM in the microsphere that has been thus fabricated, with the light coupled by the tapered fibre, are shown in Fig. 6.11.

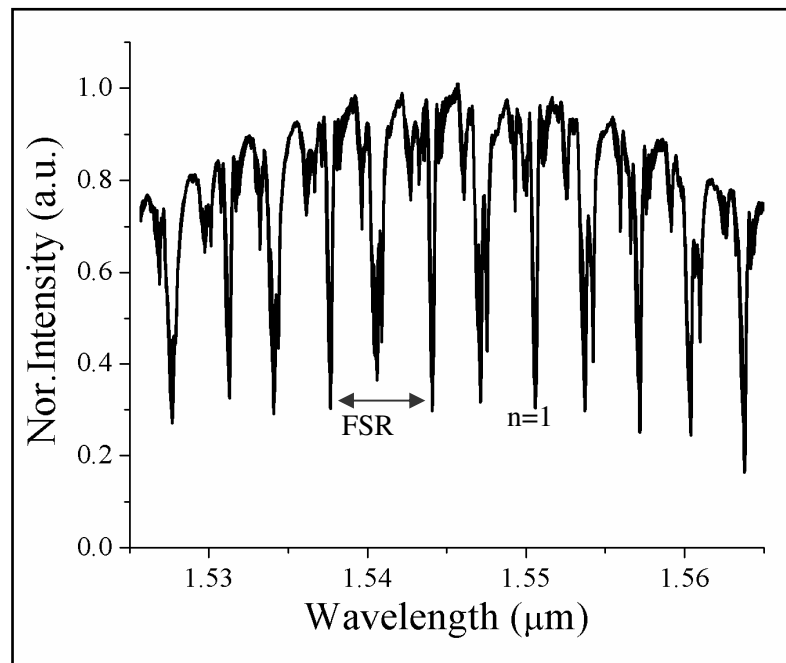


Fig. 6.11 Resonances in the microsphere coupled with a tapered fibre

Using a typical spectrometer with a resolution of 0.01 nm at an operating wavelength of 1.5  $\mu\text{m}$ , the maximum measured  $Q$ -factor ( $\lambda/\Delta\lambda$ ) is of the order of  $10^4$ ; however, higher  $Q$  value can be expected by employing high resolution measurement setup. The measured WGM- FSR of 6.412 nm indicates that the diameter of microsphere is 75  $\mu\text{m}$ , a result which is in good agreement with the estimated diameter measured directly using the microscope and the graticule calibration. The measured WGM spectrum provides an indication of the location of WGMs over a wide spectral window, which is important for selecting the appropriate excitation wavelength for lasing.

The lasing process in the Tm-doped microsphere, under excitation with light at a wavelength around 1.6  $\mu\text{m}$  is rather complex, owing to a number of factors: the large number of high  $Q$  modes that are present in the sphere, the spatial selectivity of the pump, the loading of the sphere as a result of the taper, the large spectral gain bandwidth, and the variations in the emission and absorption cross-sections with wavelength in the Tm-doped silica materials. Depending on the nature of the gain region within the sphere, lasing occurred at wavelengths ranging from 1.9 to 2.1  $\mu\text{m}$ , in both multi-mode and single-mode fashions. Single-mode lasing has been obtained by tuning the pump wavelength to a fundamental WGM resonance that produced a narrow equatorial-ring gain region while multi-mode lasing was obtained by pumping non-fundamental WGMs. By adjusting the position between the tapered fibre and the sphere, switching between multi-mode and single-mode lasing action has been achieved. Fig. 6.12 and 6.13 show the spectral outputs over the wavelength range 1.9 to 2.0  $\mu\text{m}$ , indicating the multi-mode and single-mode lasing operations respectively.

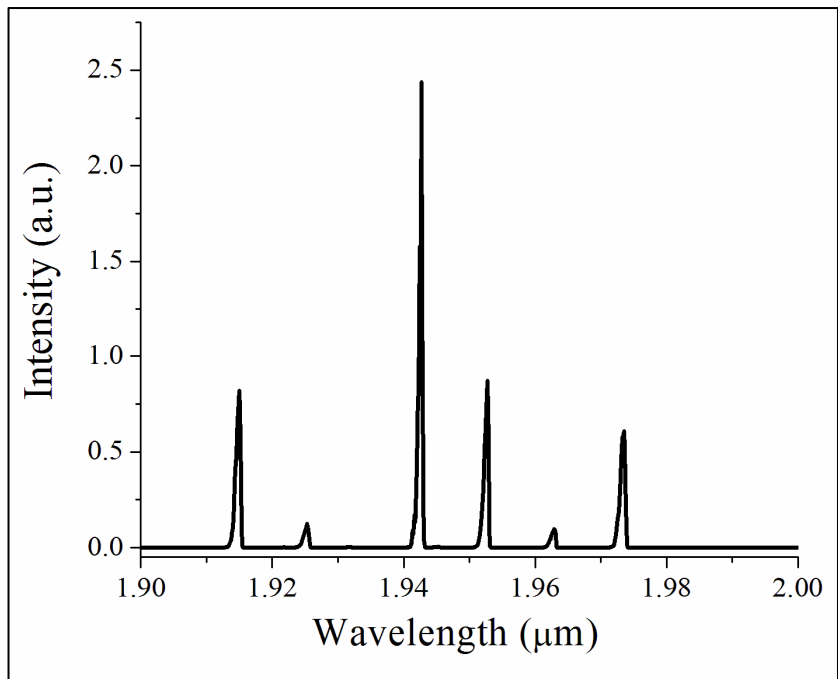


Fig. 6.12 Spectral outputs showing multi-mode lasing in the Tm-doped microsphere laser

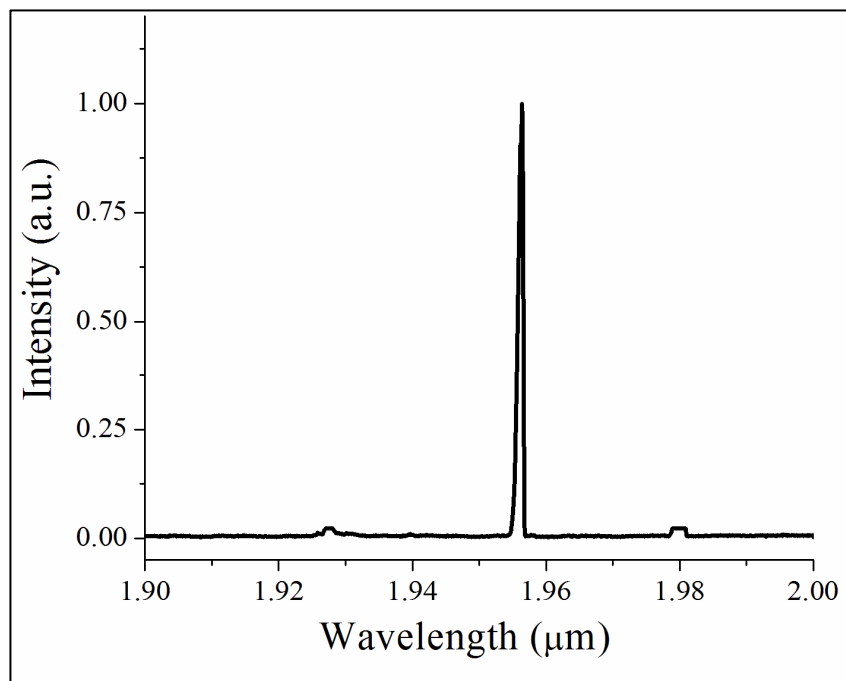


Fig. 6.13 Spectral output showing single-mode lasing in the Tm-doped microsphere laser

To evaluate further the laser performance, a series of experiments has been undertaken by subjecting the microsphere laser cavity to similar coupling conditions and to excitation at different wavelengths. The corresponding laser action achieved at different wavelengths is illustrated clearly in Fig. 6.14. In the multi-mode laser case, although most of the peaks are regularly spaced, irregularly spaced peaks occur as both the transverse electric and transverse magnetic modes of the WGMs are allowed in the microsphere.

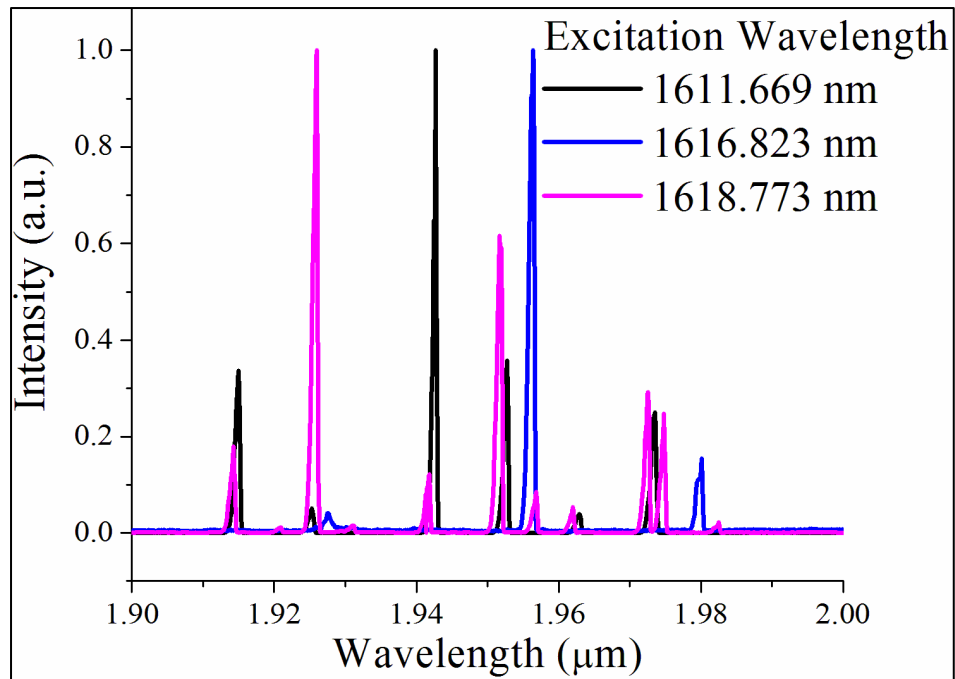


Fig. 6.14 Multi-mode lasing for different excitation wavelengths and identical coupling

For the 2 μm laser emission from what is a 3-level system, the red shift of the laser wavelength (centre wavelength of the emission spectrum of Tm in silica is around 1.85 μm) results from the mode mismatch between the pump and the signal laser. The radial distribution of the WGMs of the pump and signal laser do not overlap strongly. Part of the 2 μm laser WGM area is not covered by the pump laser and therefore the re-absorption arising from those ‘un-pumped’ Tm-ions causes the lower transition laser to operate at longer wavelengths. The difference in lasing performance of the laser (in terms

of laser wavelength) under different pump wavelengths, shown in Fig. 6.14, is due to the excitation of various WGMs existing in the laser resonator.

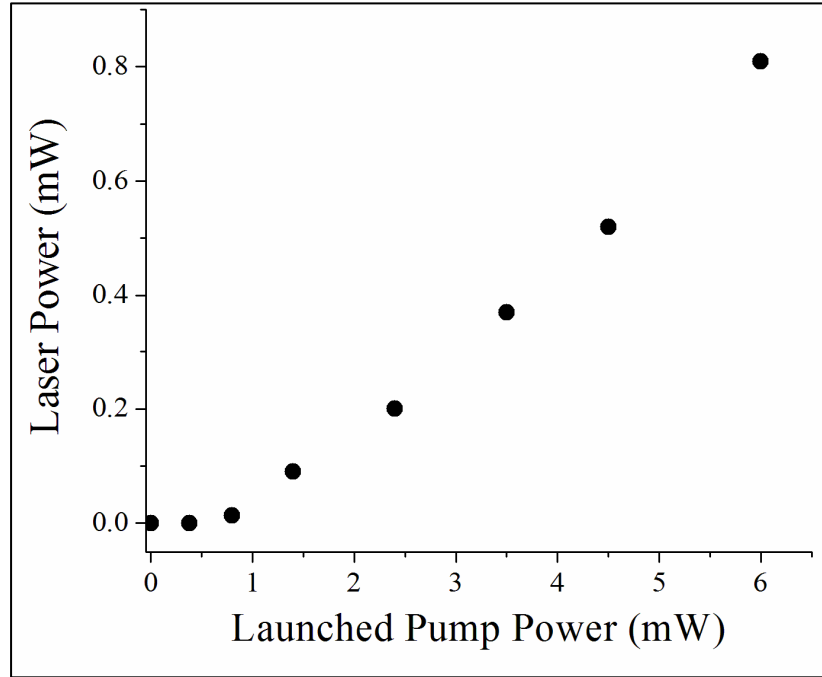


Fig. 6.15 Variation of laser output power with pump power

A plot of laser power available at the tapered fibre end as a function of the launched pump power at the input end is shown in Fig. 6.15. The lasing threshold is estimated to be only 50  $\mu\text{W}$  and the laser reaches an output power of 0.3 mW while remaining single-mode in operation. For multi-mode lasing, a total power of 0.8 mW was obtained. This low threshold value has its origin in a combination of the small mode volume available and the high finesse of the cavity. It is worth noting from Fig. 6.15 that the laser emission shows a linear relationship with pump power, above the threshold.

## 6.5 Summary

A novel silica based microsphere-based fibre laser system in the wavelength region of 2  $\mu\text{m}$  has been demonstrated successfully. The microsphere cavity design based on Tm-

doped silica glass provides a threshold of as low as  $50 \mu\text{W}$  and high  $Q$ . The lasing can be obtained throughout the gain medium ( $\text{Tm}$  in silica glass) and the morphological resonance can be tailored by changing the size of the sphere. Switching between single-mode and multi-mode operation is made possible by changing the coupling of tapered fibre and microsphere, i.e. the gap between tapered fibre and microsphere. Additionally, under similar coupling conditions, the lasing wavelength can be altered by changing the excitation wavelength.

The compact laser system discussed above is designed for the intended application in gas sensing, with a high  $Q$  (and thus narrow line-width) and the output power achieved, suitable for applications both in the laboratory and in the field. Coupled with a proper detector, a compact gas sensor system can thus be created to monitor a number of interesting and environmentally-important gases such as  $\text{CO}_2$ , which will be discussed in detail in Chapter 7.

## References

- [1] D K Armani, T J Kippenberg, S M Spillane and K J Vahala ‘Ultra-high-Q toroid microcavity on a chip’, *Nature*, Vol. 421, pp. 925-928 (2003)
- [2] V Sandoghdar, F Treussart, J Hare, V Lefe`vre-Seguin, J M Raimond and S Haroche ‘Very low threshold whispering-gallery-mode microsphere laser’, *Physical Review A*, Vol. 54, pp. R1777-R1780 (1996)
- [3] M Pollnau, C Grivas, L Laversenne, J S Wilkinson, RW Eason and D P Shepherd ‘Ti:Sapphire waveguide lasers’, *Laser Physics Letters* Vol. 4, pp. 560–571 (2007)
- [4] A J Campillo, J D Eversole and H B Lin ‘Cavity quantum electrodynamic enhancement of stimulated emission in microdroplets’, *Physical Review Letters*, Vol. 67, pp. 437–440 (1991)

- [5] D W Vernooy, V S Ilchenko, H Mabuchi, E W Steed and H J Kimble ‘High-Q measurements of fused-silica microspheres in the near infrared’, *Optics Letters*, Vol. 23, pp. 247–249 (1998)
- [6] M L Gorodetsky, A A Savchenkov and V S Ilchenko ‘Ultimate Q of optical microsphere resonators’, *Optics Letters*, Vol. 21, pp. 453-455 (1996)
- [7] K Sasagawa, K Kusawake, J Ohta and M Nunoshita ‘Nd-doped tellurite glass microsphere laser’, *Electronics Letters*, Vol.38, pp. 1355-1357 (2009)
- [8] M Cai, O Paw-ter, K J Vahala and P C Sbrchel ‘Fiber-coupled microsphere laser’, *Optics Letters*, Vol. 25, pp. 1430-1432 (2000)
- [9] B Richards, A Jha, Y Tsang, D Binks, J Lousteau, F Fusari, A Lagatsky, C Brown and W Sibbett ‘Tellurite glass lasers operating close to  $2\mu\text{m}$ ’, *Laser Physics Letters*, Vol. 7, pp. 177–193 (2010)
- [10] J Wu, S Jiang and N Peyghambarian ‘1.5- $\mu\text{m}$ -band thulium-doped microsphere laser originating from self-terminating transition’, *Optics Express*, Vol. 13, pp. 10129-10133 (2005)
- [11] B E Little, J P Laine and H A Haus ‘Analytic Theory of Coupling from Tapered Fibers and Half-Blocks into Microsphere Resonators’, *Journal of Lightwave Technology*, Vol. 17, pp. 704-715 (1999)
- [12] D W Vernooy, V S Ilchenko, H Mabuchi, E W Streed and H J Kimble ‘High-Q measurements of fused-silica microspheres in the infrared’, *Optics Letters*, Vol. 23, pp. 247–249 (1998)
- [13] J C Knight, G Cheung, F Jacques and T A Birks ‘Phase-matched excitation of whispering-gallery-mode resonances by a fiber taper’ *Optics Letters*, Vol. 22, pp. 1129–1131 (1997)
- [14] A Serpenguzel, S Arnold and G Griffel ‘Excitation of resonances of microspheres on an optical fiber’ *Optics Letters*, Vol. 20, pp. 654–656 (1995)
- [15] V S Ilchenko and A B Matsko ‘Optical resonators with whispering-gallery modes— Part II: Applications’, *IEEE Journal of Selected Topics of Quantum Electron*, Vol. 12, pp. 15-32 (2006)

- [16] J A Stratton, P M Morse, L J Chu and R A Hutner 'Elliptic cylinder and spheroidal wave functions including tables of separation constants and coefficients', Wiley, New York (1941)
- [17] V V Vassiliev, V L Velichansky, V S Ilchenko, M L Gorodetsky, L Hollberg and A V Yarovitsky 'Narrow-line-width diode laser with a high-Q microsphere resonator', Optics Communication, Vol. 158, pp. 305-312 (1998)
- [18] S Schiller 'Asymptotic expansion of morphological resonance frequencies in Mie scattering', Applied Optics, Vol. 32, pp. 2181-2185 (1993)
- [19] J C Knight, G Cheung, F Jacques and T A Birks 'Phase-matched excitation of whispering-gallery-mode resonances by a fiber taper', Optics Letters, Vol. 22, pp.1129-31 (1997)

# Chapter 7

## Detection of CO<sub>2</sub> Using a Novel Tuneable Thulium-doped ‘All-fibre’ Laser

*Abstract:* This chapter reports the experimental results obtained from a novel gas sensor system incorporating a tuneable Thulium-doped fibre laser designed and developed specifically for gas sensing and discussed in Chapters 5. The laser operating wavelength range centred at a wavelength of 1.995  $\mu\text{m}$  has been selected to detect the R(50) transition ( $\nu_1 + 2\nu_2 + \nu_3$ ) of CO<sub>2</sub> based on its line-strength and on its isolation from interfering high-temperature water absorption features. The laser line-width and tuning range are optimized accordingly. The modulation of the fibre laser, achieved through pump source modulation and a ‘locking’ detection mechanism, has been utilized to reduce significantly the laser intensity noise and therefore to create a compact gas sensor system with a high sensitivity. The absorption spectrum, as well as the line-strength and the concentration level of CO<sub>2</sub>, have been monitored through absorption spectroscopy techniques. The measured minimum detectable concentration of CO<sub>2</sub> obtained using this sensor system shows that it is quite capable of detecting trace gases in the ppm level. The stable laser performance achieved in the sensor system illustrates its potential for the development of practical, compact yet sensitive fibre laser based gas sensor systems.

### 7.1 Introduction

Detection and quantification of pollutant gases such as methane, acetylene, carbon monoxide and carbon dioxide are important in environmental and pollution monitoring, which remains a major concern for society [1]. Desirable performance characteristics for

recent gas sensors are: fast temporal response, highly selectivity of particular species, long-term stability without maintenance and re-calibration and real time measurement in just few seconds. It is well known that compared to the conventional ionization and electrochemical gas sensors, the advantages of the optical-based sensors are their simple structure, small size, fast response, low cost, remote detection capability, high sensitivity and safety in hazardous environment [2]. The use of infrared (IR)-absorption spectroscopy in gas sensing is considered to be one of the finest technologies for use in industrial, environmental and safety monitoring [2], as most of the gases have strong fundamental absorption in the mid-infrared (MIR) region of the spectrum (over the wavelength range between 2 and 20  $\mu\text{m}$ ) and weaker overtones/combination overtones of the fundamental absorption in the near-infrared (NIR) (over the wavelength range between 1 and 2  $\mu\text{m}$ ). Consequently, the IR-absorption spectroscopic technique has been widely used for high-resolution, non-destructive, sensitive and fast detection and quantification of important gas species. Using this technique, the detector does not directly interact with the gases (often corrosive and reactive), therefore it is a non-contact and safe approach for measurements.

MIR spectroscopy can provide ultra-sensitive analysis of gases as their fundamental vibrational/rotational molecular absorption exhibits strong absorption and their absorption cross sections in the MIR are around 20–200 times stronger than those in the NIR region. In the past few decades, extensive research has been carried out to develop compact laser sources in the MIR that includes semiconductor lasers such as inter-band cascade lasers (ICLs) and quantum cascade lasers (QCLs) [3], high power gas lasers (e.g.,  $\text{CO}_2$  and CO lasers) [4-5], nonlinear frequency conversion based MIR sources such as difference frequency generation sources or optical parametric oscillators [6-7]. However, some key aspects such as low power level, laser wavelength instability, high maintenance cost and non-room temperature operation strongly limit their reliability and the range of field applications. Nevertheless, MIR spectroscopy remains to be a promising technique for gas sensing although there is a limitation in the availability of key MIR optical components [8]. On the other side, fuelled by the growth of the

telecommunications industry, fibre optic components, including sources and detectors operating in room temperature, are readily available for the NIR spectral region to develop an effective commercial system. Improved detection mechanisms have allowed the widespread applications using NIR sensing techniques to achieve sensitive and selective gas monitoring, thereby overcoming the problems with accessing the weaker absorption line-strength that is seen than is present for the MIR wavelength range [9-10].

Semiconductor lasers, such as the Distributed Feedback (DFB) laser operating in the NIR range, are popular in sensing applications, exploiting their wavelength stability, narrow line-width, compact nature and cost [11]. While a known and carefully controlled operating wavelength is vital in absorption spectroscopy, semiconductor lasers are not readily available at the specific wavelengths and at reasonable cost to provide a close 'match' to the key absorption features of the gases of interest. These are generally gas specific and hence a separate DFB laser is often needed for each gas absorption line of interest. Well-designed fibre lasers, however, can overcome this limitation by offering potentially much wider wavelength ranges, in addition to distinctive and valuable features such as stability, narrow line-width and high tuneability at room temperature. A fibre Bragg grating (FBG)-based laser resonator can be readily created to target the specific signature absorption bands of the gas(es) of interest, eliminating the need for more expensive optical components, while at the same time allowing a wide tuning range.

CO<sub>2</sub> is an important gas used in various industries such as the food, oil as well as the chemical industries and therefore the detection of CO<sub>2</sub> concentrations over the ppb to ppm range is very important. With the advances seen in laser technology, in the last decade, DFB lasers as well as quantum cascade lasers in the NIR and MIR wavelength range have been used extensively as sources in CO<sub>2</sub> detection systems [12-14]. The utilization of a tuneable fibre laser at a wavelength of around 1.5 μm for CO<sub>2</sub> sensing has also been reported [15], in spite of a number of difficulties known by using a shorter wavelength for the sensitive detection of the target gas. The utilization of the 2 μm wavelength region is more advantageous as the absorption of CO<sub>2</sub> over the 2 μm

wavelength band is hundreds of times stronger than that of 1.5  $\mu\text{m}$  region [16]. The broad fluorescence spectrum of the Thulium (Tm)-ion in silica glass allows the fabrication of a widely tuneable fibre laser with a tuning range from 1.7 to 2.1  $\mu\text{m}$ , thus providing an excellent overlap with the strong absorption lines that are suitable for  $\text{CO}_2$  measurement [17]. Furthermore, there is a major benefit in having available compact systems for ‘in-the-field’ use for environmental monitoring and an ‘all-fibre’ laser has the advantage of being more robust than many other systems, as well as showing a low loss, making it more rugged and reliable for installation and thereby reducing maintenance needs.

The main objective of this work is to design an ‘all-fibre’ laser based compact gas sensors with potential for industrial use. Thus a Tm-doped ‘all-fibre’ tuneable laser in the 2  $\mu\text{m}$  wavelength region has been designed using a similar approach discussed in Chapter 5 with the key laser parameters such as output power, line-width and tuning range being optimized to align with the signature absorption band of  $\text{CO}_2$  in this wavelength range. The modulation of the fibre laser is achieved by modulating the pump light and through monitoring the absorption spectrum using the ‘locking’ detection principle both the concentration level of  $\text{CO}_2$  and the minimum detectable concentration can thus be measured. The stability of laser performance as the key element of the sensor system has also been studied with a view to develop a prototype sensor system that meets the needs of practical, ‘in-the-field’ applications.

## 7.2 Sensor Principle

$\text{CO}_2$  has four classically-described vibrational modes, of which two bending modes are degenerate. Only the vibrations that induce a dipole moment are spectroscopically active in the IR wavelength region. Thus the inactive fundamental  $\nu_1$  appears only in combination bands, but  $\nu_2$  at 15  $\mu\text{m}$  and  $\nu_3$  at 4.3  $\mu\text{m}$  absorb intensely while the NIR wavelength region is populated by weak overtone and combination bands. Some of the important IR absorption of  $\text{CO}_2$  is tabulated in Table 7.1 [from HITRAN2008 database]

Table.7.1 Absorption bands of CO<sub>2</sub> in IR region

CO <sub>2</sub> band	Wavelength $\lambda$		Line Strength S cm/molecules
	(cm <sup>-1</sup> )	( $\mu$ m)	
$\nu_2$	667	15	$5 \times 10^{-18}$
$\nu_3$	2361.466	4.235	$3.524 \times 10^{-18}$
$\nu_1 + \nu_3$	3597.963	2.779	$3.525 \times 10^{-20}$
$\nu_1 + 2\nu_2 + \nu_3$	4989.972	2.004	$1.332 \times 10^{-21}$
$2\nu_1 + \nu_3$	5109.311	1.957	$4.003 \times 10^{-23}$
$\nu_1 + 4\nu_2 + \nu_3$	6240.105	1.603	$1.838 \times 10^{-23}$
$2\nu_1 + 2\nu_2 + \nu_3$	6359.968	1.572	$1.846 \times 10^{-23}$

If the laser emission is resonant with a particular CO<sub>2</sub> absorption line, the intensity of light transmitted through the gas cell will be reduced by the CO<sub>2</sub> absorption and the transmitted light level changes with the variation of the gas concentration. The key features of NIR spectroscopy are governed by the Beer-Lambert law. According to the Beer-Lambert law, the relationship between the intensity of the emergent light,  $I$ , the intensity of the incident light,  $I_0$ , and the density,  $N$ , is given by [18]

$$I(\lambda) = I_0(\lambda) \exp[-LC\alpha(\lambda)] \quad (7.1)$$

where  $L$  is the interaction length of gas with light and  $\sigma$  is the absorption cross section. As  $L$  and  $\sigma$  are known, the density of the gas,  $N$ , can be obtained by measuring the light intensities,  $I$  and  $I_0$ . The use of this approach in this application is based on two assumptions being valid: the incident radiation is monochromatic and each absorbing centre is independent of all others, regardless of the type or concentration of the target gas(es).

## 7.3 Experimental Work

### 7.3.1 Selection of laser wavelength

As discussed in Chapter 5, a known length of Tm-doped fibre can provide amplified spontaneous emission (ASE) over the wavelength range from 1.75  $\mu\text{m}$  to 2.1  $\mu\text{m}$ , under pumping at 1.6  $\mu\text{m}$ . The laser resonator can be formed to operate at any wavelength in this range by using a suitable FBG pair. Fig. 7.1 shows the recorded ASE spectrum of a Tm-doped (Tm<sup>3+</sup> concentration:  $\sim 0.3$  mol%, Al<sup>3+</sup> concentration:  $\sim 6.8$  mol%) Alumino-silicate fibre (active fibre length: 15 cm), pumped at a wavelength of 1.6  $\mu\text{m}$ . The spectrum shows excellent overlap with the  $\nu_1 + 2\nu_2 + \nu_3$  combination absorption band of CO<sub>2</sub>, centred at 2.004  $\mu\text{m}$ . Fig. 7.1 also includes the absorption spectra of CO<sub>2</sub> at wavelengths of around 1.875  $\mu\text{m}$  and 1.998  $\mu\text{m}$  with more details being illustrated in the inset figures. The absorption line strengths shown in the figure are obtained from the HITRAN2008 database.

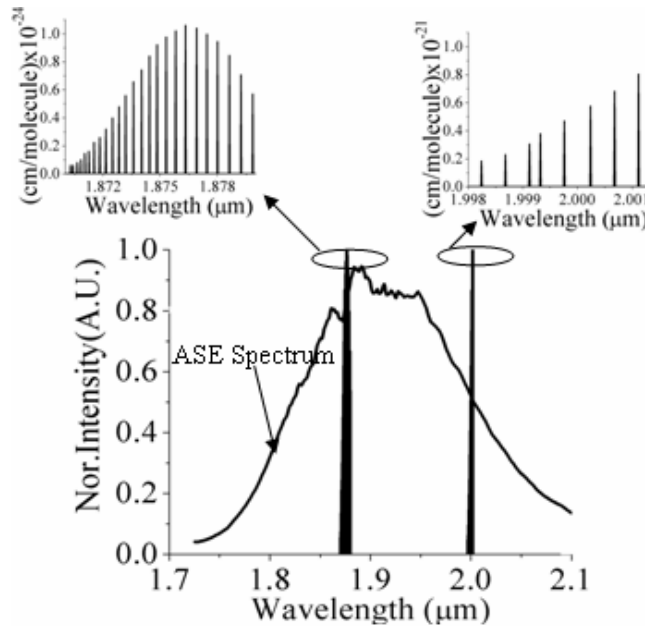


Fig. 7.1 ASE spectrum from Tm-doped fibre overlapped with the absorption spectrum of CO<sub>2</sub>. Inset: Higher resolution spectra of CO<sub>2</sub> showing absorption line strength on the Y-axis

The operating wavelength range of  $1.998 \mu\text{m}$  was chosen for use in this sensor application for the following reasons: (a) it has approximately one thousand times stronger absorption line strength than is seen at  $1.875 \mu\text{m}$  and (b) it shows isolation from interfering high temperature water absorption features [13]. Therefore a laser wavelength at  $1.995 \mu\text{m}$  was selected and, coupled with a suitable laser tuning mechanism, the laser can thus be tuned with wavelengths up to  $2.001 \mu\text{m}$ . It has been estimated that the wavelength difference between the absorption lines in the operating wavelength range is around  $0.28 \text{ nm}$  and thus the line-width of the laser should be smaller than that value to avoid overlapping with two absorption lines simultaneously.

### 7.3.2 Experimental set-up

The schematic of the gas sensor system using the Tm-doped tuneable fibre laser is shown in Fig.7.2.

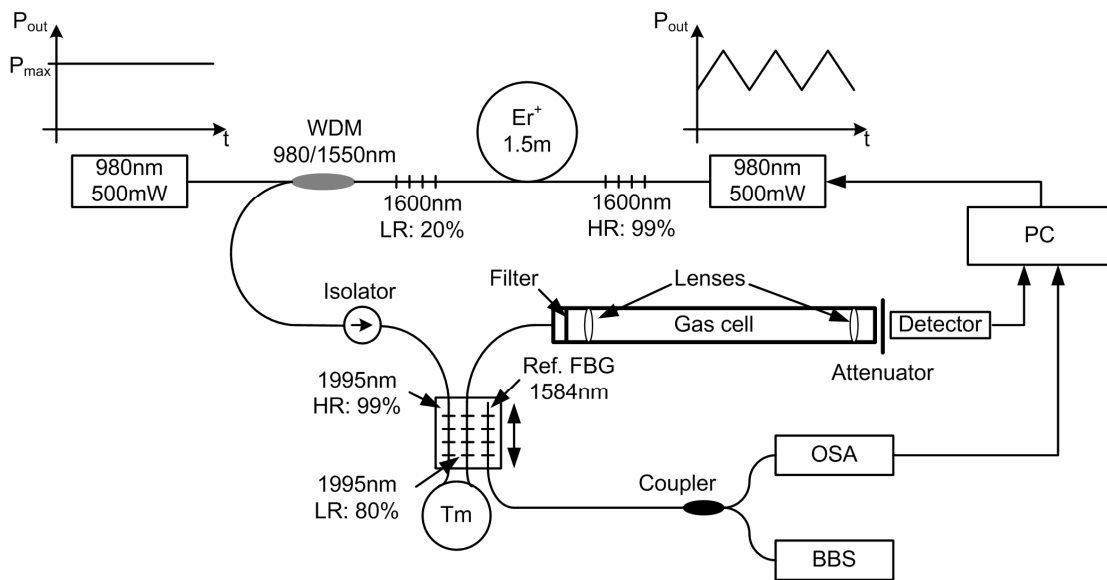


Fig. 7.2 Schematic of the gas sensor system using the Tm-doped tuneable fibre laser (HR: High reflective FBG; LR: low reflective FBG; BBS: broadband source)

An Erbium (Er)-doped fibre laser operating at 1.6  $\mu\text{m}$  was designed by using (a) 1.5 m length of Er-doped active fibre, (b) a FBG pair at 1.6  $\mu\text{m}$ , with the High Reflectivity (HR) being 99.98 % and the Low Reflectivity (LR) being 20% and (c) a bi-directional pump at 0.98  $\mu\text{m}$  each with an output power of 500 mW, all in order to pump Tm-doped fibre laser. The backward pump source was connected to the resonator by using a 0.98/1.55  $\mu\text{m}$  Wavelength Division Multiplexer (WDM) while the forward pump source is connected directly to the resonator. Both the 0.98  $\mu\text{m}$  pump sources were driven by using two Wavelength Electronic WLD3343 laser drivers. The forward pump source was modulated by changing the set-point voltage of the WLD3343 laser driver using the analogue output from the NI PCI-6110 DAQ card and a LabView program. The 1.55  $\mu\text{m}$  output of the WDM coupler was connected to the input end of the Tm-doped fibre laser, designed for lasing at 1.995  $\mu\text{m}$ , through an isolator with a centre wavelength at 1.6  $\mu\text{m}$  (to avoid back-coupling of light). The Tm-doped fibre laser at 1.995  $\mu\text{m}$  consisted of a 15 cm of Tm-doped Alumino-silicate fibre (Tm<sup>3+</sup> concentration: ~0.3 mol%, Al<sup>3+</sup> concentration: ~ 6.8 mol%), a FBG pair (HR: 99%; LR: 80%) and the modulated fibre laser pump source operating at 1.6  $\mu\text{m}$ . The output end of the 1.995  $\mu\text{m}$  fibre laser was connected to a 0.36 m long gas cell containing the gas to be measured and in order to allow only light from the 1.995  $\mu\text{m}$  fibre laser to be coupled into the gas cell, a long pass filter (LP-1700 nm) having a cut-off wavelength at around 1.7  $\mu\text{m}$  was placed in front of the gas cell. Furthermore, the light within the gas cell was collimated and a photodetector (Thorlabs PDA10D) was placed at the other end of the gas cell to record the laser light intensity variations with an attenuator in the front to keep the modulated light to be within the dynamic range of the detector. The details of the construction of the gas cell were reported in Ref. [19]. The NI PCI-6110 DAQ card, an anti-aliasing filter and LabView software were used to record as well as to process the output voltage signal obtained from the photodetector.

As described in Chapter 5, the centre wavelength of the 1.995  $\mu\text{m}$  fibre laser can be tuned by applying equal compression to the resonator formed by the FBG pair. In order to monitor the actual centre wavelength of the tuneable laser at around 1.995  $\mu\text{m}$  and to

avoid the use of an expensive Optical Spectrum Analyzer (OSA) designed for extended wavelengths, a simple interrogation system has been created in this work by using a reference FBG with a Bragg wavelength of 1.584  $\mu\text{m}$ . To tune the laser wavelength, both the 1.995  $\mu\text{m}$  FBG pair and the reference FBG were embedded into a flexible material (Makroform vivak clear 099) having a Young's modulus of 2050  $\text{N}/\text{mm}^2$ , by using cyanoacrylic adhesive (Loctite 435). The gratings are firmly adhered to the material, in that way to prevent any drift during the tuning process and to assure equal strain distribution. In the compression mount, a displacement ( $\Delta z$ ) was achieved by driving the fixing mount through a micro-screw. The wavelength change of the 1.584  $\mu\text{m}$  FBG was interrogated by using an OSA (AQ6370), when it is connected to an Er-doped fibre based Broadband Source (BBS) via a 1x2 3dB coupler. An Ethernet link was established between the OSA and LabView in order to capture and automatically process the measured reference FBG spectrum. The photographs of tuneable fibre laser and gas cell used during the experimentation are presented in Fig. 7.3. Data Acquisition was done using NI PCI-6110 DAQ card where the acquisition frequency is set to the modulation frequency of the fibre laser as well as the detector. The signals were generated and processed by using LabView.

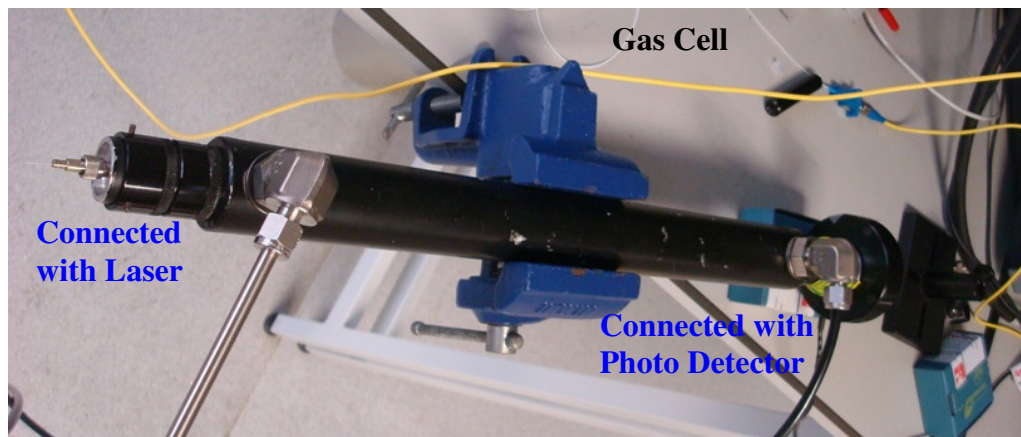
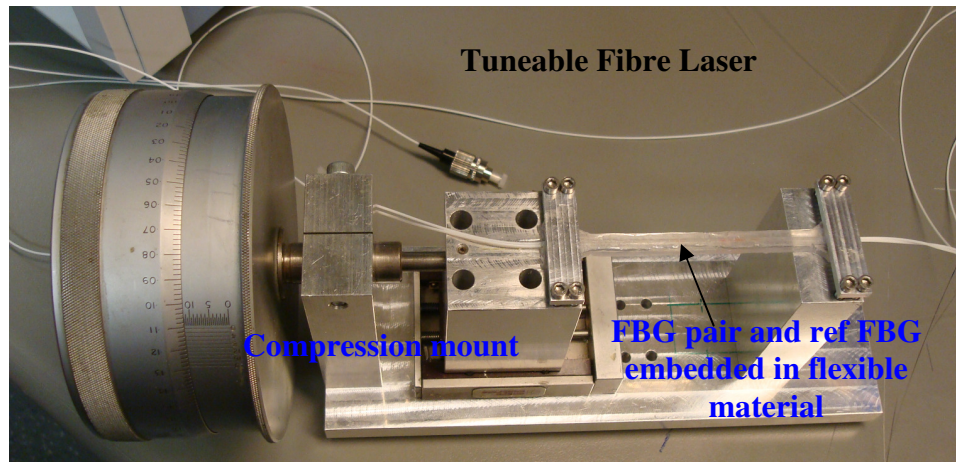


Fig.7.3 Images of Tm-doped tuneable fibre laser and gas cell used in sensor system

### 7.3.3 Laser characteristics

The output power of the laser at 1.995  $\mu\text{m}$ , monitored as a function of the set-point voltage of the WLD3343 laser driver of the forward 0.98  $\mu\text{m}$  pump source, is shown in Fig. 7.4. The output power of the 1.995  $\mu\text{m}$  laser was measured by using a Power Meter (Ophir Nova). Beyond the threshold, the laser output power is seen to be linearly dependent on the input set voltage of the forward 0.98  $\mu\text{m}$  pump source. The maximum output power of the Tm-doped fibre laser when the bidirectional pump is set to maximum, i.e. both forward and backward pumping is set at the maximum was 3 mW and power stability of the laser was tested for 4 hours. Furthermore, the line-width of the

laser measured by use of OSA AQ6375 (with a resolution of 0.05 nm) is 0.14 nm which is well suited to matching the tuneable laser light to a specific absorption line of the CO<sub>2</sub> gas.

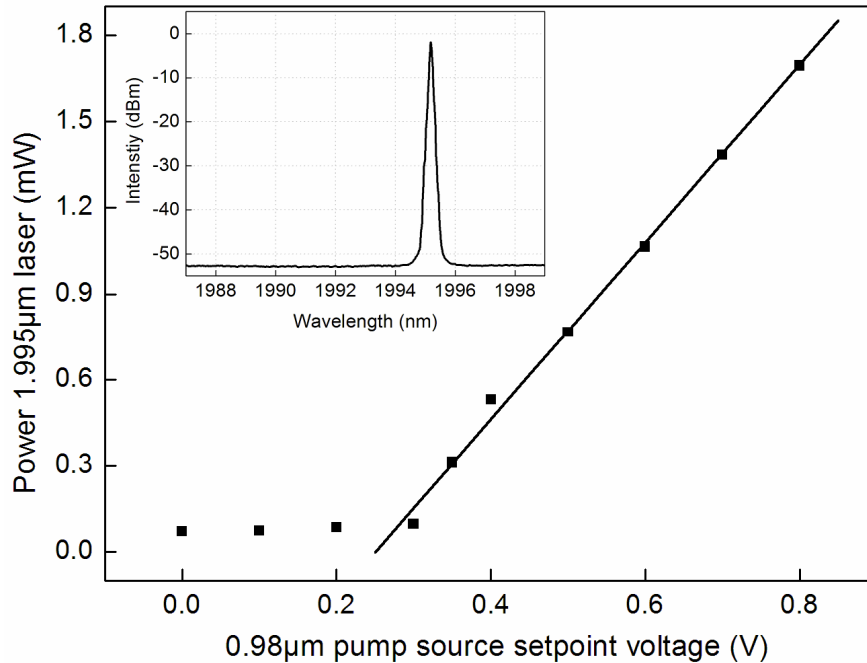


Fig. 7.4 Laser output spectrum and variation of laser output power at 1.995 μm with the set-point voltage of the forward 0.98 μm pump source laser diver

For fibre lasers, in the absence of the external modulation, the response of the laser exhibits a sharp peak in the power spectrum at the relaxation oscillation frequency,  $f_0$ . The relaxation oscillations are quasi-sinusoidal, exponentially damped oscillations about the steady state laser output [20]. The nature of the response depends on several factors such as the populations of the different laser levels, the pump power, cavity loss and upper state lifetime. Fig. 7.5 shows the transient response of the 1.995 μm laser when the 0.98 μm pump laser was switched on, followed by switch off. The laser output initially shows spiking which settles down to relaxation oscillations as the system approaches steady state. As illustrated in Fig. 7.5 with a sampling frequency of 100 kHz and anti-aliasing filtering, the frequency  $f_0$  of the relaxation oscillation is around 26 kHz.

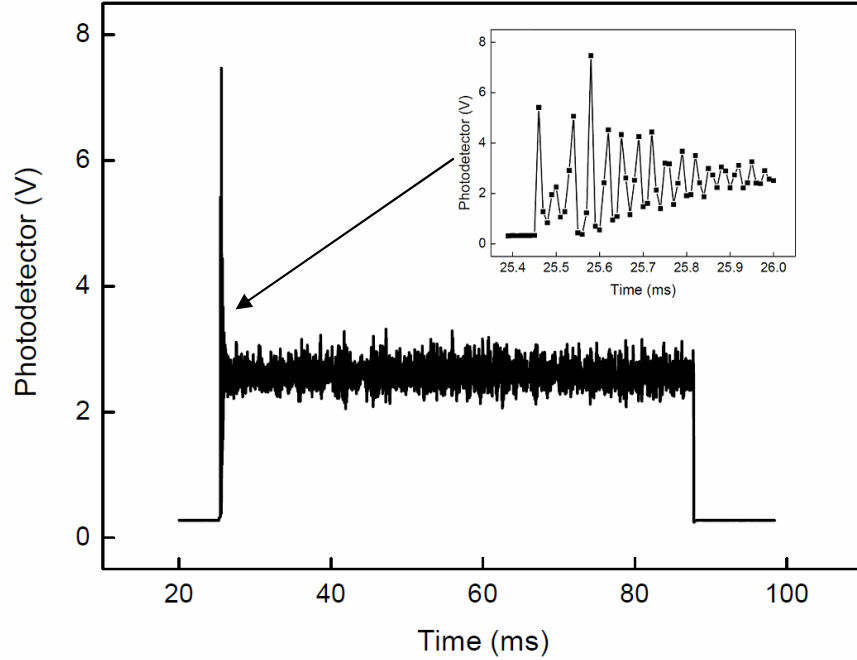


Fig. 7.5 Transient behaviour of Tm-doped fibre laser

As already outlined in Equation (7.1), the concentration of a particular gas can be monitored directly by measuring the emergent laser light intensity. However, laser intensity noise limits the minimum detectable gas concentration and therefore usually either wavelength or frequency modulation is used as a harmonic detection technique to enhance the sensitivity [21]. In the past, fibre lasers have been wavelength modulated by either dynamically straining or heating the FBGs [21]. However, in both cases the optical fibre is permanently under mechanical stress and therefore this region might lead to failure. Consequently the lifetime of this kind of fibre laser is restricted.

In order to avoid permanent stressing the optical fibres of the fibre laser, the 1.995  $\mu\text{m}$  laser is sinusoidally modulated with the modulation frequency  $f_m$ , given by the signal:

$$y(t) = A_0 + A_m \sin(2\pi f_m t) \quad (7.2)$$

and applied to the set-point voltage of the WLD3343 laser driver of the forward 0.98  $\mu\text{m}$  pump source using the analogue output of the NI PCI-6110 DAQ card. In Equation (7.2),  $A_0$  and  $A_m$  are the offset and modulation amplitudes respectively.  $A_0$  is required in order

to set the laser beyond the threshold, as illustrated in Fig. 7.4. The modulation frequency,  $f_m$ , was fixed to a value below half of the fundamental laser frequency ( $f_m < f_0/2$ ) to suppress self-pulsation [17]. Hence a frequency,  $f_m$ , of 1 kHz was used as the modulation frequency of the input set voltage of the forward pump source. The measured output power, when the Tm-doped fibre laser was modulated, is shown in Fig. 7.6 and this indicates that the resulting modulated intensity from the fibre lasers was dominated (as revealed by in-phase and in-frequency match) by the modulation of the input set voltage of the 0.98  $\mu\text{m}$  forward pump source.

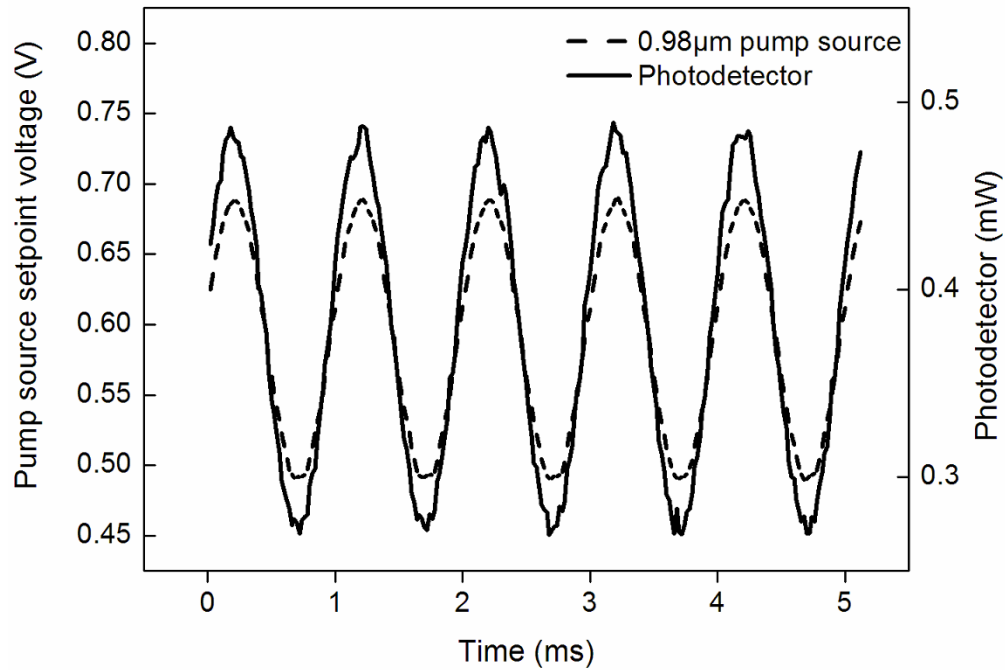


Fig. 7.6 Modulated intensity of the Tm-doped fibre laser at 1.995  $\mu\text{m}$

The linear variation of the reference FBG wavelength with the laser tuning wavelength is shown in Fig. 7.7, thereby offering an effective solution capable of practical implementation for determining the laser wavelength in the 2  $\mu\text{m}$  range through using a simple interrogator operating in the telecommunications range at wavelengths around 1.55  $\mu\text{m}$ , rather than through the use of an expensive OSA in the longer wavelength range. The data on the variation of laser wavelength with the Bragg wavelength of the

reference FBG was captured using a long wavelength Optical Spectrum Analyser (AQ6375) and utilized only to calibrate the sensor system.

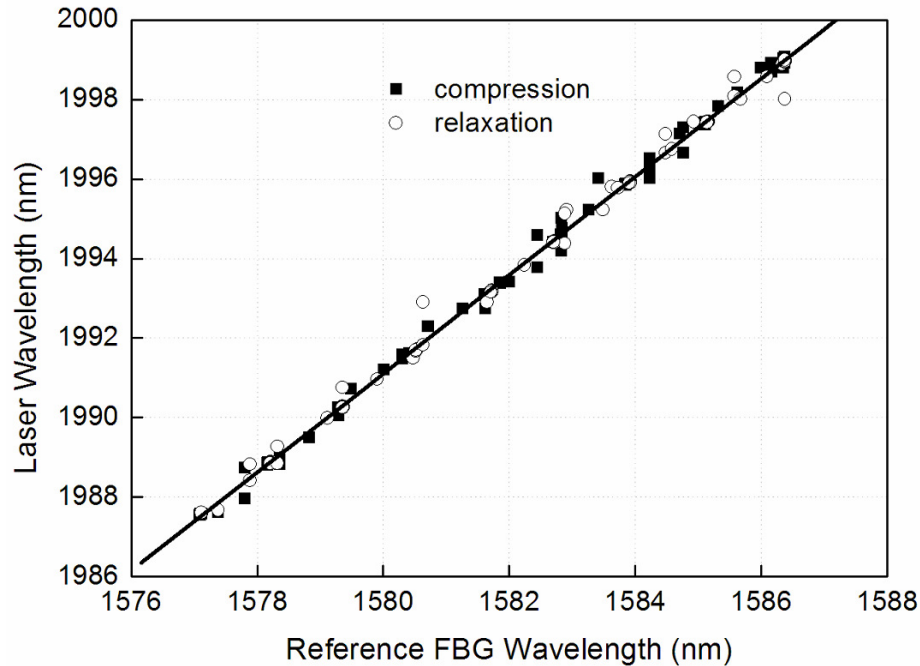


Fig. 7.7 Linear relationship between the centre wavelength of the tuneable laser at 1.995  $\mu\text{m}$  and the Bragg wavelength of reference FBG at 1.584  $\mu\text{m}$

### 7.3.4 CO<sub>2</sub> detection

In order to measure the variation of the laser intensity due to the absorption by the gas at different centre wavelengths, a ‘locking’ mechanism was applied. The ‘locking’ mechanism used calculates the FFT of the captured photodetector voltage and subsequently allows the monitoring of the absolute amplitude at the modulation frequency  $f_m$  of 1 kHz. The absolute amplitude obtained is in unit voltage and can be converted in intensity by using the transimpedance gain, responsivity and active area of the photodetector.

At the beginning, the gas chamber was pressurized to 2 bar with Nitrogen (N<sub>2</sub>) gas and the amplitudes  $A_m$  were measured for each centre wavelength when the laser was tuned over the full range. Following this the short-term noise and the long-term drift of the gas

sensor at a single laser wavelength of  $1.996\ \mu\text{m}$  were measured under conditions where the gas cell was pressurized with  $\text{N}_2$ . In Fig. 7.8, the constant amplitude obtained is illustrated, seen by observation over a period of 45 min and thereby establishing the stability of the sensor system. From the test shown in Fig. 7.8, a standard deviation of 0.67% for the short-term noise and 0.21% for the long-term drift of the fibre laser system was measured. The noise of the fibre laser system is mainly caused by the accuracy obtained from the analogue input of the NI PCI-6110 DAQ card, which is defined as  $\pm 0.011\text{V}$  for the used configuration used. Therefore, the stability of the fibre laser system could be further enhanced by developing an analogue front-end for the DAQ card that allows a higher accuracy to be obtained.

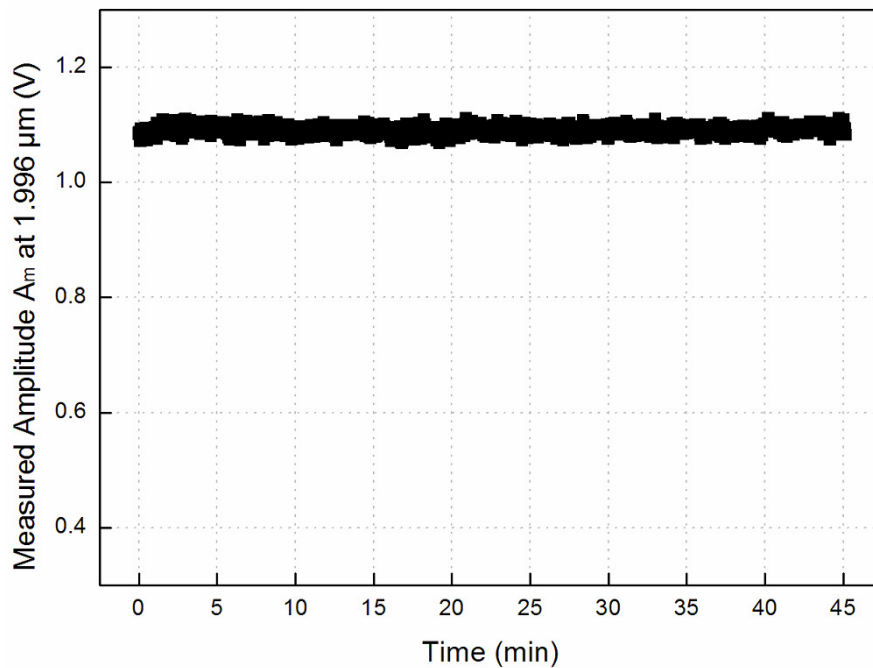


Fig. 7.8 Stability of the  $\text{Tm}$ -doped fibre laser based gas sensor system over time

The chamber was then evacuated and pressurised to 1.5 bar using  $\text{CO}_2$  and a similar experiment on the laser tuning and detection was carried out. In Fig. 7.9, the spectrum of the tuneable laser is illustrated when the chamber was under 1.5 bar  $\text{CO}_2$  and 2 bar  $\text{N}_2$ . Under the condition where it was filled with  $\text{N}_2$ , the intensity of the fibre laser over the

tuning range was almost constant and there is no distortion seen in laser spectrum as  $N_2$  does not have any absorption in this wavelength range. The small attenuation at a higher wavelength is likely due to the compression of the HR and LR FBG of the Tm-doped fibre laser and consequently the attenuation of the light within the laser resonator. Furthermore, the negligible sinusoidal modulation observed was due to light interference within the gas cell between the fibre end face and the filter, as shown in Fig. 7. 2. The interference can be avoided by tilting the filter. However, when the laser was exposed to the chamber filled with  $CO_2$ , the laser light was strongly absorbed on a different absorption line of  $CO_2$ .

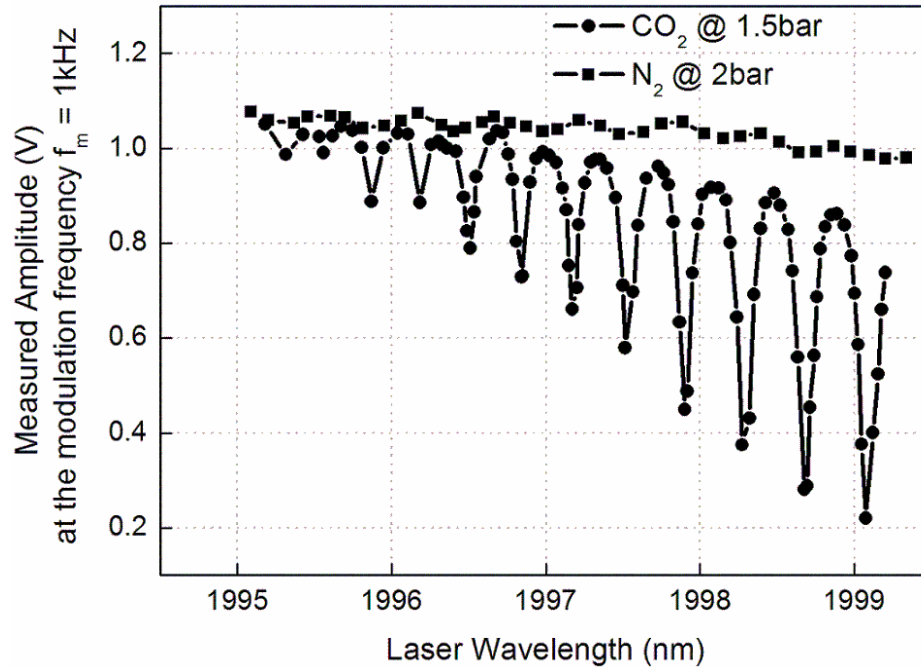


Fig.7.9 Measured amplitudes  $A_m$  of the modulated tuneable Tm-doped fibre laser exposed in the gas cell

The information about the absorption spectrum is valuable to tune and thus fix the laser wavelength at one convenient absorption line to measure the concentration level of  $CO_2$  present. The intensities of the laser at the two different fixed wavelength of  $1.9975 \mu\text{m}$  and  $1.9979 \mu\text{m}$  were recorded subsequently at different concentrations of  $CO_2$  within the

chamber and the variation of detected voltage with CO<sub>2</sub> concentration compared to the reference voltage  $V_0$ , which was obtained at 2 bar N<sub>2</sub>, are shown in semi logarithmic scale in Fig. 7.10.

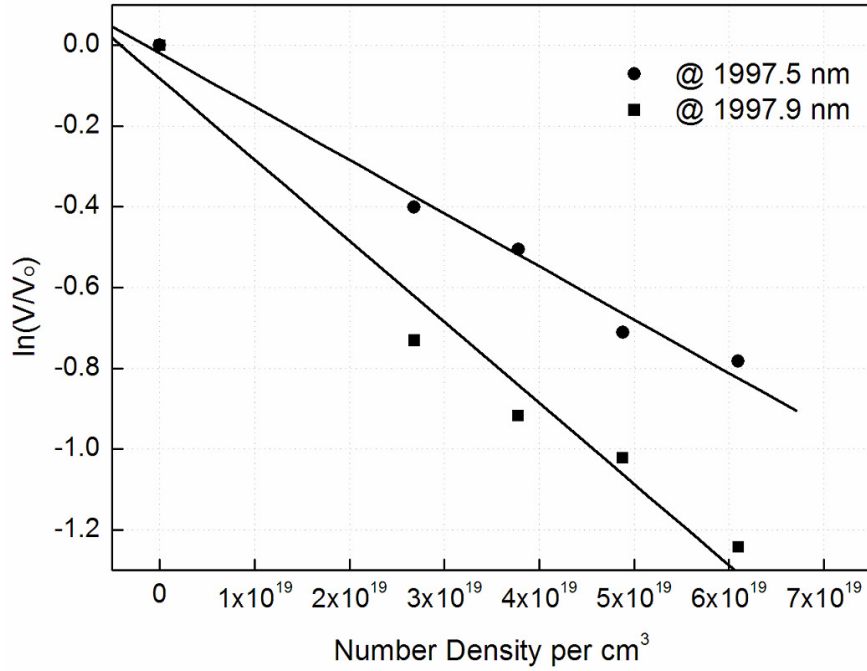


Fig.7.10 Measured amplitudes  $A_m$  of the modulated Tm-doped fibre laser (at 1.9975  $\mu\text{m}$  and 1.9979  $\mu\text{m}$ ) with CO<sub>2</sub> gas concentration

As illustrated in Fig. 7.10 the normalized and logarithmic emergent laser light intensities depends linear on the CO<sub>2</sub> gas concentration, which is consistent with Equation (1). Furthermore, to obtain the absorption cross sections,  $\sigma$ , for both wavelengths, linear functions were fitted into the graphs shown in Fig. 7.10. The slopes of the linear functions, which are equal to  $\sigma L$ , were calculated at  $2.01 \times 10^{-20} \text{ cm}^3/\text{molecule}$  with a standard deviation of  $8.6 \times 10^{-2}$  for 1.9979  $\mu\text{m}$  and  $1.32 \times 10^{-20} \text{ cm}^3/\text{molecule}$  with a standard deviation of  $3.6 \times 10^{-2}$  for 1.9975  $\mu\text{m}$ . From this, the values of  $\sigma$  were obtained at  $5.6 \times 10^{-22} \text{ cm}^2/\text{molecule}$  for 1.9979  $\mu\text{m}$  and  $3.7 \times 10^{-22} \text{ cm}^2/\text{molecule}$  for 1.9975  $\mu\text{m}$  considering  $L = 0.36 \text{ m}$  (length of gas cell).

Pressure broadening effects of the CO<sub>2</sub> absorption lines at different pressures could not be measured directly due to the relative broad line width of the 1.995 μm laser source. However, as a result of the broad line-width of the fibre laser, it was assumed that the pressure broadening of the absorption lines also affect the emergent laser light intensities at different CO<sub>2</sub> densities. Therefore, the line strengths,  $S$ , of the absorption lines can be obtained by normalizing the measured absorption cross sections using the measured laser line-width of 0.35 cm<sup>-1</sup>. From this, the line strengths of 1.95×10<sup>-22</sup> cm/molecule and 1.28×10<sup>-22</sup> cm/molecule were obtained for wavelengths of 1.9979 μm and 1.9975 μm, respectively. The measured line strengths of CO<sub>2</sub>, using the gas sensor designed, are in good agreement with the HITRAN database, as shown in Fig. 7.1.

The minimum detectable density,  $N_{\min}$ , has been derived by manipulating Equation (1) and is written as:

$$N_{\min} = \frac{\ln\left(1 - \frac{1}{SNR}\right)}{-\sigma \cdot L} \quad (3)$$

Equation 3 reveals that the detection limit is determined by the path length,  $L$ , the absorption cross section,  $\sigma$ , at a specific wavelength and the signal-to noise (SNR) ratio in the spectrum, where 1/SNR is defined by the standard deviation of the short-term noise of the fibre laser gas sensor. From Fig. 7.8 and Fig. 7.10, the minimum detectable concentration,  $N_{\min}$ , of the fibre laser-based gas sensor constructed has been calculated to be 3.34×10<sup>17</sup> molecule/cm<sup>3</sup>, which is equivalent to 1.2% volume. The minimum detectable concentration could be further reduced by removing the attenuator at the front of the detector and eliminating the noise seen from the analogue input of the DAQ card. Consequently the system as designed shows real potential for the detection of CO<sub>2</sub> in the atmosphere and potentially the accuracy could be enhanced further with an improved electronic system.

## 7.4 Summary

The designed Tm-doped fibre laser based gas detection system has shown itself to be successful in offering a stable means of detection of CO<sub>2</sub> using its optical spectrum. The system designed laser is superior in terms of the selection of the operating wavelength and its fit to a specific absorption line of the gas showing a stronger absorption cross-section, in a particular longer wavelength absorption band. In addition, the employment of the modulated laser and the 'locking' detection technique shows a low level of noise in the detection system. The detected CO<sub>2</sub> spectrum in the range of 1.998 μm has been shown to be comparable with the spectral features available from the HITRAN data base.

The use of the reference FBG offers the potential for the use of a simple FBG interrogator, as a much less expensive alternative to using an OSA specifically designed for longer wavelength range detection, to allow the laser wavelength to be monitored readily over the tuning range used. However, when the absorption feature of the targeted gas is known, the HR and LR FBG for the Tm-doped fibre laser can be fabricated such that their centre wavelengths are equal to an absorptions line of the targeted gas and consequently the reference FBG would not be further required. As a consequence the total detection and signal processing scheme for the resulting fibre laser gas sensor requires relatively inexpensive and relatively available equipment.

This work has thus presented preliminary work which presents an effective 'proof-of-principle' on the implementation of a compact tunable 'all-fibre' laser for gas sensing in the 2 μm wavelength range. There is a considerable scope for enhancing the detection system for the selective and sensitive detection of a range of different gases, involving the optimization of the dynamic range of the detector and with that removing the attenuator as well as improving the signal processing algorithm used. This builds on the inexpensive, compact and easy to use system demonstrated in this work.

## References

- [1] G Stewart 'Optical Fiber Sensors Technology', Chapter 5, Kluwer Academic Publishers, Dordrecht, Ed: K T V Grattan and B T Meggitt, (1999)
- [2] G Stewart, G Whitenett, P Shields, J Marshall and B. Culshaw 'Design of fibre laser and sensor systems for gas spectroscopy in the near-IR', in Proc. Industrial and Highway Sensors Technology, Bellingham, WA, pp. 172 – 180 (2004)
- [3] C Sirtori, J Faist, F Capasso, D L Sivco, A L Hutchinson and A Y Cho 'Long wavelength infrared (~11  $\mu\text{m}$ ) quantum cascade lasers', Applied Physics Letters, Vol. 69, pp. 2810–2812 (1996)
- [4] G C Bijnen, F J M Harren, J H P Hackstein and J Reuss 'Intracavity CO laser photoacoustic trace gas detection: cyclic CH<sub>4</sub>, H<sub>2</sub>O and CO<sub>2</sub> emission by cockroaches and scarab beetles', Applied Optics, Vol. 35, pp. 5357–68 (1996)
- [5] A Romann and M W Sigrist 'Photoacoustic gas sensing employing fundamental and frequency-doubled radiation of a continuously tunable high-pressure CO<sub>2</sub> laser', Applied Physics B, Vol. 75, pp 377-383 (2002)
- [6] N Matsuoka, S Yamaguchi, K Nanri, T Fujioka, D Richter and F K Tittel 'Yb Fiber Laser Pumped Mid-IR Sorce Based on Difference Frequency Generation and Its Application to Ammonia Detection', Jpn. J. Appl. Phys. Vol.40, pp.625-628 (2001)
- [7] A J Henderson, P M Roper, L A Borschowa and R D Mead 'Stable, continuously tunable operation of a diode-pumped doubly resonant optical parametric oscillator', Optics Letters, Vol. 25, pp. 1264-1266 (2000)
- [8] H Gunzler and H U Gremlich 'IR Spectroscopy: An Introduction', Wiley VCH; 1<sup>st</sup> edition (August 15, 2002)
- [9] Y Zhang, M Zhang, W Jin, H L Ho, M S Demokan, X H Fang, B Culshaw and G Stewart 'Investigation of erbium-doped fiber laser intracavity absorption sensor for gas detection', Optics Communications, Vol. 234, pp. 435–441 (2004)
- [10] J Cousin, P Masselin, W Chen, D Boucher, S Kassi, D Romanini and P Szriftgiser, 'Application of a continuous-wave tunable erbiumdoped fiber laser to molecular spectroscopy in the near infrared', Applied Physics B, Vol. 83, pp-261–266, (2006)

- [11] P Werle, R.Mücke, F D'Amato and T Lancia 'Near-infrared trace-gas sensors based on room-temperature diode lasers', Applied Physics B, Vol. 67, pp-307–315 (1998)
- [12] A Rocco, G De Natale, P De Natale, G Gagliardi and L Gianfrani 'A diode-laser-based spectrometer for in-situ measurements of volcanic gases', Applied Physics B, Vol. 78, pp- 235–240 (2004)
- [13] M E Webber, S Kim, S T Sanders, D S Baer, R K Hanson and Y Ikeda 'In situ combustion measurements of CO<sub>2</sub> by use of a distributed-feedback diode-laser sensor near 2.0 μm', Applied Optics, Vol. 40, pp. 821-828 (2001)
- [14] V L Kasyutich, P A Martin 'A CO<sub>2</sub> sensor based upon a continuous-wave thermoelectrically-cooled quantum cascade laser', Sensors and Actuators B Vol.157, pp. 635– 640 (2011)
- [15] G Whitenett, G Stewart, H Yu and B Culshaw 'Investigation of a Tuneable Mode Locked Fiber Laser for Application to Multipoint Gas Spectroscopy', Journal of Lightwave Technology, Vol. 22, pp-813-819 (2004)
- [16] 'HITRAN'2008 Database' <http://www.cfa.harvard.edu/hitran/vibrational.html>
- [17] W A Clarkson, N P Barnes, P W Turner, J Nilsson and D C Hanna 'High-power cladding pumped Tm-doped silica fiber laser with wavelength tuning from 1860 to 2090 nm', Optics Letters, Vol. 27, pp-1989-1991 (2002)
- [18] N L Alpert, W E Keiser and H A Szymanski 'IR: Theory and Practice of Infrared Spectroscopy', Second ed. New York: Plenum Press (1970)
- [19] J Mulrooney 'An Optical Fibre Sensor for the Measurement of Carbon Dioxide Exhaust Emissions from Land Transport Vehicles', PhD- Thesis, University of Limerick, Ireland (2006)
- [20] A E Siegman 'Lasers', University Science Books, Mill Valley, CA (1986)
- [21] S Michelsen 'Optical fiber grating based sensors', PhD-Thesis, Technical University of Denmark, Denmark (2003)

# Chapter 8

## Conclusion and Future Work

### 8.1 Conclusion

The thesis has discussed and reported several significant advances in Thulium-doped fibre laser starting from the fabrication of Thulium-doped optical preforms and fibres. A successful prototype of tuneable ‘all-fibre’ laser based sensor for the detection of trace gases, has also been conceptualized and developed in the work presented in the thesis. Feasibility of the technique and relevance of selection of operating wavelength at 1.995  $\mu\text{m}$ , tuned at 1.998  $\mu\text{m}$ , has been established during laboratory demonstration of CO<sub>2</sub> detection, while detected CO<sub>2</sub> spectrum including absorption strength in the range of 1.998  $\mu\text{m}$  is in good agreement with the spectral features available from the HITRAN data base. Thulium-doped ‘all-fibre’ tuneable laser in the single-mode single-clad fibre configuration proves great potential to construct a compact, rugged, reliable and easy installable and maintainable system for ‘in-the-field’ use for environmental monitoring. Implementation of modulation in laser and ‘locking’ detection technique enables a low level of noise in the detection system.

Thus the major achievements made in response to the aims and objectives highlighted in Chapter 1 can be summarised as follows.

- Successful fabrication of active fibres (Thulium- and Thulium/Ytterbium-doped fibre) with good quality, desired characteristics and repeatability through standardization of fabrication process parameters in Modified Chemical Vapour Deposition (MCVD) process coupled with solution doping technique to enable the incorporation of rare-earth ions into the preforms.

- Rigorous characterization of waveguide, transmission and spectroscopic properties of the fabricated Thulium- and Thulium/Ytterbium-doped fibres to identify a suitable active fibre for use in laser design. As a gain medium of such laser system, aluminosilicate and aluminogermanosilicate glass with suitable amount of aluminium proves good host materials for Thulium. It has been found that an efficient Ytterbium to Thulium energy transfer occurs when Ytterbium:Thulium proportion is approximately equal to unity.
- Successful design and development of optimized fibre laser resonator in the 2  $\mu\text{m}$  wavelength region
- Both Thulium-doped fibre under pumping at 1.6  $\mu\text{m}$  and Ytterbium sensitized Thulium-doped fibre under dual pumping comprising a 1.6  $\mu\text{m}$  auxiliary pumping to support 0.98  $\mu\text{m}$  primary pumping has been explored to identify more economic pumping scheme.
- The laser resonator created with the combination of a high reflective fibre Bragg grating and a broadband mirror coated at the end of the fibre produced a wider tuning range compared to that created with a fibre Bragg grating-pair, which is limited by the non-uniform strain transfer to both gratings during compression/relaxation based tuning process.
- A novel Thulium-doped microsphere-based fibre laser system with very low threshold and narrow line-width in the wavelength region of 2  $\mu\text{m}$  has also been demonstrated successfully.

## 8.2 Future Work

Future work to arise from this body of the work could include the utilization of fibre laser in medical diagnostic, such as noninvasive optical blood glucose monitoring, and laser surgery; because of the distinctive absorption spectrum of human tissue being in the 2  $\mu\text{m}$  wavelength range.

The concept of noninvasive blood glucose sensing involves passing a band of near infrared light through a vascular region of the body. The concentration of glucose is then

obtained by analyzing the resulting transmission spectrum. Three unique peaks can be seen in the absorbance spectrum at 2.12  $\mu\text{m}$ , 2.27  $\mu\text{m}$ , and 2.32  $\mu\text{m}$  wavelengths [1]. Thus these wavelengths are helpful for pinning down presence of glucose, but are not readily absorbed by tissues. Compact fibre laser with power level in the mW range will be suitable for such detection. Extension of the operating wavelength in the mentioned region can be possible through doping thulium and holmium in novel host glass. This noninvasive testing would be a boon to diabetics who are not thrilled about pricking their fingers regularly.

Lasers are widely used in urology surgery. When combined with fibre laser technology, 2  $\mu\text{m}$  laser proves to be valuable in the therapy of urological disease. The centre wavelength of 2  $\mu\text{m}$  Thulium-doped fibre laser is tuneable between 1.75 and 2.1  $\mu\text{m}$ , allowing the wavelength to exactly match the 1.94  $\mu\text{m}$  water absorption peak in tissue. Such 2  $\mu\text{m}$  laser is a new surgical laser with optional continuous or pulse-wave modes. The Thulium fibre laser offers several advantages over the presently used Holmium:YAG laser for surgical Urology: (i) centre wavelength is tuneable between 1.75 and 2.22  $\mu\text{m}$ , allowing the wavelength to exactly match the 1.94  $\mu\text{m}$  water absorption peak in tissues, reducing thermal damage by a factor of four from Holmium laser at 2.12  $\mu\text{m}$ ; (ii) Thulium fiber laser is diode pumped, allowing it to be operated in either the continuous-wave mode for applications requiring maximum hemostasis and coagulation, or, with an external modulation, in the pulsed mode for applications requiring precision cutting. Holmium laser is limited to operation in a pulsed mode with a pulse length of the order of 250  $\mu\text{sec}$ , which is not ideal for applications requiring cutting or coagulation; (iii) Thulium fiber laser produces a single-mode, perfect Gaussian spatial beam profile with a beam diameter of only 18  $\mu\text{m}$ . This high-quality, small-diameter beam can easily be coupled with a collimating lens into any standard silica optical fiber (e.g., 150 or 200- $\mu\text{m}$ -core fibers) for potential use with the smallest ureteroscopes in the most challenging applications, such as access to the lower pole of the kidney for lithotripsy [2].

Based on current work, the above mentioned futuristic applications demand an average laser power of several Watts. Double-clad Thulium-doped silica fibres are suitable for

such high power scaling in lasers. The double clad designs allow efficient coupling and guiding of the pump light through the inner clad of the fibre that results lower thermal damages and nonlinear effects. The Thulium-doped fibre lasers can be pumped directly in-band, but the system efficiency is limited by the 1.6  $\mu\text{m}$  pump sources. Alternatively, the pumping at 0.79  $\mu\text{m}$  via the “2-for-1” cross-relaxation path is capable of scaling the power with an efficiency of around 55-60%. The core of the fibre needs to be doped to a high concentration in order to reduce the length of fibre required for efficient operation of the laser and to exploit favourable energy transfer processes allowing cross-relaxation mechanism. The reasonably high background losses associated with silica and the OH impurity that is unfortunately incorporated into the core during fabrication sets limits on the length of fibre that can be used. This is particularly true for Thulium-doped silica fibre lasers because the laser operating wavelength of around 2  $\mu\text{m}$  is close to the 1<sup>st</sup> overtone absorption band of water. A suitable large mode area fibre design is important to maintain a level of Thulium-ion concentration in the core for efficient lasing as well as for the single mode operation of the fibre.

## References

- [1] J T Olesberg, M A Arnold, C Mermelstein, J Schmitz and J Wagnerb ‘Tunable laser diode system for noninvasive blood glucose measurements’ *Optical Diagnostics and Sensing* , Proc. Of SPIE Vol. 5702, pp. 23-29 (SPIE, Bellingham, WA, 2005)
- [2] N M Fried and K E Murray ‘High-Power Thulium Fiber Laser Ablation of Urinary Tissues at 1.94  $\mu\text{m}$ ’, *Journal of Endourology*, Vol. 19, pp. 25-31 (2005)

# List of Publications

1. K Bremer, **A Pal**, S Yao, E Lewis, R Sen, T Sun and K T V Grattan ‘Sensitive Detection of CO<sub>2</sub> Implementing Tuneable Thulium-doped ‘All-fibre’ Laser’, Applied Optics, Vol. 52, Issue 17, pp. 3957-3963 (2013)
2. **A Pal**, S Y Chen, R Sen, T Sun, and K T V Grattan ‘High-Q low threshold Thulium-doped silica microsphere laser in the 2  $\mu$ m wavelength region designed for gas sensing applications’, Laser Physics Letters, Vol. 10, 085101 (6 pages) (2013)
3. **A Pal**, R Sen, K Bremer, S Yao, E Lewis, T Sun and K T V Grattan ‘All-fibre’ Tunable Laser in the 2  $\mu$ m region, designed for CO<sub>2</sub> detection’ Applied Optics, Vol. 51, Issue 29, pp.7011-7015 (2012)
4. **Pal, Atasi**; Dhar, Anirban; Das, Shyamal; Annapurna, K; Schwuchow, Anka; Sun, Tong; Grattan, Kenneth T V; Sen, Ranjan ‘Energy-transfer parameters in a Tm/Yb doped single mode silica fibre’ JOSA B, Vol. 27, Issue 12, pp.2714-2720 (2010)
5. **Atasi Pal**, Anirban Dhar, Shyamal Das, Shu Ying Chen, Tong Sun, Ranjan Sen, Kenneth T V Grattan ‘Ytterbium sensitized Thulium doped fibre laser at near IR with 980 nm pump’ Optics Express, Vol. 18, Issue. 5, pp. 5068-50745 (2010)
6. **Pal, Atasi**; Chen, Shu Ying; Das, Shyamal; Bhattacharya, Archi; Sun, Tong; Sen, Ranjan; Grattan, K T V ‘Low Threshold Fiber Taper Coupled Silica Microsphere Laser in the 2 micron Wavelength Region’ The European Conference on Lasers and Electro-Optics 2011 paper: CJ\_P10
7. **Atasi Pal**, Shyamal Das, Shu Ying Chen, Tong Sun, Kenneth T. V. Grattan and Ranjan Sen ‘The Influence of Tm and Yb Proportion on Multi-step Energy Transfer Process’ Photon10 Optics and Photonics conference, UK, Aug, 2010
8. **Atasi Pal**, Shyamal Das, Shu Ying Chen, Tong Sun, Kenneth T. V. Grattan and Ranjan Sen, ‘All-Fiber Thulium Doped Fiber Laser by Utilizing Pump at 980 nm’ XXXVI OSI Symposium on Frontiers in Optics and Photonics (FOP11)